

11-12-2020

Fundamental Studies of the Singlet Oxygenation of Water Soluble Biological and Environmental Important Molecules

Marcela Jaramillo

Florida International University, mjara009@fiu.edu

Follow this and additional works at: <https://digitalcommons.fiu.edu/etd>

 Part of the [Environmental Chemistry Commons](#)

Recommended Citation

Jaramillo, Marcela, "Fundamental Studies of the Singlet Oxygenation of Water Soluble Biological and Environmental Important Molecules" (2020). *FIU Electronic Theses and Dissertations*. 4555.
<https://digitalcommons.fiu.edu/etd/4555>

This work is brought to you for free and open access by the University Graduate School at FIU Digital Commons. It has been accepted for inclusion in FIU Electronic Theses and Dissertations by an authorized administrator of FIU Digital Commons. For more information, please contact dcc@fiu.edu.

FLORIDA INTERNATIONAL UNIVERSITY

Miami, Florida

FUNDAMENTAL STUDIES OF THE SINGLET OXYGENATION OF WATER
SOLUBLE BIOLOGICAL AND ENVIRONMENTAL IMPORTANT MOLECULES

A dissertation submitted in partial fulfillment of

the requirements for the degree of

DOCTOR OF PHILOSOPHY

in

CHEMISTRY

by

Marcela Jaramillo Arcila

2020

To: Dean Michael R. Heithaus
College of Arts, Sciences and Education

This dissertation, written by Marcela Jaramillo Arcila entitled Fundamental Studies of the Singlet Oxygenation of Water Soluble Biological and Environmental Important Molecules, having been approved in respect to style and intellectual content, is referred to you for judgment.

We have read this dissertation and recommend that it be approved.

Jeffrey A. Joens

Christopher J. Dares

Shekhar Bhansali

Stanislaw Wnuk

Kevin O'Shea, Major Professor

Date of Defense: November 12, 2020

The dissertation of Marcela Jaramillo Arcila is approved.

Dean Michael R. Heithaus
College of Arts, Sciences and Education

Andrés G. Gil
Vice President of Research and Economic Development
and Dean of the University Graduate School

Florida International University, 2020

© Copyright 2020 by Marcela Jaramillo Arcila

All rights reserved.

DEDICATION

I dedicate this dissertation to

My mom, Blanca I. Arcila, my sister, Natalia Jaramillo, my great friends and supporters,
Ulises Franco and Ingrid Lehman, all my nieces and nephews, blood and soul family, my
mentor, professor Kevin O'Shea

and

Especially to my daughter, Valeria Franco, and God,

for their love, support, patience, encouragement, and helping me see the silver linings in
difficult times and keep a strong faith throughout my Ph.D. journey.

ACKNOWLEDGMENTS

I feel profound gratitude towards my mentor, Professor Dr. Kevin O'Shea, for his trust, encouragement, inspiration, leadership, patience, and scientific insights. I am grateful for selecting me to work and learn from him. It has been an honor to have his outstanding mentorship. May God bless Professor O'Shea and his family.

I want to acknowledge my committee members, Dr. Jeffrey A. Joens, Dr. Christopher J. Dares, Dr. Shekhar Bhansali, and Dr. Stanislaw Wnuk, for their time, insightful comments, suggestions, and warm approach. They elevated my research and Ph.D. experience. A special thanks to Dr. Jeffrey A. Joens for helping my research and academic journey. I feel deep admiration and respect for him.

I want to recognize my research lab members for your support and friendship. My Ph.D. journey was blessed by being part of such a brilliant, committed, and caring group of people. Ya-Li Hsu, Armando Perez, and Magali Autie thank you very much for your constant and kind help; I truly appreciate you.

I am also highly appreciative of the continuous faith in me, mentorship, and financial support kindly offered by Dr. Shekhar Bhansali, Dr. Alla Mirzoyan, Dr. Sonja Montas-Hunter, and the NSF Bridge to Doctorate Fellowship, and the NSF Graduate Research Fellowship Program. Finally, I would like to acknowledge the Department of Chemistry and the University Graduate School of FIU support.

ABSTRACT OF THE DISSERTATION

FUNDAMENTAL STUDIES OF THE SINGLET OXYGENATION OF WATER SOLUBLE BIOLOGICAL AND ENVIRONMENTAL IMPORTANT MOLECULES

by

Marcela Jaramillo Arcila

Florida International University, 2020

Miami, Florida

Professor Kevin O'Shea, Major Professor

Singlet oxygen, $^1\text{O}_2$, can be easily generated by a sensitizer, solar radiation, and molecular oxygen. $^1\text{O}_2$ is very important in a range of biological and environmental systems. The products and mechanisms of the $^1\text{O}_2$ reactions are well studied in organic solvents, and despite well-established solvent effects, studies on the reactions of the singlet oxygen in aqueous media are limited. Herein, $^1\text{O}_2$ reactions with biologically and environmentally relevant conjugated π systems in aqueous solutions are presented.

Water-soluble isomeric 1, 3-hexadienes are simple mechanistic probes for the $^1\text{O}_2$ reactions since concerted and non-concerted pathways produce distinct products. The isomerization of sorbic acid and sorbic alcohol is commonly used as triplet dissolved organic matter ($^3\text{DOM}^*$) quenchers. However, contributions from the singlet oxygenation of sorbic acid or alcohol during $^3\text{DOM}^*$ quantification has been neglected. The major reaction of $^1\text{O}_2$ with Sorbic Acid, SCO_2H , and sorbic alcohol, SOH , was the [4+2] pathway

to produce the endoperoxide. The singlet oxygenation of SCOOH and SOH in D₂O produced minor products from the [2+2] reaction pathways not observed in methanol-d₄ or chloroform-d₃.

Domoic acid (DA), a potent marine toxin, was readily oxidized upon reaction with ¹O₂. The [2+2] cycloaddition and ene reactions at the Z double bond were the major singlet oxygenation reaction pathways observed in aqueous media. The bimolecular rate constant for the DA reaction with ¹O₂ was 5.1 x 10⁵ M⁻¹ s⁻¹. The ¹O₂ reaction product mixture of DA did not exhibit significant biological activity indicating that singlet oxygenation could be an essential natural detoxification process.

Melanin, a pyrrole containing photoprotective pigment in the skin, is subject to irreversible damage by photooxidation. The reactions of singlet oxygen with the model pyrroles produced hydroxypyrrolones (HPOnes) as the major products. The singlet oxygenation of several pyrroles despite varying substitution at the α-carbon yielded identical major products. The bimolecular rate constants of singlet oxygen reactions with the studied pyrroles were from 1.2 to 18.9 x 10⁸ M⁻¹s⁻¹. 1H-pyrrole-2,3,4-tricarboxylic acid (TCOOH-Py), a marker to assess melanin photoaging, reacted with ¹O₂ at rates near diffusion control, $k(^1\text{O}_2+\text{TCOOH-Py})=18.9\pm 0.05 \times 10^8 \text{ M}^{-1}\text{s}^{-1}$. TCOOH-Py concentrations may underestimate skin damage.

TABLE OF CONTENTS

CHAPTER	PAGE
CHAPTER 1 INTRODUCTION TO THE REACTIONS OF SINGLET OXYGEN	1
1.1. General pathways and mechanism of the singlet oxygen reactions with conjugated dienes	5
1.2. Compounds of interests	8
1.2.1. Hexadienes: Sorbic Acid and Sorbic Alcohol	8
1.2.2. Domoic Acid.....	9
1.2.3. Pyrroles.....	11
1.3. The Relative Rate Technique:	12
1.4. Concluding Remarks	14
1.5. References	14
CHAPTER 2 SINGLET OXYGEN REACTIONS WITH WATER SOLUBLE HEXADIENES	19
2.1. Abstract.....	20
2.2. Introduction	21
2.3. Materials and Methods	23
2.4. Results and Discussion	25
2.5. Mechanistic Studies:.....	41
2.6. References	48
CHAPTER 3 FUNDAMENTAL STUDIES OF THE SINGLET OXYGEN REACTIONS WITH THE POTENT MARINE TOXIN DOMOIC ACID	51
3.1. Abstract.....	52
3.2. Introduction	53
3.3. Materials and methods.....	57
3.4. Results and discussion	61
3.5. References	83
CHAPTER 4 REACTIONS OF THE SINGLET OXYGENATION OF WATER-SOLUBLE PYRROLES: PRODUCTS, KINETICS, AND MECHANISTIC STUDIES	88
4.1. Abstract.....	89
4.2. Introduction	90
4.3. Materials and methods.....	94
4.4. Results and discussion	97
4.5. Kinetic studies	105
4.6. References	108
VITA.....	113

LIST OF TABLES

Table	Page
Table 2.1 ^{13}C NMR data for (6-methyl-3,6-dihydro-1,2-dioxin-3-yl)methanol.....	39
Table 2.2. ^{13}C NMR data for (5-methylfuran-2-yl)methanol	40
Table 2.3 The estimated product distribution of UV isomerization of SCOOH using NMR data C_3	43
Table 2.4. The estimated product distribution of UV isomerization of MuOH using NMR data C_3	46
Table 3.1. Summary of HPLC and LC-HR/MS analyses of Domoic acid and major products of singlet oxygenated Domoic acid.....	72
Table 3.2. The half-life of Domoic acid based on the reaction with reactive species ..	81
Table 4.1. Summary of the $^1\text{O}_2$ reactions with Pyrroles	107

LIST OF FIGURES

Figure	Page
Figure 1.1. Structures of Common $^1\text{O}_2$ photosensitizers.	3
Figure 1.2. Structures of Sorbic acid and Sorbic alcohol.	9
Figure 1.3. Structures of Domoic acid (left), L-glutamic acid (center), and Kainic acid (right). Homologous structural features are in blue, and the diene functionalities are in red.	10
Figure 1.4. Examples of structures of biological molecules containing pyrrole functionality.	12
Figure 2.1. Structures of sorbic acid (SCOOH) and sorbic alcohol (SOH) and sorbic amine (SNH ₂).	22
Figure 2.2. Aliphatic signals of ^1H NMR spectrum of singlet oxygenation of 5 mM SCOOH. The solutions prepared with 10 μM RB in D ₂ O were continuously purged with oxygen as it was irradiated with a 150 W Xenon lamp. The temperature was maintained at $\sim 5^\circ\text{C}$. The NMR spectra were obtained in the 400 Bruker NMR spectrometer.	26
Figure 2.3. ^{13}C NMR spectrum of singlet oxygenation of 5 mM SCOOH. The solutions prepared with 10 μM RB in D ₂ O were continuously purged with oxygen as it was irradiated with a 150 W Xenon lamp. The temperature was maintained at $\sim 5^\circ\text{C}$. The NMR spectra were obtained in the 400 Bruker NMR spectrometer.	27
Figure 2.4 NOESY NMR spectrum of singlet oxygenation of 5 mM SCOOH. The solutions prepared with 10 μM RB in D ₂ O were continuously purged with oxygen as it was irradiated with a 150 W Xenon lamp. The temperature was maintained at $\sim 5^\circ\text{C}$. The NMR spectra were obtained in the 400 Bruker NMR spectrometer.	28
Figure 2.5. Half-chair conformations of SCOOH _{cis} and SCOOH _{cis} , modified from Yong et al., 2012 and Parekh, P. K. et.al., 2012 (2, 26).	30
Figure 2.6. ^1H spectrum of the singlet oxygenation of 5 mM SCOOH for 2 hours (Top) 1 ^1H spectrum of the singlet oxygenation of 5 mM SCOOH for 2 hours and 1 hour of heating at 60°C	31
Figure 2.7. Aliphatic region of the ^1H spectrum of the singlet oxygenation of 5 mM SCOOH for 2 hours (Top). ^1H spectrum of the singlet oxygenation of 5 mM SCOOH for 2 hours and 1 hour of heating at 60°C	32
The singlet oxygenation of SOH was conducted in an NMR tube in D ₂ O at $\sim 5^\circ\text{C}$, using a Xenon lamp as the light source. No direct photolysis or energy transfer from RB pathways was observed in control experiments (without O ₂ or RB). The proton NMR	

time profile of the reaction of $^1\text{O}_2$ with 5 mM SOH is shown in Figure 2.8. As the reaction proceeded, the characteristic signals of SOH steadily decreased with the appearance of new complementary peaks.....33

Figure 2.9. Aldehyde region of the ^1H NMR spectra singlet oxygenated SOH. The solutions prepared with 10 μM RB in D_2O were continuously purged with oxygen as it was irradiated with a 150 W Xenon lamp. The temperature was maintained at $\sim 5^\circ\text{C}$. The NMR spectra were obtained in the 400 Bruker NMR spectrometer.35

Figure 2.10. ^1H NMR spectra of *trans* crotonaldehyde (top) acetaldehyde (bottom) and singlet oxygenated SOH product mixture (middle).36

Figure 3.1. ^1H NMR spectra of Domoic acid and singlet oxygenated Domoic acid. ^1H NMR spectrum of 3.21 mM DA (top) and after 25 minutes of reaction with $^1\text{O}_2$ reaction (bottom). The solutions were prepared with 10 μM RB in D_2O , buffered at pH 8 in an NMR tube, constantly purged with oxygen, and irradiated with a 150 W Xenon lamp while maintaining the temperature at $\sim 5^\circ\text{C}$. The NMR spectra were recorded in the 400 Bruker NMR spectrometer.....63

Figure 3.2. ^1H NMR of 10 mg (2*S*, 3*S*, 4*R*)-4-acetyl-3-(carboxymethyl)pyrrolidine-2-carboxylic acid, PAC, authentic per mL of D_2O standard (top). ^1H NMR of 25 min $^1\text{O}_2$ reaction with 3.21 mM DA (bottom). The peaks labeled with * are assigned to the ene reaction products. The 3.21 mM DA solution was prepared with 10 μM RB in D_2O , buffered at pH=8 in an NMR tube, continuously purged with oxygen, and irradiated with at 150 W Xenon lamp while maintaining the temperature at $\sim 5^\circ\text{C}$. The NMR spectra were recorded in the 400 Bruker NMR spectrometer.....66

Figure 3.3. Time profile of aldehyde and aliphatic regions of the ^1H NMR spectrum of singlet oxygenated Domoic acid. The ratio of MOP- H_e and PAC- H_f signals over the course of the reaction is shown. The integration of PAC- H_f corresponds to the 3 hydrogens of the methyl group. The solutions were prepared with 10 μM RB in D_2O , buffered at pH ~ 8 in an NMR tube, constantly purged with oxygen, and irradiated with a 150 W Xenon lamp temperature while maintaining the temperature at $\sim 5^\circ\text{C}$. The NMR spectra were recorded in the 400 Bruker NMR spectrometer.68

Figure 3.4. The ^1H NMR time profile of the singlet oxygenation of Domoic acid showing characteristic (*R*, *E*)-2-methyl-5-oxopent-3-enoic acid, MOP, and enol-(*R*, *E*)-2-methyl-5-oxopent-3-enoic acid, enol-MOP signals. Spectrum (bottom) was recorded 1 hour in the dark after the photooxidation. Spectrum (middle) was taken 3 hours in the dark the photooxidation. The spectrum at the top is the difference between the bottom and middle spectra. The signals for the enol tautomer, enol-MOP, are labeled. The NMR spectra were recorded in the 600 Bruker NMR spectrometer.69

Figure 3.5. Proposed Transformation of (*R*, *E*)-2-methyl-5-oxopent-3-enoic acid (MOP) under $^1\text{O}_2$ reaction conditions. Proposed MOP (1) enolization to molecule 2 extends conjugation, and subsequently, intermolecular cyclization and dehydration produce 3-methyl-2H-pyran-2-one (4), which is locked in an *s-cis* conformation, which

is highly susceptible to [4+2] cycloaddition of $^1\text{O}_2$. The resulting 5 can decompose to CO_2 and (Z)-4-oxopent-2-enal.70

Figure 3.6. ^1H NMR spectra of singlet oxygenated Domoic acid illustrating the integration ratio of (2*S*, 3*S*, 4*R*)-4-acetyl-3-(carboxymethyl)pyrrolidine-2-carboxylic acid (PAC) to (2*S*,3*S*,4*S*)-4-((6*R*,*E*)-6-carboxy-3-hydroperoxyhepta-1,4-dien-2-yl)-3-(carboxymethyl) pyrrolidine-2-carboxylic acid (HP1). The solutions were prepared in 10 μM Rose Bengal in D_2O , buffered at pH \sim 8 in an NMR tube, constantly purged with oxygen and irradiated with a 150 W Xenon lamp temperature while maintaining the temperature at \sim 5 $^\circ\text{C}$. The NMR spectra were recorded in the 400 Bruker NMR spectrometer.71

Figure 3.7. COSY NMR of singlet oxygenated Domoic acid. The proton correlations for the ene product, HP1 is shown. Protons in the azolidine ring are not shown for simplicity. HP1- H_e chemical shift is expected to be around 5 ppm, which coincides with the water peak. The solutions were prepared with 10 μM Rose Bengal in D_2O , buffered at pH \sim 8 in an NMR tube, constantly purged with oxygen and irradiated with a 150 W Xenon lamp temperature while maintaining the temperature at \sim 5 $^\circ\text{C}$. The NMR spectra were recorded in the 400 Bruker NMR spectrometer.74

Figure 3.8. LC-HR/MS spectra of singlet oxygenation of Domoic acid and Domoic acid after singlet oxygenation. The proposed fragmentation pattern for HP1 and HP2. LC-HR/MS of 32.1 μM DA Standard (Top) LC-HR/MS of 1:100 dilution of 25 min $^1\text{O}_2$ reaction with 3.21 mM DA, HP1 (middle), and HP2 (bottom). Left to right are squared the proposed fragmentation patterns for HP1 and HP2. The solutions were prepared in 10 μM Rose Bengal in D_2O , buffered at pH \sim 8 in an NMR tube, constantly purged with oxygen, and irradiated with a 150 W Xenon lamp while maintaining the temperature at \sim 5 $^\circ\text{C}$. The MS data were obtained employing a Surveyor HPLC for chromatographic separation, and HR/MS detection was performed by a 7 T Bruker Solarix FT-ICR mass spectrometer equipped with an ESI source.76

Figure 3.9. Red and black circles represent the rate of singlet oxygenation of 200 μM of Domoic acid and FFA. The solutions were prepared in 10 μM RB Millipore filtered water (18 M Ω) buffered by 20 mM KH_2PO_4 at pH=8. The photochemical reaction was carried out in a Pyrex test tube (12 x 75 mm) and constantly purged with oxygen. A 150 W Xenon lamp equipped with a water-filled Pyrex filter, was used for irradiation at a reaction temperature of \sim 5 $^\circ\text{C}$. The reactions were monitored using the Varian Pro star 210 HPLC.78

Figure 4.1. Elucidation of the product from 20 min Photooxidation of 0.5 M, 5-acetyl-2,4-dimethyl-1*H*-pyrrole-3-carboxylic acid (Ac-Py), 2-hydroxy-2,4-dimethyl-5-oxo-2,5-dihydro-1*H*-pyrrole-3-carboxylic acid (OHOxo-Py). The ^1H (Top) and ^{13}C (Bottom) NMR spectra were recorded in the 400 Bruker NMR spectrometer. The solution was prepared with 10 μM RB in D_2O , continuously purged with oxygen, and irradiated with at 150 W Xenon lamp while maintaining the temperature at \sim 5 $^\circ\text{C}$98

Figure 4.2. Structure of mechanistic probes for the $^1\text{O}_2$ reactions with pyrroles.99

Figure 4.3. Synthesis of methyl 5-acetyl-2,4-dimethyl-1H-pyrrole-3-carboxylate, Ac-Py-DM. The esterification of 50 mg Ac-Py was modified from the procedure initially described by Bagal et al., 2010 (36). 5-Acetyl-2,4-dimethyl-1H-pyrrole-3-carboxylic acid (50 mg, 70.4 mmol) was added to solution of MeI (18 μ L, 70.4 mmol) and K₂CO₃ (155 mg, 281 mmol) in DMF (2 mL) while stirring. The mixture was stirred for 24 hours at room temperature. The product was extracted with H₂O/Et₂O, the final extraction of the organic layer was done with a NaCl saturated brine solution, and then dried over CaCl₂. The solvent was evaporated in vacuo to give AC-Py-ES. ¹H NMR δ ppm (400 MHz, CDCl₃) 3.76 (3H, s, CO₂CH₃), 2.55 (3H, s, COCH₃), 2.43 (3H, s, CH₃), 2.41 (3H, s, CH₃).....101

Figure 4.4. Synthesis of methyl 5-acetyl-1,2,4-trimethyl-pyrrole-3-carboxylate, Ac-Py-TM. The esterification of 50 mg Ac-Py was modified from the procedure initially described by Bagal et al., 2010 (36). 5-Acetyl-2,4-dimethyl-1H-pyrrole-3-carboxylic acid (50 mg, 70.4 mmol) was added to solution of MeI (36 μ L, 140.8 mmol) and K₂CO₃ (155 mg, 281 mmol) in DMF (2 mL) while stirring. The mixture was stirred for 24 hours at room temperature. The product was extracted with H₂O/Et₂O, the final extraction of the organic layer was done with a NaCl saturated brine solution, and then dried over CaCl₂. The102

Figure 4.5. Photooxidation of 0.5 M Synthesis of methyl 5-acetyl-2,4-dimethyl-1H-pyrrole-3-carboxylate, Ac-Py-DM, in CD₂Cl₂. ¹H NMR Ac-Py-DM (bottom) and ¹H NMR product upon 25 min photooxidation, OHoxoEs-Py, methyl 2-hydroxy-2,4-dimethyl-5-oxo-2,5-dihydro-1H-pyrrole-3-carboxylate. The solutions were prepared with 10 μ M Rose Bengal in D₂O in an NMR tube, constantly purged with oxygen and irradiated with a 150 W Xenon lamp temperature while maintaining the temperature at ~ 5 °C. The spectra were recorded in the 400 Bruker NMR spectrometer.103

Figure 4.6 Photooxidation of 0.5 M methyl 5-acetyl-1,2,4-trimethyl-pyrrole-3-carboxylate, Ac-Py-TM, in CD₂Cl₂. ¹H NMR Ac-Py-TM (bottom) and ¹H NMR product mixture upon 90 seconds photooxidation. The solutions were prepared with 10 μ M Rose Bengal in D₂O in an NMR tube, constantly purged with oxygen and irradiated with a 150 W Xenon lamp temperature while maintaining the temperature at ~ 5 °C. The spectra were recorded in the 400 Bruker NMR spectrometer.104

Figure 4.7. ¹H NMR of the photooxidation of 0.5 M 1H-pyrrole-2,3,4-tricarboxylic acid (TCOOH-Py) in 1 ml⁻¹ D₂O. ¹H NMR TCOOH-Py before reaction (bottom) and ¹H NMR of the product of 10 min photooxidation of TCOOH-Py (top). The solutions were prepared with 10 μ M Rose Bengal in D₂O in an NMR tube, continuously purged with oxygen and irradiated with a 150 W Xenon lamp temperature while maintaining the temperature at ~ 5 °C. The spectra were recorded in the 400 Bruker NMR spectrometer.105

Figure 4.8. The relative reaction rate of singlet oxygenation of 0.5 M model Pyrrole and 0.5 M FFA. Detailed reaction conditions are provided in the experimental section. Red triangles represent COOH-Py, gray squares represent TCOOH-Py, black diamond represent F-Py, yellow circles represent Ac-Py, and blue circles represent H-Py.....106

LIST OF SCHEMES

Scheme	Page
Scheme 1.1. General mechanisms of the photosensitized reactions.....	3
Scheme 1.2. General pathways of the singlet oxygen reactions with conjugated dienes.	5
Scheme 1.3. Proposed mechanism for the ene $^1\text{O}_2$ reaction.	6
Scheme 1.4. Reaction $^1\text{O}_2$ with <i>trans</i> anthracenes producing the cis endoperoxide derivative. Scheme simplified from Zehm, D. et al., 2007.....	8
Scheme 2.1. Illustration of competing for $^1\text{O}_2$ reaction pathways with SCOOH. Possible products for each pathway $^1\text{O}_2$ reaction with SCOOH are SCOOH-EP, SCOOH-HP, [2+2] ₁ acetaldehyde and (<i>E</i>)fumaric acid, [2+2] ₂ (<i>E</i>) croton aldehyde and formic acid.	26
Scheme 2.2. Illustration of products from the [4+2] concerted and non-pathways of the reaction of $^1\text{O}_2$ with SCOOH producing <i>cis</i> and <i>trans</i> SCOOH-EP.....	29
Scheme 2.3. Decarboxylation of SCOOH-EP to (<i>Z</i>)-4-hydroxypent-2-enal and enol tautomer-driven isomerization to the thermodynamically favored (<i>E</i>)-4-hydroxypent-2-enal.....	32
Scheme 2.4. Illustration of competing for $^1\text{O}_2$ reaction pathways with SOH. Possible products for each pathway of $^1\text{O}_2$ reaction with SOH are SOH-EP [4+2] (6-methyl-3,6-dihydro-1,2-dioxin-3-yl)methanol, SOH-HP 1(ene1) (<i>E</i>)-4-hydroperoxyhexa-2,5-dien-1-ol, HPSOH 2(ene2) (1 <i>Z</i> or <i>E</i> , 4 <i>E</i>)-3-hydroperoxyhexa-1,4-diene, [2+2] ₁ acetaldehyde and (<i>E</i>)-4-hydroxybut-2-enal, [2+2] ₂ (<i>E</i>)-but-2-enal, crotonaldehyde and 2-hydroxyacetaldehyde.	34
Scheme 2.5. Isomerization and <i>s-cis</i> conformations of hexadienes.....	42
Scheme 3.1. The [2+2] cycloaddition reaction of $^1\text{O}_2$ with the <i>Z</i> double of the diene functionality of Domoic acid. PAC and MOP, (<i>R</i> , <i>E</i>)-2-methyl-5-oxopent-3-enoic acid are the products of the reaction.	65
Scheme 3.2. The ene reaction of $^1\text{O}_2$ pathway at the <i>E</i> and <i>Z</i> double of the diene functionality of Domoic acid. HP1 ((2 <i>S</i> ,3 <i>S</i> ,4 <i>S</i>)-4-((6 <i>R</i> , <i>E</i>)-6-carboxy-3-hydroperoxyhepta-1,4-dien-2-yl)-3-(carboxymethyl) pyrrolidine-2-carboxylic acid) and HP2 ((2 <i>S</i> ,3 <i>S</i> , <i>Z</i>)-4-((6 <i>R</i> , <i>E</i>)-6-carboxy-3-hydroperoxyhept-4-en-2-ylidene)-3-(carboxymethyl)pyrrolidine-2-carboxylic acid) are the products of the reaction at the <i>Z</i> double bond. HP3, ((2 <i>S</i> ,3 <i>S</i> ,4 <i>S</i>)-4-((2 <i>Z</i> ,5 <i>E</i>)-6-carboxy-4-hydroperoxyhepta-2,5-dien-2-yl)-3 (carboxymethyl)pyrrolidine-2-carboxylic acid) was not observed.	73
Scheme 3.3. Major photosensitized transformations of Domoic acid	79

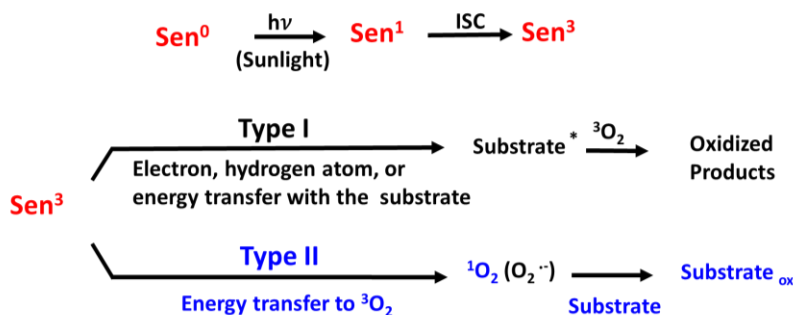
Scheme 4.1. Proposed mechanism for the 5-acetyl-2,4-dimethyl-1H-pyrrole-3-carboxylic acid, Ac-Py, endoperoxide rearrangement into 2-hydroxy-2,4-dimethyl-5-oxo-2,5-dihydro-1H-pyrrole-3-carboxylic acid, OHoxo-Py.....99

CHAPTER 1 INTRODUCTION TO THE REACTIONS OF SINGLET OXYGEN

Introduction to Singlet Oxygen

Singlet oxygen ($^1\text{O}_2$) can be produced via photosensitized reactions, as illustrated in Scheme 1.1. Photosensitization is initiated when a photon excites a sensitizer from the ground state to a singlet excited state, which may intersystem cross to a triplet state (I). The triplet state can transfer its excess energy to ground state molecular oxygen ($^3\text{O}_2$), also a triplet by a spin allowed process to generate $^1\text{O}_2$ (I). Singlet oxygen possesses a degenerate and vacant orbital at the highest occupied molecular orbitals (HOMO) energy level. Singlet oxygen is, therefore, electrophilic and capable of accepting electrons (I). Electron-rich substrates, such as dienes, alkenes, sulfides, and phenols, can be oxidized by $^1\text{O}_2$ (2). The excitation energy of $^1\text{O}_2$ is relatively low, only 22 kcal mol $^{-1}$ above the ground state (I). Thus $^1\text{O}_2$ can be generated by the absorption of relatively low energy photons in the visible region of the electromagnetic radiation spectrum (I).

Photooxidation can lead to various products, and the reactions have been defined as Type I and Type II. For the type I reactions, the excited triplet sensitizer reacts directly with the substrate in one-electron, energy, or hydrogen atom transfer processes to produce radicals and excited species, producing oxidized products (3). The direct reactions of $^1\text{O}_2$ with substrates are referred to as type II photosensitized processes (3). The main factors dictating the partitioning between the type I and II reaction pathways are the wavelength of the photon absorbed, the substrate concentration, and the structure and reactivity of the substrate and the sensitizer (I).



Scheme 1.1. General mechanisms of the photosensitized reactions (1).

Most singlet oxygen photosensitizers are highly conjugated compounds capable of absorbing visible light and transferring energy to molecule oxygen (4). Quantum yield, the ratio of molecules of singlet oxygen produced per photons of light absorbed, describes the sensitizer efficiency of producing singlet oxygen (4). The quantum yield is proportional to the probability of the singlet state sensitizer to the intersystem cross into the triplet excited state (5). The presence of heavy atoms, such as iodine and bromine, in the sensitizer often increases quantum yield, namely the heavy atom effect (5).

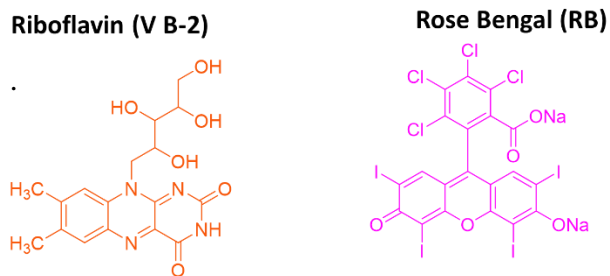


Figure 1.1. Structures of Common ${}^1\text{O}_2$ photosensitizers.

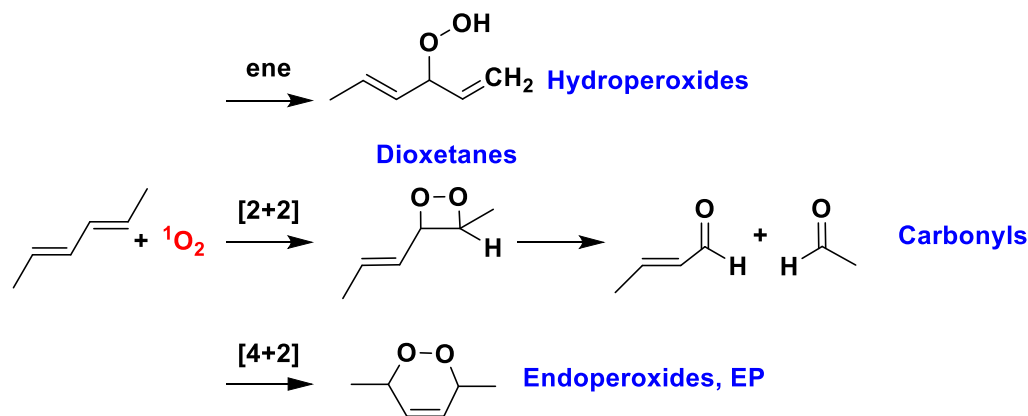
Dissolved organic matter (DOM) consists of a complex variety of soluble organic materials in aquatic systems. (2). Chromophoric DOM (cDOM) has a large content of phenolic and aromatic functionalities (2). cDOM can absorb solar radiation and participate in photochemical reactions (2). Riboflavin (VB-2) shown in Figure 1.1, a component of

DOM, is present in the sea in concentrations up to ~ 780 ppm (6). Riboflavin, VB-2, has been proposed as a natural sensitizer for the photooxidative degradation of contaminants in water, particularly pesticides and herbicides (6). The VB-2 quantum yield for singlet oxygen is 0.47, with maximum absorption at 440 nm (6). Rose Bengal (RB) with maximum absorption at 545 nm, Figure 1.1, is a synthetic organic compound commonly used as a vegetable dye, ophthalmological agent, and photobactericide (5). The RB quantum yields for singlet oxygen are 0.75, 0.76, and 0.68 and in water, deuterated water, and methanol, respectively (5). Rose Bengal is an excellent $^1\text{O}_2$ sensitizer and chosen for the experiments described herein.

In biological and environmental systems, $^1\text{O}_2$ is exceptionally important, requiring only sensitizer, solar radiation, and molecular oxygen. Singlet oxygen is ubiquitous in the photic zone of aquatic bodies and involved in the natural photochemical transformation and fate of organic pollutants and toxins (2, 6). Singlet oxygen is also proposed as an oxidant for some solar-based water purification techniques and disinfection (7). Photodynamic therapy (PDT) uses cytotoxic $^1\text{O}_2$ to treat cancer lesions with excellent specificity (4, 8). PDT can also be used for the treatment of blood (4). While these systems and applications involve aqueous media, and there is a rich literature on the products and mechanisms of the $^1\text{O}_2$ reactions in organic solvents (9–12), there are minimal product and mechanistic studies of singlet oxygen in aqueous media (13, 14).

1.1. General pathways and mechanism of the singlet oxygen reactions with conjugated dienes

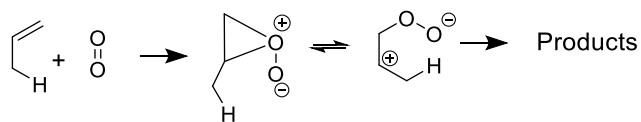
Singlet oxygen can react with conjugated π systems via [4+2] cycloaddition, ene reactions, and [2+2] cycloaddition reactions, Scheme 1.2 (15). In general, the [4+2] cycloaddition of $^1\text{O}_2$ yields modestly stable endoperoxide (EP) (15). The ene reaction involves the abstraction of an allylic proton by $^1\text{O}_2$ to form the corresponding hydroperoxide (HP) (15), while the [2+2] reaction produces dioxetanes, which are unstable and typically collapse into their corresponding carbonyl compound (15).



Scheme 1.2. General pathways of the singlet oxygen reactions with conjugated dienes.

The reaction mechanisms of $^1\text{O}_2$ have been a topic of serious debate for decades, with evidence for both concerted and non-concerted reaction mechanisms. Some of the recent advances in the $^1\text{O}_2$ reaction mechanisms are discussed in the following sections. Noteworthy, the literature on the mechanism of $^1\text{O}_2$ in organic solvents is extensive; thus, the following discussion is abbreviated.

Strong experimental evidence for the intermediacy of a perepoxyde in equilibrium with an open zwitterionic intermediate, Scheme 1.3, for ene pathway, has been reported in the last decades (16).



Scheme 1.3. Proposed mechanism for the ene $^1\text{O}_2$ reaction.

Intramolecular kinetic isotope effects (KIEs) for the cis-6-d6 ($k_{\text{H}}/k_{\text{D}}=1.04\text{--}1.09$), trans-6-d6 ($k_{\text{H}}/k_{\text{D}}=1.45$), and gem-6-d6 ($k_{\text{H}}/k_{\text{D}}=1.38\text{--}1.41$) deuterated tetramethylethylenes (TMEs) were reported (16). The isotope effect was significant only when the H and D had cis orientation, such as trans-6-d6 and gem-6-d6 compounds (17). The observed KIEs suggest that hydrogen abstraction is not the rate-determining step for the reactions since the values indicate secondary KIE. The perepoxyde intermediate prefers to abstract H rather than D based on relative bond strength (C-D stronger than C-H), providing evidence for an intermediate in the $^1\text{O}_2$ ene reaction with the structural features of the perepoxyde (17).

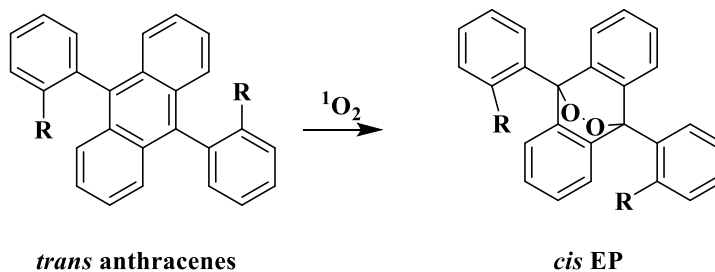
Solvent effect studies of the singlet oxygenation of α,β -unsaturated esters showed that the hydroperoxide (HP) geminal production to the ester group was gradually favored as the dielectric constant of the solvent was increased (18). The transition state (TS) of the perepoxyde producing the geminal HP is much more polar than the TS producing the vicinal HP, supporting a polar intermediate's stabilization for ene the reactions (18). The $^1\text{O}_2$

reaction with the sterically strained trans-cyclooctene in the presence of the reducing agent, triphenyl phosphite, chemically trapped the perepoxide as the trans-epoxide (19).

The hydroxyl directing effect refers to the stabilization of $^1\text{O}_2$ perepoxide structure by hydrogen bonding to a hydroxyl group. The [2+2] cycloaddition of $^1\text{O}_2$ to adamantylidene-substituted allylic alcohol produced a 95:5 threo-dioxetane to erythro-dioxetane ratio (11). The perepoxide transition state to form the threo-dioxetane may easily hydrogen bond to the hydroxyl group, while the transition state of erythro-product is sterically hindered (11). In methanol- d_4 , the threo to erythro selectivity significantly drops to 89:11, since the methanol- d_4 can, also, hydrogen bond (11).

The singlet oxygenation of *E,E*, *E,Z*, and *Z,Z* hexadienes produced both *cis* and *trans* EPs indicating non-concerted mechanisms based on Woodward Hoffman rules [4+2] cycloaddition mechanisms (20). Several solvent trapped intermediates were also observed. Thus an open zwitterionic intermediate was proposed as the intermediate of the reactions (21). The $^1\text{O}_2$ reaction with *trans* 9,10-bisarylanthracenes showed a full rotation of a phenyl group producing the *cis* EP derivative, Figure 1.2 (22). A zwitterionic intermediate for these reactions is more feasible than a biradical since the activation energies of such biradicals are larger than the bisarylanthracenes rotation barriers. (22). The bimolecular rate constants increased by a factor of ten when bisarylanthracenes were substituted with electron-donating groups instead of electron-withdrawing substituents (23). Electron-donating groups stabilize the positive charged at the carbon of the zwitterionic intermediates, while electron-donating groups and electron-withdrawing stabilize radicals in the same way. The kinetics of the reaction would be unchanged based on the substitution

for a reaction with radical intermediate. On the other hand, a reaction with zwitterionic intermediate would show faster reaction rates when substituted with electron-donating groups (23).



Scheme 1.4. Reaction $^1\text{O}_2$ with trans anthracenes producing the cis endoperoxide derivative. Scheme simplified from Zehm, D. et al., 2007.

1.2. Compounds of interests

1.2.1. Hexadienes: Sorbic Acid and Sorbic Alcohol

Sorbic acid (SCOOH) and sorbic alcohol (SOH), Figure 1.2, are attractive probes for the singlet oxygen reaction in aqueous media. Sorbic acid is used food preservative, while SOH serves as a flavoring and aromatizing agent (28). Hence, SCOOH and SOH are considered safe for human consumption. The $^1\text{O}_2$ reactions of these compounds may be implicated in food spoilage and may produce toxic derivatives. Triplet CDOM ($^3\text{CDOM}^*$) is a key player in environmental photochemistry; thus, $^3\text{CDOM}^*$ is vital for the photochemical transformation and fate of pollutants and toxins (29–32). Isomerization of the diene system of SCOOH, SOH, and sorbic amine (SNH₃) (2,4-hexadien-1-amine) is employed to quantify $^3\text{CDOM}^*$ with energies at wavelengths above 250 nm (29–32).

Although $^1\text{O}_2$ has not been reported to produce isomerization of these dienes and can quench the probes adding error to the estimation of $^3\text{CDOM}^*$.

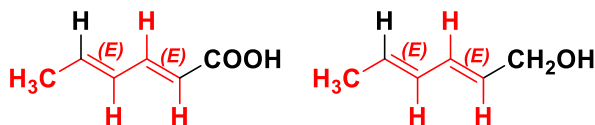


Figure 1.2. Structures of Sorbic acid and Sorbic alcohol.

1.2.2. Domoic Acid

Harmful algal blooms refer to the proliferation of toxin-producing aquatic microorganisms caused by the increase of nutrient above-normal conditions (33). Among the harmful effects is the production of secondary metabolites that can be toxic to other organisms (33). Domoic Acid (DA) is an example of these toxic secondary metabolites (34). It is produced by the bloom of the marine photosynthetic diatom, *Pseudonitzschia* (34). Shellfish, clams, and mussels bioaccumulated the potent toxin, which can be biomagnified at each level of the food chain (34). The first reported incident of human intoxication due to DA was in Canada in 1987 when three elderly patients died, and other victims suffered long-term neurological problems. Because the victims suffered from memory loss, the term "amnesic" shellfish poisoning is commonly used for the DA intoxication. The primary route of exposure is ingestion of contaminated seafood and water (35). Contaminated water and food with DA have terrible consequences on human health, wildlife, and the environment (34). It is estimated that DA contamination causes the crab fishery industry \$110 thousand to \$10.57 million income loss per closure, depending upon the closures (36). Also, DA contamination causes the death and illness of seals, sea lions, whales, and other mammals. The EPA regulates DA with a maximum allowed

concentration in seafood of $20 \mu\text{g g}^{-1}$ (37). Domoic acid contamination is very problematic on the US west coast, having severe adverse health impacts on humans and wildlife (37).

The biological activity of DA originates from the homologous structural features of glutamic acid shown in Figure 1.3. Domoic acid binds the glutamate receptors, abundantly expressed in the brain and the heart, causing an over-excitation that leads to cellular loss of function, damage, and death (34). The conjugated diene functionally has been reported to play an essential role in the toxicity of the molecule since the different geometrical isomers display different levels of toxicity. The *Z, E* diene containing DA, is the most toxic (38). Isodomoic acid, which diene is not conjugated, has 240 –fold less affinity to the glutamate receptors (38).

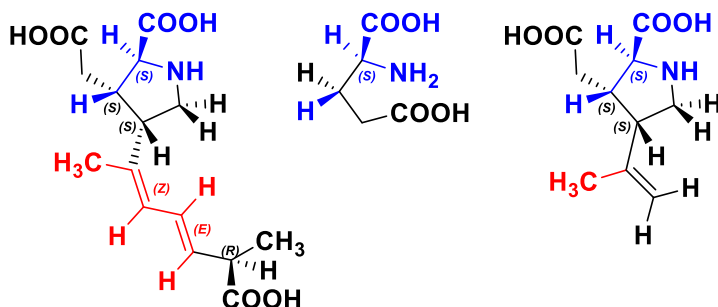


Figure 1.3. Structures of Domoic acid (left), L-glutamic acid (center), and Kainic acid (right). Homologous structural features are in blue, and the diene functionalities are in red.

Domoic acid contains a variety of functional groups, carboxylic acid, cyclic amine, and a diene. The diene moiety is particularly susceptible to the $^1\text{O}_2$ reaction and may undergo one or more of the main pathways shown in section. The reactions of $^1\text{O}_2$ with DA may represent an essential pathway for the photochemical transformation of DA in the environment and an alternative detoxification strategy for DA contaminated water and

food. Singlet oxygen can be generated under algal bloom conditions light, oxygen, and natural pigments are abundant. Singlet oxygen may react with the diene functionality in DA to weakening its harmful biological effects. Kainic Acid (KA) (Figure 1.3) is a natural marine toxin present in some seaweed (39). Kainic Acid is also an agonist of glutamic acid, but it is much less toxic than DA (39).

1.2.3. Pyrroles

Melanin, a vital natural pigment, plays a protective role against Ultra Violet (UV) radiation and reactive oxygen species damage, including $^1\text{O}_2$. While melanin provides photoprotection, it also can be damaged by photooxidation. 1 (40, 41). The heterogeneous melanin polymer is composed of indole and pyrrole subunits (40, 42, 43). In the presence of light, melanin in hair produced $^1\text{O}_2$ through self-sensitization (44). Melanin can efficiently quench of $^1\text{O}_2$ (45, 46). 1H-pyrrole-2,3,4-tricarboxylic acid (TCOOH-Py), commonly used as a marker to assess melanin photoaging. Using_TCOOH-Py concentrations as a measure of melanin damage under photodynamic conditions may underestimate skin damage due to sun exposure.

The reactions of $^1\text{O}_2$ with water-soluble pyrroles (Py) were studied as model compounds to understand the photooxidative damage to the primary melanin structure. Besides, pyrrole functionalities are essential in several biological systems such as bilirubin and the freshwater contaminants atorvastatin, fluvastatin, and fludioxonil (Figure 1.4). The bimolecular rate constant of the reaction of $^1\text{O}_2$ with bilirubin is one of the fastest reported, $k_r=4\times 10^8 \text{ M}^{-1}\text{sec}^{-1}$, accounting for the rapid disappearance of bilirubin during phototherapy of neonatal jaundice (47). Mechanistic and kinetic studies of the singlet oxygenation of

pyrroles are well documented in organic solvents. Reports of the reaction of $^1\text{O}_2$ with pyrroles in aqueous media are scarce (13, 14).

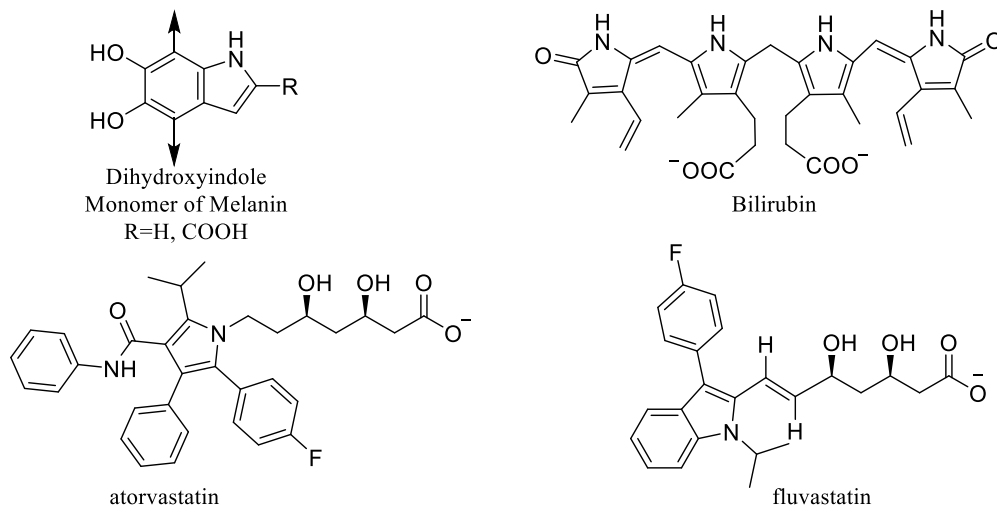


Figure 1.4. Examples of structures of biological molecules containing pyrrole functionality.

1.3. The Relative Rate Technique:

The relative rate method, summarized below, was used to determine the second-order rate constant for the reaction of $^1\text{O}_2$ with the compounds studied (24). The rate of the reaction of furfuryl alcohol (FFA) with $^1\text{O}_2$ is well-established and has been extensively used in competition kinetics with a variety of organic compounds (25–27). The rate equations for the reactions of an organic molecule (OM) and FFA with $^1\text{O}_2$ are expressed in Equations 1 and 2,

$$\frac{d\text{Ln}(OM)}{dt} = -k_{(^1\text{O}_2+OM)}[{}^1\text{O}_2] \quad (1)$$

$$\frac{d\text{Ln}(FFA)}{dt} = -k_{(^1\text{O}_2+FFA)}[{}^1\text{O}_2] \quad (2)$$

The rate equations for the reactions of an organic molecule (OM) and FFA with $^1\text{O}_2$ are expressed in Equations 1 and 2,

The kinetic Equation 3, based on the reactions' ratio, can be derived from Equations 1 and 2.

$$\text{Ln} \frac{[\text{OM}]_t}{[\text{OM}]_0} = \frac{k(^1\text{O}_2+\text{OM})}{k(^1\text{O}_2+\text{FFA})} \text{Ln} \frac{[\text{FFA}]_t}{[\text{FFA}]_0} \quad (3)$$

Multiplying the slope of the natural log of the $^1\text{O}_2$ degradation rate of FFA versus that of the OM by the FFA second-order rate constant, $k(^1\text{O}_2+\text{FFA})=0.94\pm 0.01 \times 10^8 \text{ M}^{-1} \text{ s}^{-1}$ yields $k(^1\text{O}_2+\text{OM})$ (25–27). Assuming a $^1\text{O}_2$ steady-state concentration $[^1\text{O}_2]_{\text{ss}}$ in Equation 1, the half-life expression of the OM upon reaction with $^1\text{O}_2$ ($t_{1/2} (^1\text{O}_2+\text{OM})$) equation 9 can be derived (Equation 4-8).

$$\frac{d\text{Ln} ([\text{OM}]_0)}{dt} = -k(^1\text{O}_2+\text{OM}) [^1\text{O}_2]_{\text{ss}} \quad (1)$$

$$\int \frac{d\text{Ln} ([\text{OM}]_0)}{dt} = \int_{t=0}^{t=t} -k(^1\text{O}_2+\text{OM}) [^1\text{O}_2]_{\text{ss}} \quad (4)$$

At half-life, $t_{1/2}$,

$$\text{Ln} ([\text{OM}]_0) = -k(^1\text{O}_2+\text{OM}) t_{1/2} [^1\text{O}_2]_{\text{ss}} \quad (5)$$

$$\frac{\text{Ln} ([\text{OM}]_0)}{2} = -k(^1\text{O}_2+\text{OM}) [^1\text{O}_2]_{\text{ss}} t_{1/2} + \text{Ln} ([\text{OM}]_0) \quad (6)$$

$$\text{Ln} ([\text{OM}]_0) - \text{Ln} (2) = -k(^1\text{O}_2+\text{OM}) [^1\text{O}_2]_{\text{ss}} t_{1/2} + \text{Ln} ([\text{OM}]_0) \quad (7)$$

$$t_{1/2} = \frac{\text{Ln} (2)}{k(^1\text{O}_2+\text{OM}) [^1\text{O}_2]_{\text{ss}}} \quad (8)$$

1.4. Concluding Remarks

In the following chapters, the reactions of $^1\text{O}_2$ with the compounds of interest will be presented. The reactions products were characterized. In the case of DA, the biological activity of the products as compared to DA. The competition kinetics allowed to elucidate the bimolecular rate constants for the reactions.

1.5. References

- (1) Foote, C. S. Mechanisms of Photosensitized Oxidation. *Science*. **1968**, *162* (3857), 963–970.
- (2) Kieber, D. J.; Peake, B. M.; Scully, N. M. Chapter 8 Reactive oxygen species in aquatic ecosystems. *UV Effects in Aquatic Organisms and Ecosystems*; Helbling, E. W., Zagarese, H., Eds.; Comprehensive Series in Photochemical & Photobiological Sciences; Royal Society of Chemistry: Cambridge, 2007; Vol. 1, pp 251-276., and references within.
- (3) Foote, C. S. Definition of Type I and Type II. *Photochem. Photobiol.* **1991**, *54* (5), 659.
- (4) DeRosa, M. Photosensitized Singlet Oxygen and Its Applications. *Coord. Chem. Rev.* **2002**, *233–234*, 351–371.
- (5) Murasecco-Suardi, P.; Gassmann, E.; Braun, A.; Oliveros, E. Determination of Quantum Yield of Intersystem Crossing of Rose Bengal. *Helv. Chim. Acta* **1987**, *70*, 1760.
- (6) García, N. A.; Pajares, A. M.; Bregliani, M. M. Singlet Oxygen Mediated Photodegradation of Water Contaminants. In *Singlet Oxygen: Applications in Biosciences and Nanosciences*; The Royal Society of Chemistry, **2016**; 447–457.
- (7) Kim, H.; Kim, W.; MacKeyev, Y.; Lee, G. S.; Kim, H. J. K.; Tachikawa, T.; Hong, S.; Lee, S.; Kim, J.; Wilson, L. J.; Majima, T.; Alvarez, P. J. J.; Choi, W.; Lee, J. Selective Oxidative Degradation of Organic Pollutants by Singlet Oxygen-Mediated Photosensitization: Tin Porphyrin versus C60 Aminofullerene Systems. *Environ. Sci. Technol.* **2012**, *46* (17), 9606–9613.
- (8) Tian, J.; Huang, B.; Nawaz, M. H.; Zhang, W. Recent Advances of Multi-Dimensional Porphyrin-Based Functional Materials in Photodynamic Therapy. *Coord. Chem. Rev.* **2020**, *420*, 213410.

- (9) Adam, W.; Michael, P. π -Facial Diastereoselectivity in the [4+2] Cycloaddition of Singlet Oxygen as a Mechanistic Probe. *Acc. Chem. Res.* **1996**, *29* (6), 275–283.
- (10) Tzirakis, M. D.; Alberti, M. N. On the Mechanism of the [4+2] Cycloaddition of 1O_2 with 1,3-Dienes: Identifying the Putative Biradical / Dipolar Intermediate by Employing the Gem-Diphenylcyclopropylcarbinyl Radical Clock as a Mechanistic Probe. *Arch. Org. Chem.* **2015**, *iii*, 83–100.
- (11) Adam, W.; Saha-Möller, C. R.; Schambony, S. B. A Highly Diastereoselective Dioxetane Formation by the Hydroxy-Directed [2+2] Cycloaddition of Singlet Oxygen to a Chiral Allylic Alcohol. *J. Am. Chem. Soc.* **1999**, *121* (9), 1834–1838.
- (12) Stratakis, M.; Orfanopoulos, M. Regioselectivity in the Ene Reaction of Singlet Oxygen with Alkenes. *Tetrahedron* **2000**, *56*, 1595–1615.
- (13) Lightner, D. A.; Bisacchi, G. S.; Norris, R. D. On the Mechanism of the Sensitized Photooxygenation of Pyrroles. *J. Am. Chem. Soc.* **1976**, *98* (3), 802–807.
- (14) Apell, J. N.; Pflug, N. C.; McNeill, K. Photodegradation of Fludioxonil and Other Pyrroles: The Importance of Indirect Photodegradation for Understanding Environmental Fate and Photoproduct Formation. *Environ. Sci. Technol.* **2019**, *53* (19), 11240–11250.
- (15) Clennan, E. L. Synthetic and Mechanistic Aspects of 1,3-Diene Photooxidation. *Tetrahedron* **1991**, *47* (8), 1343–1382.
- (16) Grdina, B.; Orfanopoulos, M.; Stephenson, L. M. Stereochemical Dependence of Isotope Effects in the Singlet Oxygen-Olefin Reaction. *Am. Chem. Soc.* **1979**, *39* (22), 3–5.
- (17) Fudickar, W.; Linker, T. Intermediates in the Formation and Thermolysis of Peroxides from Oxidations with Singlet Oxygen. *Aust. J. Chem.* **2014**, *67* (3), 320.
- (18) Orfanopoulos, M. Solvent Effects on the Side Selectivity of Singlet Oxygen with Alpha, Beta Unsaturated Esters. New Evidence for a Peroxide Intermediate. *Tetrahedron Lett.* **1991**, *32* (49), 7321–7324.
- (19) Poon, T. H. W.; Pringle, K.; Foote, C. S. Reaction of Cyclooctenes with Singlet Oxygen. Trapping of a Peroxide Intermediate. *J. Am. Chem. Soc.* **1995**, *117* (29), 7611–7618.
- (20) Hoffmann, R.; Woodward, R. B. Selection Rules for Concerted Cycloaddition Reactions. *J. Am. Chem. Soc.* **1965**, *87* (9), 2046–2048.
- (21) O'Shea, K. E.; Foote, C. S. Chemistry of Singlet Oxygen. 51. Zwitterionic Intermediates from 2,4-Hexadienes. *J. Am. Chem. Soc.* **1988**, *110* (21), 7167–7170.

- (22) Zehm, D.; Fudickar, W.; Linker, T. Molecular Switches Flipped by Oxygen. *Angew. Chemie - Int. Ed.* **2007**, *46* (40), 7689–7692.
- (23) Fudickar, W.; Linker, T. Remote Substituent Effects on the Photooxygenation of 9,10-Diarylanthracenes: Strong Evidence for Polar Intermediates. *Chem. Commun.* **2008**, No. 15, 1771.
- (24) Atkinson, R.; Aschmann, S. M.; Pitts, J. N. Rate Constants for the Gas-Phase Reactions of the OH Radical with a Series of Monoterpenes at 294 ± 1 K. *Int. J. Chem. Kinet.* **1986**, *18* (3), 287–299.
- (25) Jaramillo, M.; Joens, J. A.; O’Shea, K. E. Fundamental Studies of the Singlet Oxygen Reactions with the Potent Marine Toxin Domoic Acid. *Environ. Sci. Technol.* **2020**, acs.est.9b07380.
- (26) Haag, W. R.; Hoigne, J. Singlet Oxygen in Surface Waters. 3. Photochemical Formation and Steady-State Concentrations in Various Types of Waters. *Environ. Sci. Technol.* **1986**, *20* (4), 341–348.
- (27) Appiani, E.; Ossola, R.; Latch, D. E.; Erickson, P. R.; McNeill, K. Aqueous Singlet Oxygen Reaction Kinetics of Furfuryl Alcohol: Effect of Temperature, PH, and Salt Content. *Environ. Sci. Process. Impacts* **2017**, *19* (4), 507–516.
- (28) Fujiyoshi, T.; Ikami, T.; Kikukawa, K.; Kobayashi, M.; Takai, R.; Kozaki, D.; Yamamoto, A. Direct Quantitation of the Preservatives Benzoic and Sorbic Acid in Processed Foods Using Derivative Spectrophotometry Combined with Micro Dialysis. *Food Chem.* **2018**, *240* (January 2017), 386–390.
- (29) McNeill, K.; Canonica, S. Triplet State Dissolved Organic Matter in Aquatic Photochemistry: Reaction Mechanisms, Substrate Scope, and Photophysical Properties. *Environ. Sci. Process. Impacts* **2016**, *18* (11), 1381–1399.
- (30) Parker, K. M.; Mitch, W. A. Halogen Radicals Contribute to Photooxidation in Coastal and Estuarine Waters. *Proc. Natl. Acad. Sci. U. S. A.* **2016**, *113* (21), 5868–5873.
- (31) Grebel, J. E.; Pignatello, J. J.; Mitch, W. A. Sorbic Acid as a Quantitative Probe for the Formation, Scavenging and Steady-State Concentrations of the Triplet-Excited State of Organic Compounds. *Water Res.* **2011**, *45* (19), 6535–6544.
- (32) Zhou, H.; Yan, S.; Ma, J.; Lian, L.; Song, W. Development of Novel Chemical Probes for Examining Triplet Natural Organic Matter under Solar Illumination. *Environ. Sci. Technol.* **2017**, *51* (19), 11066–11074.
- (33) Bricker, S. B.; Longstaff, B.; Dennison, W.; Jones, A.; Boicourt, K.; Wicks, C.; Woerner, J. Effects of Nutrient Enrichment in the Nation’s Estuaries: A Decade of Change. *Harmful Algae* **2008**, *8* (1), 21–32.

- (34) Saeed, A. F.; Awan, S. A.; Ling, S.; Wang, R.; Wang, S. Domoic Acid: Attributes, Exposure Risks, Innovative Detection Techniques and Therapeutics. *Algal Res.* **2017**, *24*, 97–110.
- (35) Perl, T.; Bedard, L.; Kosatsky, T.; Hockin, J.; Todd, E.; Remis, R. An Outbreak of Toxic Encephalopathy Caused by Eating Mussels Contaminated with Domoic Acid. *New Engl. J. Med.* **1990**, *322* (25), 1775–1779.
- (36) Huppert, D. D.; Trainer, V. L. Economics of Razor Clam Fishery Closures Due to Harmful Algal Blooms in Washington State. *PICES Sci. Rep.* **2014**, No. 47, 59–71.
- (37) Appendix 5: FDA and EPA Safety Levels in Regulations and Guidance. *Fish and Fishery Products Hazards and Controls Guidance*; SGR 129, United States Department of Health and Human Services; Food and Drug Administration; Center for Food Safety and Applied Nutrition; Office of Food Safety. <https://www.fda.gov/media/80637/download>. **2019**, A5-8.
- (38) Holland, P. T.; Selwood, A. I.; Mountfort, D. O.; Wilkins, A. L.; McNabb, P.; Rhodes, L. L.; Doucette, G. J.; Mikulski, C. M.; King, K. L. Isodomoic Acid C, an Unusual Amnesic Shellfish Poisoning Toxin from Pseudo-Nitzschia Australis. *Chem. Res. Toxicol.* **2005**, *18* (5), 814–816.
- (39) Hampson, D. R.; Manalo, J. L. The Activation of Glutamate Receptors by Kainic Acid and Domoic Acid. *Nat. Toxins* **1998**, *6* (3–4), 153–158.
- (40) Foote, C. S.; Ching, T. Y. Chemistry of Singlet Oxygen. XXI. Kinetics of Bilirubin Photooxygenation. *J. Am. Chem. Soc.* **1975**, *97* (21), 6209–6214.
- (41) Glass, K.; Ito, S.; Wilby, P. R.; Sota, T.; Nakamura, A.; Bowers, C. R.; Vinther, J.; Dutta, S.; Summons, R.; Briggs, D. E. G.; Wakamatsu, K.; Simon, J. D. Direct Chemical Evidence for Eumelanin Pigment from the Jurassic Period. *Proc. Natl. Acad. Sci. U. S. A.* **2012**, *109* (26), 10218–10223.
- (42) Xiao, M.; Chen, W.; Li, W.; Zhao, J.; Hong, Y. lee; Nishiyama, Y.; Miyoshi, T.; Shawkey, M. D.; Dhinojwala, A. Elucidation of the Hierarchical Structure of Natural Eumelanins. *J. R. Soc. Interface* **2018**, *15* (140).
- (43) Ward, W. C.; Lamb, E. C.; Gooden, D.; Chen, X.; Burinsky, D. J.; Simon, J. D. Quantification of Naturally Occurring Pyrrole Acids in Melanosomes. *Photochem. Photobiol.* **2008**, *84* (3), 700–705.
- (44) Chiarelli-Neto, O.; Pavani, C.; S. Ferreira, A.; Uchoa, A. F.; Severino, D.; Baptista, M. S. Generation and Suppression of Singlet Oxygen in Hair by Photosensitization of Melanin. *Free Radic. Biol. Med.* **2011**, *51* (6), 1195–1202.
- (45) Rodgers, M. A. J.; Snowden, P. T. Lifetime of $^1\text{O}_2$ in Liquid Water As Determined by Time-Resolved Infrared Luminescence Measurements. **1982**, (6), 5541–5543.

- (46) Lindig, B. A.; Rodgers, M. A. J.; Schaaplc, A. P. Determination of the Lifetime of Singlet Oxygen in D2O Using 9,10-Anthracenedipropionic Acid, a Water-Soluble Probe. *J. Am. Chem. Soc.* **1980**, *102* (17), 5590–5593.
- (47) Foote, C. S.; Ching, T. Y. Chemistry of Singlet Oxygen. XXI. Kinetics of Bilirubin Photooxygenation. *J. Am. Chem. Soc.* **1975**, *97* (21), 6209–6214.

**CHAPTER 2 SINGLET OXYGEN REACTIONS WITH WATER SOLUBLE
HEXADIENES**

2.1. Abstract

A mixture of water-soluble isomeric 1, 3-hexadienes, sorbic acid (SCOOH), sorbic alcohol (SOH), muconic acid, and muconic alcohol was employed as a mechanistic probe for the $^1\text{O}_2$ reactions in aqueous media. Concerted and non-concerted reaction pathways of isomeric hexadienes produce distinctly different products. The reactions of $^1\text{O}_2$ with the 1,3-diene conjugated systems react with singlet oxygen via the [4+2] pathway to produce the corresponding endoperoxides. The endoperoxide (EP) derivative of SCOOH was stable at initially degraded over time to yielded (Z)-4-hydroxypent-2-enal. The ^1H NMR spectra of SCOOH-EP yielded two sets of peaks, indicating a mixture of *cis* and *trans* isomers or conformers. However, the SOH-EP from SOH yielded only a single set of ^1H NMR peaks consistent with a single EP product. The reactions of SCOOH and SOH with singlet oxygen in D_2O also produced several products from the [2+2] pathways. The [2+2] products, however, were not observed in methanol- d_4 or chloroform- d_3 . The solvent effect on product distribution suggests that water molecules may promote the [2+2] cycloaddition by stabilizing charged or polar intermediates. In contrast, the lack of solvent effects on the [4+2] pathway suggests a concerted process or one with minimal polar character. Singlet oxygenation of sorbic acid or alcohol during photochemical experiments can introduce an error in $^3\text{DOM}^*$ measurements. The isomerization sorbic acid and sorbic alcohol are used as triplet dissolved organic matter ($^3\text{DOM}^*$) quenchers for quantification.

2.2. Introduction

Sorbic acid (SCOOH), 2*E*,4*E*-hexadienoic acid (Figure 2.1), has fungicidal and bactericidal properties (1, 2). Sorbic acid is widely used as a food preservative, cosmetics, pharmaceuticals, animal feeds, and industrial processes (2, 3). The safety of SCOOH for consumption was reported in 1954 and are nowadays plentiful (1, 4). Sorbic acid is synthesized through various methods, e.g., by the reaction of ketene and crotonaldehyde (3). The amine and ester sorbic acid derivatives similar properties and applications (2). Cytoplasmic oxidation of fatty acids forms damaging triplet carbonyls (5). The quenching of triplet acetone by SCOOH and the ester derivative of SCOOH leads to isomerization of the diene system at rates near diffusion control, 10^8 - 10^9 M⁻¹ s⁻¹ (5). The isomerization of 1, 3 hexadienes derivatives have been used to quantify triplet excited state carbonyls (5). Triplet excited state induced inflammation was reduced by the addition of SCOOH (5). The triplet quenching ability of SCOOH may be correlated to SCOOH antimicrobial activity (5). Triplet chromophoric dissolved organic matter (³CDOM*) is a key player in environmental photochemistry; thus, ³CDOM* is vital for the transformation and fate of pollutants and toxins (6–9). Sorbic acid is widely used to probe the formation rate and steady-state concentrations of ³DOM* irradiated with light >315 nm (6, 8, 9). Suwannee River DOM triplet quantum yield of 0.062 was determined using SCOOH isomerization (8). Sorbic amine, 2,4-hexadien-1-amine, and SOH, Figure 2.1, were also proposed as quenchers for triplet DOM measurements. Sorbic amine and SOH do not absorb light in the spectrum's visible range, a desirable characteristic for probes for environmental studies. The ³DOM*quenching rates were 0.42 ± 0.1 , 1.1 ± 0.1 , and $5.2 \pm 0.4 \times 10^9$ M⁻¹ s⁻¹ for SCOOH, SOH, and SNH₂, respectively (9). The sorbic derivatives have different

quenching abilities close to diffusion-controlled rates. The most efficient quencher was the amine substituted derivative. O_2 is the most efficient $^3DOM^*$ quencher and leads to the generation of 1O_2 (6). Diene isomerization induced by 1O_2 has been reported in organic solvents (10). Singlet oxygen can, also, react with the hexadiene probes, reducing the probes molecules able to accept the $^3DOM^*$ for isomerization, eventually adding error to the estimation. The detailed product study of SCOOH was reported by a previous member of Dr. O'Shea's research laboratory, Punam K. Parekh (2). Herein, the product studies are extended to the singlet oxygenation of SOH.

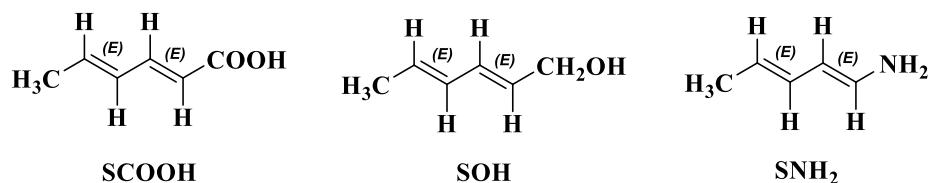


Figure 2.1. Structures of sorbic acid (SCOOH) and sorbic alcohol (SOH) and sorbic amine (SNH₂).

As presented in the introductory chapter, 1O_2 can react with conjugated π systems via ene, [2+2] cycloaddition, and [4+2] cycloaddition reactions pathways. The products, kinetics, and mechanisms are highly susceptible to experimental conditions (11). Significantly, the solvent can also have a profound effect on the reactions of 1O_2 (11). In general, the ene and [2+2] pathways are proposed to occur through a perepoxide and/or open zwitterionic intermediates, as demonstrated by kinetic isotope effects, solvent effect, chemically trapping, and product studies (11–15). Concerted and non-concerted mechanisms for the [4+2] cycloaddition have been proposed (11). Various hexadienes (10, 16) and bisarylanthracenes (17) exhibited non-concerted mechanisms in organic solvents.

The intermediate for the [4+2] pathway has been proposed to have a zwitterionic character on the basis of product and solvent studies (10, 16–19). Concerted and non-concerted [4+2] cycloaddition of isomeric hexadienes produce distinctly different products. For example, the concerted pathway of an *E, E*, SCO₂H can produce only the *cis*-endoperoxide (*cis*SCO₂H-EP) (10). A stepwise mechanism, on the other hand, can produce the *cis* and *trans* stereoisomers, and solvent trapped intermediates are also expected to be produced (Scheme 2.2) (10). Ultra Violet radiation mediated isomerization of SCO₂H, SOH, muconic acid (MuCO₂H), and muconic alcohol (MuOH) was conducted to probe the mechanisms of the ¹O₂ reactions in aqueous solutions.

2.3. Materials and Methods

Materials: Sorbic acid (CAS Number 111-28-4), sorbic alcohol (CAS Number 17102-64-6), Rose Bengal (CAS Number 632-69-9), acetaldehyde (CAS Number 75-07-0), and crotonaldehyde (CAS Number 123-73-9), muconic acid (CAS Number 3588-17-8), were purchased from Sigma Aldrich with purity higher than 95%. Dimethylformamide (DMF) (CAS Number 68-12-2), Methyl iodide (MeI) (CAS Number 78375-48-1), K₂CO₃ (CAS Number). Diisobutylaluminum hydride solution (DIBAL-H) (1.0 M in THF) (CAS Number 1191-15-7) were purchased from Fisher Scientific. The NMR tubes (OD 5 mm) were purchased from Kimble Chase. Deuterium oxide (D₂O), chloroform-d₃ (CDCl₃), Methylene chloride-d₂ (CD₂Cl₂), methanol-d₄ (MeOD₄), the NMR solvents were purchased from Cambridge Isotope Laboratories Incorporated.

Stock Solutions: A stock solution of 5 mM diene and 1×10^{-4} M Rose Bengal was prepared in deuterium oxide for NMR studies.

Photooxidation: A reaction vessel containing the stock solution was placed in a water-ice bath in a Pyrex windowed Dewar flask to maintain the reaction temperature at ~ 5 °C. Samples were irradiated with a 150 W and 7.5 Amps Xenon lamp (Oriel), fitted with a heat filter containing deionized water and a focusing lens. The Pyrex glass filters wavelengths shorter than 310 nm. The reactions products were analyzed using advanced NMR techniques. NMR spectra were obtained in the 400 Bruker NMR spectrometer.

Controls for the reactions: In the absence of a photosensitizer (direct photolysis control) and in the absence of oxygen (under argon saturation), no or negligible hexadiene transformation was observed.

Product studies: the stock solution was photooxidized using an NMR tube as the oxidation reaction vessel. The proton NMR spectra were collected at specific times. COSY NMR spectrum was also collected. The 400 and 600 MHz Bruker NMR spectrometers were used to assess product stability and to resolve coupling constants.

Synthesis of muconic alcohol, (2Z,4Z)-hexa-2,4-diene-1,6-diol, MuOH: Following a literature report (20), a solution of muconic acid (0.50 g, 70.4 mmol) was made to dimethylformamide (DMF), for a total volume of 10 ml. MeI (9.59 mL, 155mmol) was added to the mixture, followed by the addition of K_2CO_3 (1.9 g, 281 mmol). The reaction was stirred at room temperature for 24 hours. The product was extracted using water and ether simultaneously, then dried in vacuo yielding dimethyl (2Z,4Z)-hexa-2,4-dienedioate,

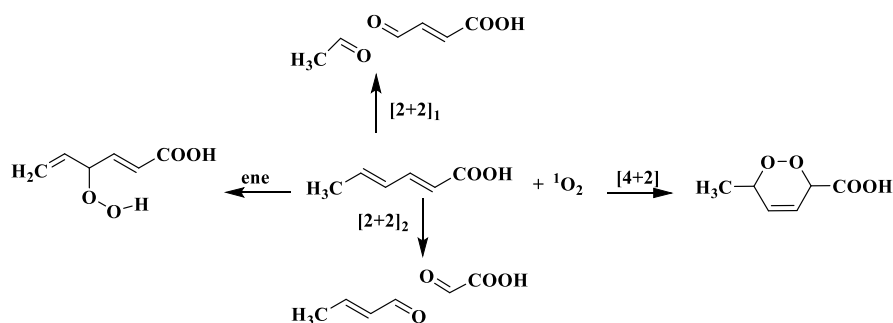
MuCOOCH₃ (0.4 g, 80%) (¹H NMR δH ppm (400 MHz, CDCl₃) 3.76 (6H, s), 6.00 (2H, m), 7.90 (2H, m).

Diisobutylaluminum hydride solution (1.0M in THF) was added to a stirred solution of MuCOOCH₃ (0.4 g) in CH₂Cl₂ at 0 °C. The solution was stirred for 16 h at room temperature. The reaction mixture was subsequently cooled to 0°C and quenched with MeOH. The reaction mixture of MuOH was diluted in MeOH, filtered through Celite and dried in vacuo (0.28 g, 70%) (¹H NMR δH ppm (400 MHz, CD₃OD) 4.22 (6H, s), 5.60 (2H, m), and 6.45 (2H, m).

2.4. Results and Discussion

Product Studies of the singlet oxygenation of SCOOH:

Parekh, P., a previous member of professor O'Shea's research group, reported the detailed elucidation of singlet oxygenation products of SCOOH (2). Parekh, P. characterized the endoperoxide (~78%) and hydroperoxide as the major products, and crotonaldehyde (~1.5%), fumaraldehydic acid (~1%), and acetaldehyde (~0.2%) as the products of the reactions using ¹H and COSY NMR (2). In the present study, her findings were supported with about 30% transformation of 5 mM SCOOH obtained after 2 hours of ¹O₂ reaction based on ¹H NMR. As Parekh, P. observed, the reaction ¹O₂ produced a pair of doublets appeared at 1.2 ppm in the ¹H NMR spectrum, and the olefinic region became confused with peaks. Although minor, characteristic aldehyde peaks at ~ 9-10 ppm also emerged in the spectrum. Herein, ¹³C and HOESY NMR of the SCOOH are presented, and previous and current results are compared to the singlet oxygenation of SOH, and a degradation product for the SCOOH-EP is proposed.



Scheme 2.1. Illustration of competing for $^1\text{O}_2$ reaction pathways with SCOAH. Possible products for each pathway $^1\text{O}_2$ reaction with SCOAH are SCOAH-EP, SCOAH-HP, $[2+2]_1$ acetaldehyde and (*E*)fumaric acid, $[2+2]_2$ (*E*) croton aldehyde and formic acid.

As reported by Parekh, P. the ^1H NMR of oxidized SCOAH shows a pair of doublets in a 1:1 ratio at 1.23 ppm ($J=6.56$ Hz) and 1.17 ppm ($J=6.52$ Hz), peak a and b shown in Figure 2.3 (2). The doublets are about 23.0 Hz apart; therefore, the protons of the two signals are not coupled (2). A slightly more deshielded and smaller doublet at 1.26 ppm ($J=6.80$ Hz) is also observed in the spectrum.

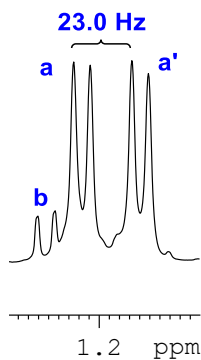


Figure 2.2. Aliphatic signals of ^1H NMR spectrum of singlet oxygenation of 5 mM SCOAH. The solutions prepared with 10 μM RB in D_2O were continuously purged with oxygen as it was irradiated with a 150 W Xenon lamp. The temperature was maintained at $\sim 5^\circ\text{C}$. The NMR spectra were obtained in the 400 Bruker NMR spectrometer.

The ^{13}C NMR (Figure 2.4) of the photooxidation of SCO₂H exhibits a pair of signals for every carbon, except for the carboxylic acid (Figure 2.5.) (^{13}C -NMR (D_2O) δ_{C} 176.35, 136.68, 136.43, 125.78, 125.61, 102.19, 101.89, 82.04, 81.49, 21.81 and 20.14 ppm). The chemical shifts in the ^{13}C NMR are consistent with the structure of SCO₂H-EP.

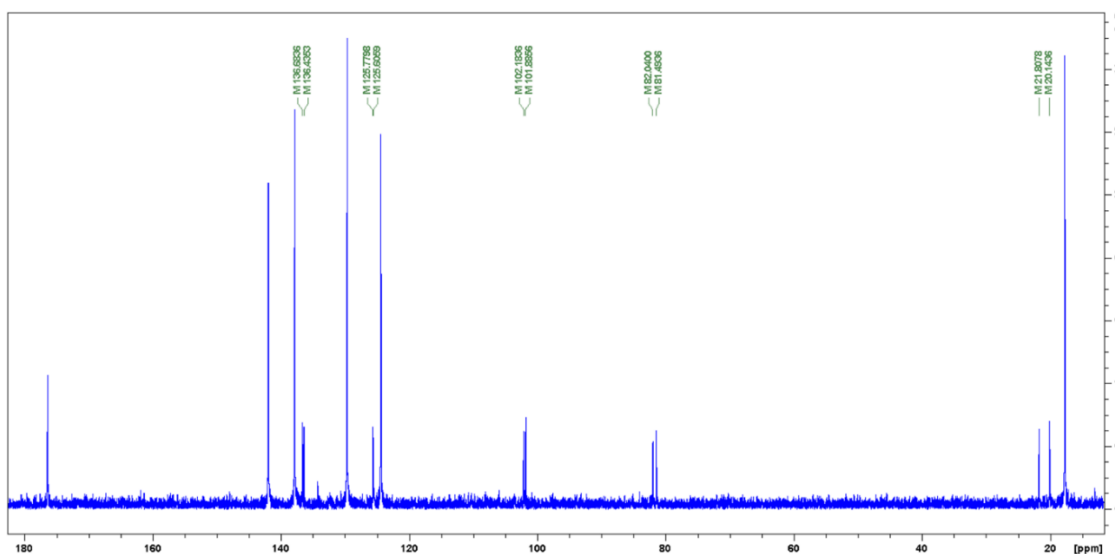


Figure 2.3. ^{13}C NMR spectrum of singlet oxygenation of 5 mM SCO₂H. The solutions prepared with 10 μM RB in D_2O were continuously purged with oxygen as it was irradiated with a 150 W Xenon lamp. The temperature was maintained at $\sim 5^\circ\text{C}$. The NMR spectra were obtained in the 400 Bruker NMR spectrometer.

The NOESY NMR spectrum of the SCO₂H-EP shows a slightly different correlation in space between the protons at C₆ to the protons at heteroatom bonded C₅, 4.56 and 4.58 ppm. The C₆ protons, also, correlate differently to the olefinic protons at C₄ at 6.10 and 6.20 ppm.

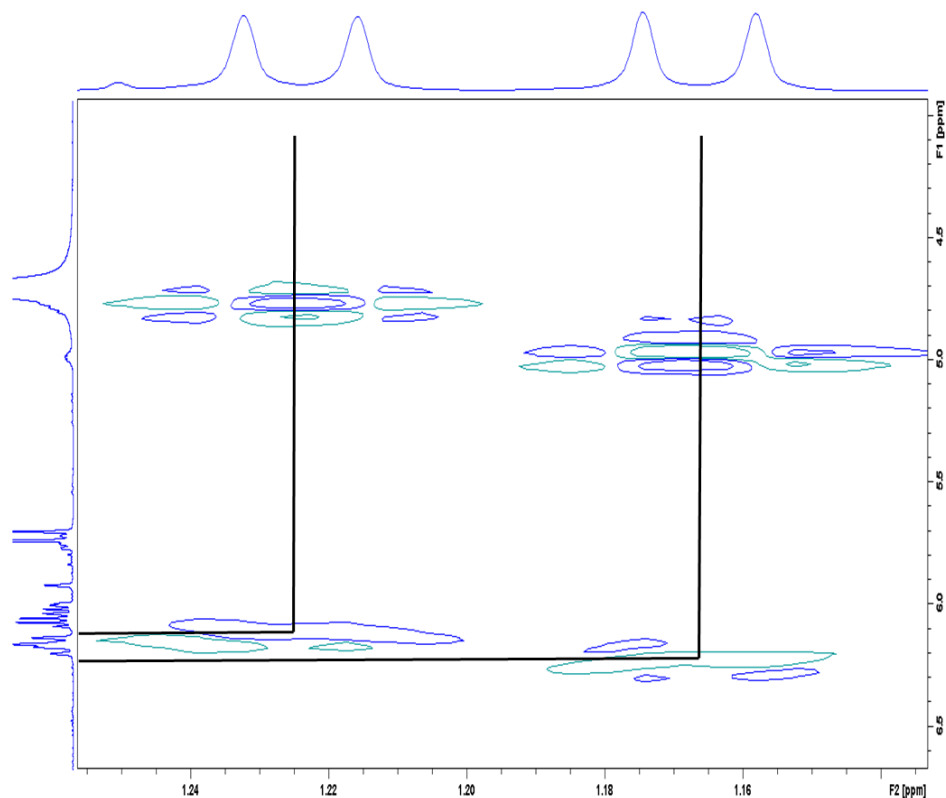
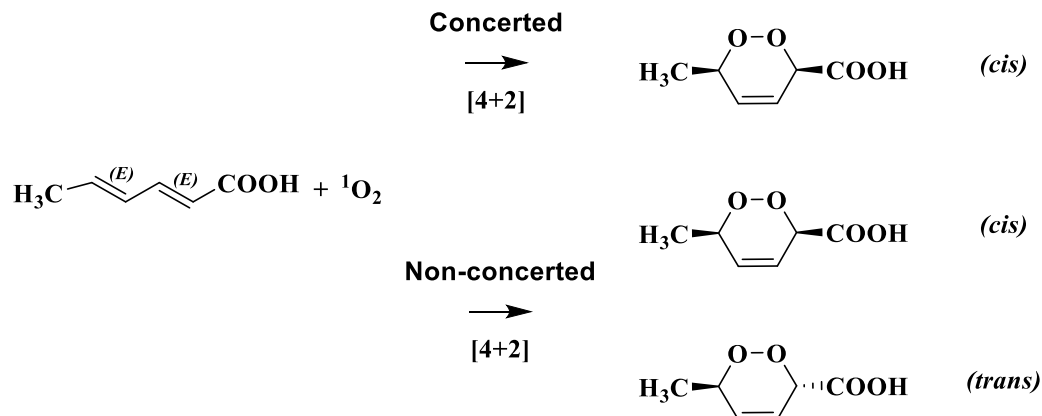


Figure 2.4 NOESY NMR spectrum of singlet oxygenation of 5 mM SCOOH. The solutions prepared with 10 μ M RB in D₂O were continuously purged with oxygen as it was irradiated with a 150 W Xenon lamp. The temperature was maintained at ~ 5 °C. The NMR spectra were obtained in the 400 Bruker NMR spectrometer.

Similar ¹³C and ¹H NMR patterns were reported for the *cis* and *trans* EP produced by isomeric 1,3-hexadienes in methanol-d₄ (*10*). The non-concerted reaction mechanism of the singlet oxygenation of SCOOH can yield both the SCOOH-EP_{*cis*} and COOH-EP_{*trans*}. (Scheme 2.2).



Scheme 2.2. Illustration of products from the [4+2] concerted and non-pathways of the reaction of ${}^1\text{O}_2$ with SCOEH producing *cis* and *trans* SCOEH-EP.

Parekh, P. K. proposed half-chair conformations of the SCOEH-EP to explain the pair of doublets at 1.23 ppm. (Figure 2.6) (2). The *cis* and *trans* diastereomers of EPs can be distinguished using variable temperature NMR (26). The *cis* half-chair conformations can oscillate between one of the larger groups at an equatorial position and the other at an axial position and vice versa (Figure 2.6), conformations close in energy (26). For the *trans*-SCOEH-EP (SCOEH-EP_{*trans*}), one of the half-chair conformations has both of the large groups at the equatorial positions, and it is favored over having both of the large groups at the axial positions (Figure 2.6) (26). Previous studies employed low-temperature NMR to elucidate *cis* and *trans* endoperoxides as the *cis* endoperoxide ${}^1\text{H}$ NMR signals split into two sets for the two conformers when cooling, while the *trans* did not (26). Parekh, P., using elevated temperature NMR experiments showed that the pair of methyl groups of the half-chair conformations of SCOEH-EP coalesce at 65°C (2).

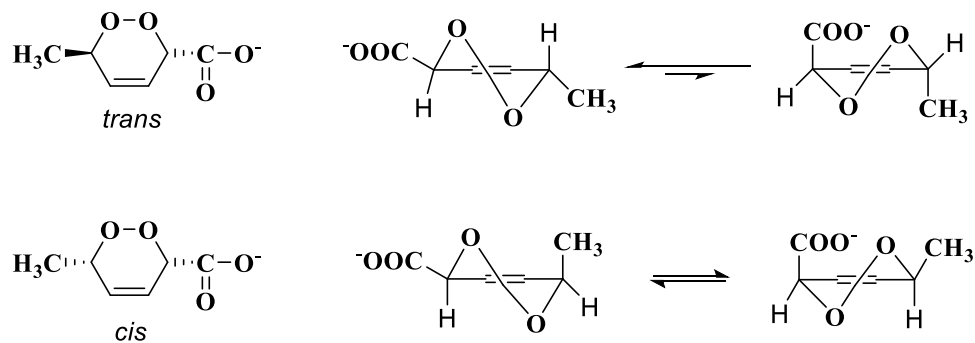


Figure 2.5. Half-chair conformations of $\text{SCOOH}_{\text{cis}}$ and $\text{SCOOH}_{\text{trans}}$, modified from Yong et al., 2012 and Parekh, P. K. et.al., 2012 (2, 26).

Only a non-concerted mechanism for [4+2] can yield both *cis* and *trans* SCOOH-EP. An open zwitterionic intermediate leading to the [4+2] cycloaddition, as has been proposed in organic solvents, would be prone to solvent trapped intermediates, which were not observed in our studies. Further support for the half-chair conformations interpretation can be gained by reacting the *E*, *Z* sorbic acid with $^1\text{O}_2$ to get the $\text{SCOOH-EP}_{\text{trans}}$, which is expected to exist in only one conformation. The double bond isomerization induced by $^1\text{O}_2$ has been reported (10). In the case of singlet oxygenation of SCOOH, such isomerization was not observed. When methanol- d_4 was the solvent for the reaction, only the SCOOH-EPs were produced without any measurable [2+2] products.

The SCOOH-EP rearranged after 15 days in the dark with the ^{13}C NMR characteristic signals of the EP carbons at 102.2, and 82.2 ppm lowered the intensity and a new signal appearing at 66.77 ppm. Also, a new signal at 198.26 ppm appeared in the spectrum of the aged SCOOH-EP, corresponding to an aldehyde or carbonyl carbon. The ^{13}C NMR spectrum is consistent with the structure of 4-hydroxypent-2-enal (^{13}C -NMR (D_2O) δ_{C} 198.26 (C_1), 128.86 (C_2), 128.86 (C_3), 66.77 (C_4), and 20.89 (C_5) ppm). The signal at 1.26 ppm ($J=6.80$ Hz) corresponding to the protons at C_5 of 4-hydroxypent-2-enal was

observed in small amounts following singlet oxygenation of SCOOH reaction (Figure 2.3, peak b). Peak b (Figure 2.3) increased with time in the dark (up to 15 days), along with a doublet at 9.37 ppm ($J=8$ Hz) and a dd at 7.05 ppm ($J=15.5$, and 8 Hz). This molecule was also formed when the oxidation mixture was heated to 60°C for 1 hour (Figure 2.6).

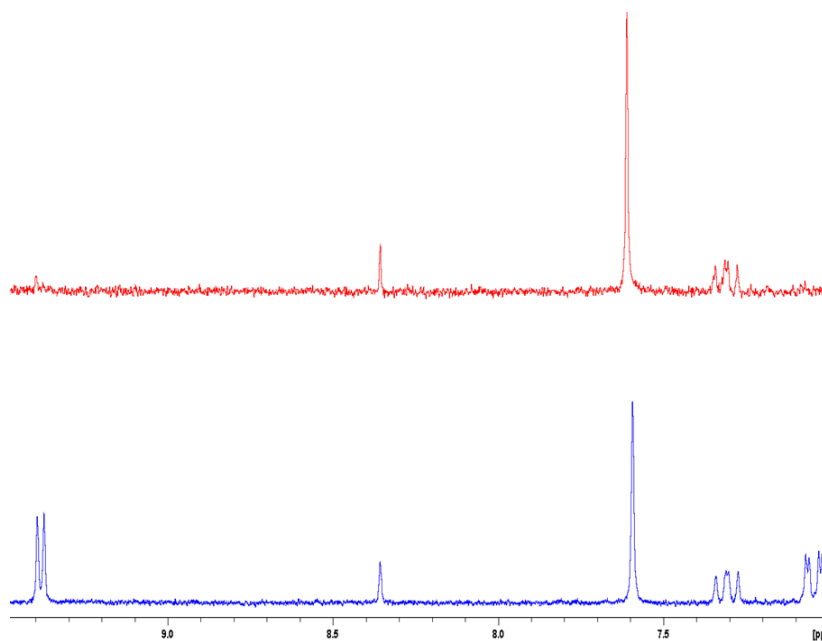
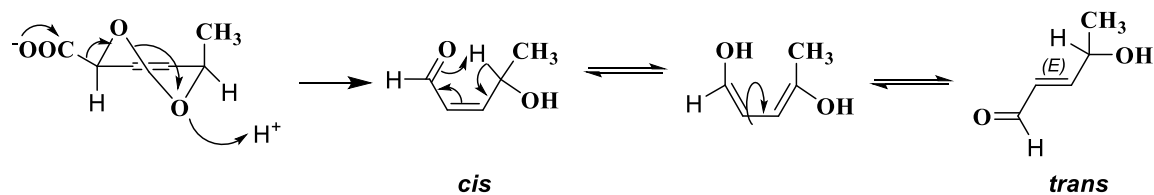


Figure 2.6. ^1H spectrum of the singlet oxygenation of 5 mM SCOOH for 2 hours (Top) ^1H spectrum of the singlet oxygenation of 5 mM SCOOH for 2 hours and 1 hour of heating at 60°C

The decarboxylation of SCOOH-EP can yield (*Z*) 4-hydroxypent-2-enal (Scheme 2.3). Decarboxylation is a common transformation of endoperoxides (24, 25). Tautomerisation of (*Z*) 4-hydroxypent-2-enal can form the thermal product, (*E*) 4-hydroxypent-2-enal.



Scheme 2.3. Decarboxylation of SCOOH-EP to (*Z*)-4-hydroxypent-2-enal and enol tautomer-driven isomerization to the thermodynamically favored (*E*)-4-hydroxypent-2-enal.

The Aliphatic peaks (Figure 2.7) at 1.255 (peak b in figure 2.2) and 1.125 ppm can be assigned to the (*E*)-4-hydroxypent-2-enal and (*Z*)-4-hydroxypent-2-enal, respectively. The doubles' a:a' integration is in 0.23:0.23:1 ratio to the methyl group of sorbic acid before heating or aging. The doubles' b:a:a':c integration is in a 0.06:0.18:0.18:0.03:1 ratio to the methyl group of sorbic acid after heating or aging. The observation supports that the peaks that emerged in the spectrum after heating or aging come from the endoperoxide (s).

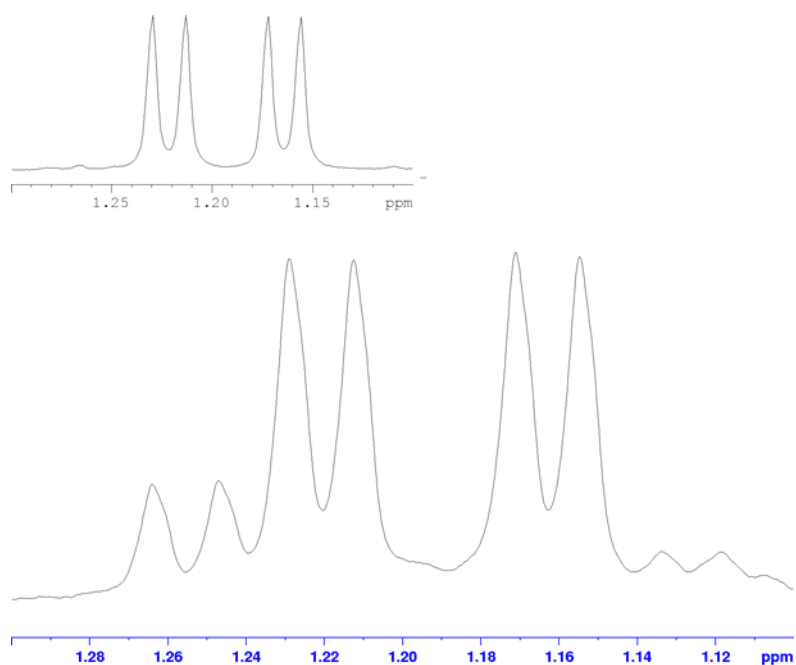


Figure 2.7. Aliphatic region of the ¹H spectrum of the singlet oxygenation of 5 mM SCOOH for 2 hours (Top). ¹H spectrum of the singlet oxygenation of 5 mM SCOOH for 2 hours and 1 hour of heating at 60°C

Product Studies of the singlet oxygenation of SOH:

The singlet oxygenation of SOH was conducted in an NMR tube in D₂O at ~ 5 °C, using a Xenon lamp as the light source. No direct photolysis or energy transfer from RB pathways was observed in control experiments (without O₂ or RB). The proton NMR time profile of the reaction of ¹O₂ with 5 mM SOH is shown in Figure 2.8. As the reaction proceeded, the characteristic signals of SOH steadily decreased with the appearance of new complementary peaks.

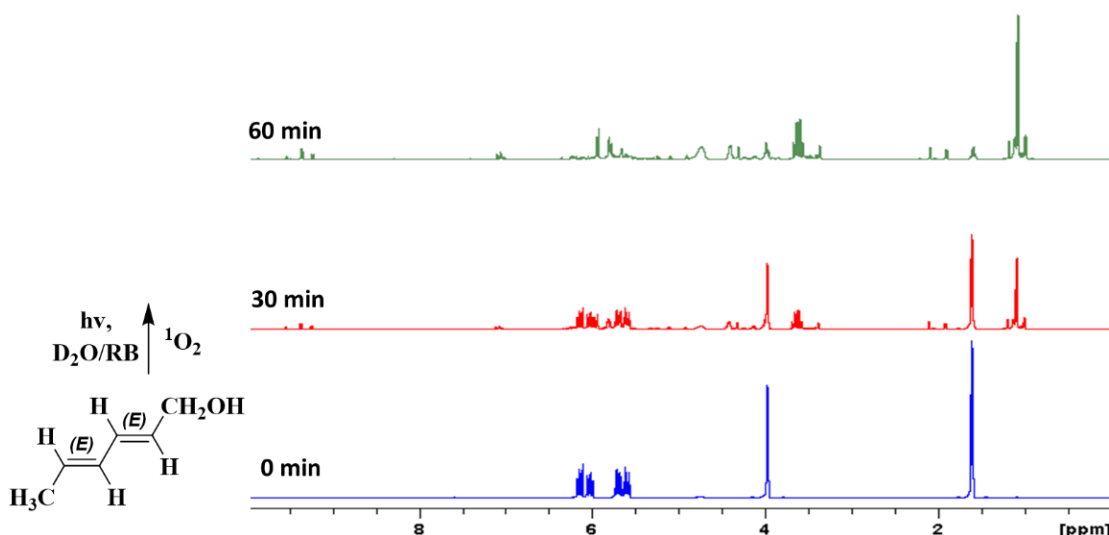
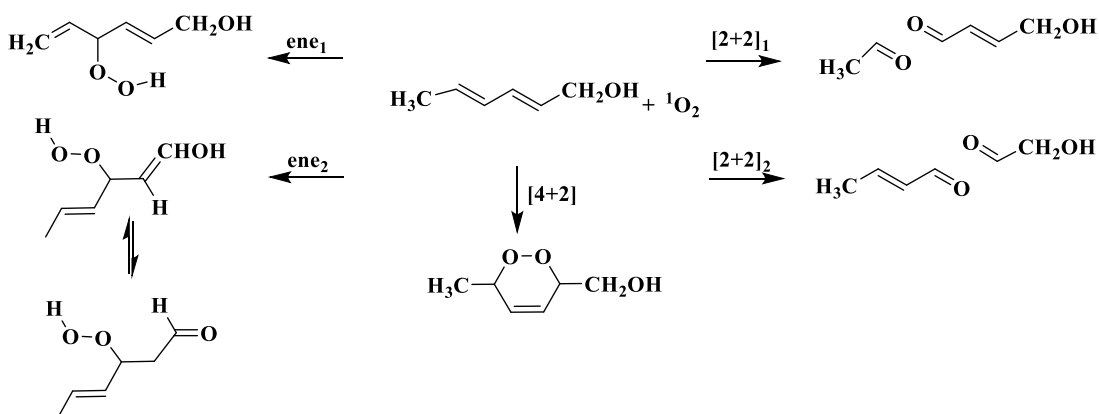


Figure 2.7. Time profile of the ¹H NMR spectrum of singlet oxygenation of 5 mM SOH. The solutions prepared with 10 μM RB in D₂O were continuously purged with oxygen as it was irradiated with a 150 W Xenon lamp. The temperature was maintained at ~ 5 °C. The NMR spectra were obtained in the 400 Bruker NMR spectrometer.

The terminal alkene of SOH-HP 1, from the ene₁ reaction pathway, can be expected to produce two broad singlets in ¹H NMR and a negative peak in ¹³C DEPT 135

NMR as previously discussed (21, 22). The characteristic SOH-HP NMR signals were not present in the spectra of singlet oxygenated SCOOH product mixture. The product of the ene₂ reaction, SOH-HP 2, may tautomerize in water in the more stable aldehyde form shown in Scheme 2.



Scheme 2.4. Illustration of competing for ¹O₂ reaction pathways with SOH. Possible products for each pathway of ¹O₂ reaction with SOH are SOH-EP [4+2] (6-methyl-3,6-dihydro-1,2-dioxin-3-yl)methanol, SOH-HP 1(ene₁) (*E*)-4-hydroperoxyhexa-2,5-dien-1-ol, HPSOH 2(ene₂) (*1Z* or *E*, *4E*)-3-hydroperoxyhexa-1,4-diene, [2+2]₁ acetaldehyde and (*E*)-4-hydroxybut-2-enal, [2+2]₂ (*E*)-but-2-enal, crotonaldehyde and 2-hydroxyacetaldehyde.

The aldehyde signal ¹H NMR of SOH-HP can be used for its identification. The aldehyde region of the ¹H NMR of the photooxidation products has four significant peaks, a doublet at 9.88 ppm (0.07), a quartet at 9.53 ppm (0.31), a doublet at 9.36 ppm (1.00), and a doublet at 9.23 ppm (0.46) (Figure 2.8). However, the ratio of the integrations of the peaks did not indicate stoichiometric relationships indicative of characteristic products from the collapse of the [2+2] dioxetane products.

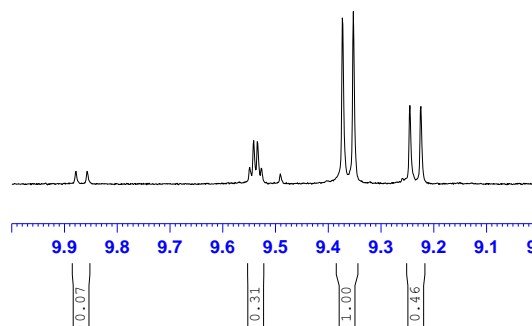


Figure 2.9. Aldehyde region of the ^1H NMR spectra singlet oxygenated SOH. The solutions prepared with $10\ \mu\text{M}$ RB in D_2O were continuously purged with oxygen as it was irradiated with a 150 W Xenon lamp. The temperature was maintained at $\sim 5\ ^\circ\text{C}$. The NMR spectra were obtained in the 400 Bruker NMR spectrometer.

The ^1H NMR of the authentic standards of acetaldehyde and crotonaldehyde were compared to the SOH oxidation mixture, Figure 2.9. Crotonaldehyde ^1H NMR signals, ^1H NMR (400 MHz, D_2O) δ 9.48 (d, 1H, $J=9$ Hz), 7.10 (dq, 1H, $J=16, 7$ Hz), 6.10 (qdd, 1H, $J=2, 9, 16$ Hz), 1.58 (dd, 3H, $J=2, 7$ Hz), are present in singlet oxygenated SOH.

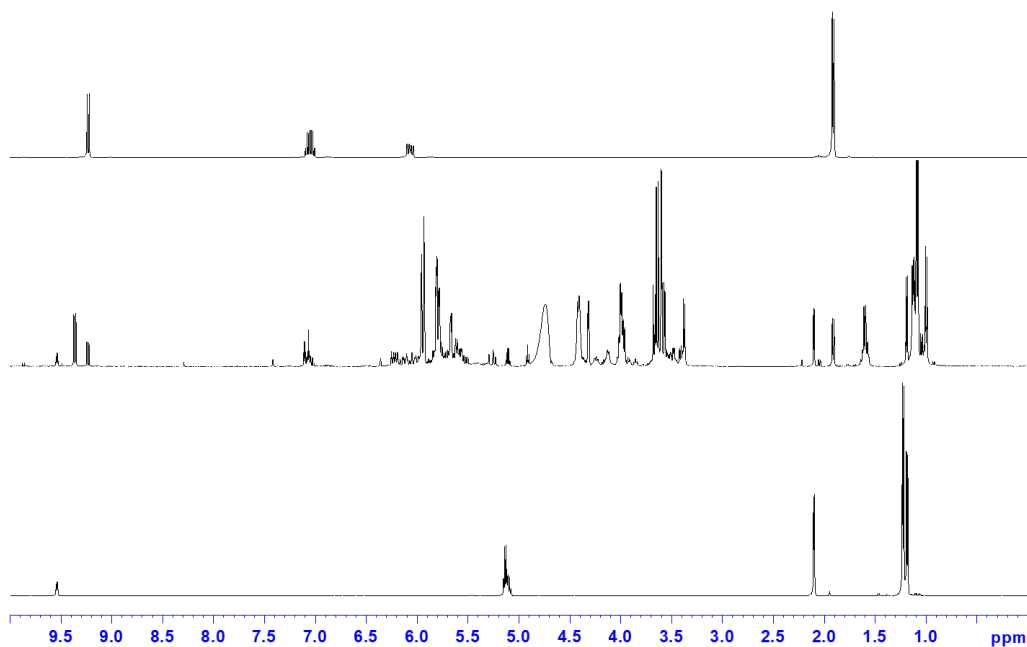


Figure 2.10. ^1H NMR spectra of *trans* crotonaldehyde (top) acetaldehyde (bottom) and singlet oxygenated SOH product mixture (middle).

The ^1H NMR signals crotonaldehyde and 2-hydroxyacetaldehyde at 9.88 ppm are 1:0.07 ratio. In aqueous solutions, low molecular weight aldehydes can be in equilibrium with their hydrated forms. The hydrate of 2-hydroxyacetaldehyde was supported using ^1H COSY NMR shown in Figure 2.10. The ratio of crotonaldehyde to 2-hydroxyacetaldehyde to 2-hydroxyacetaldehyde-hydrate was 1:0.07:0.93. Therefore, the $[2+2]_2$ yielded excellent stoichiometric balance when taking into account 2-hydroxyacetaldehyde-hydrate.

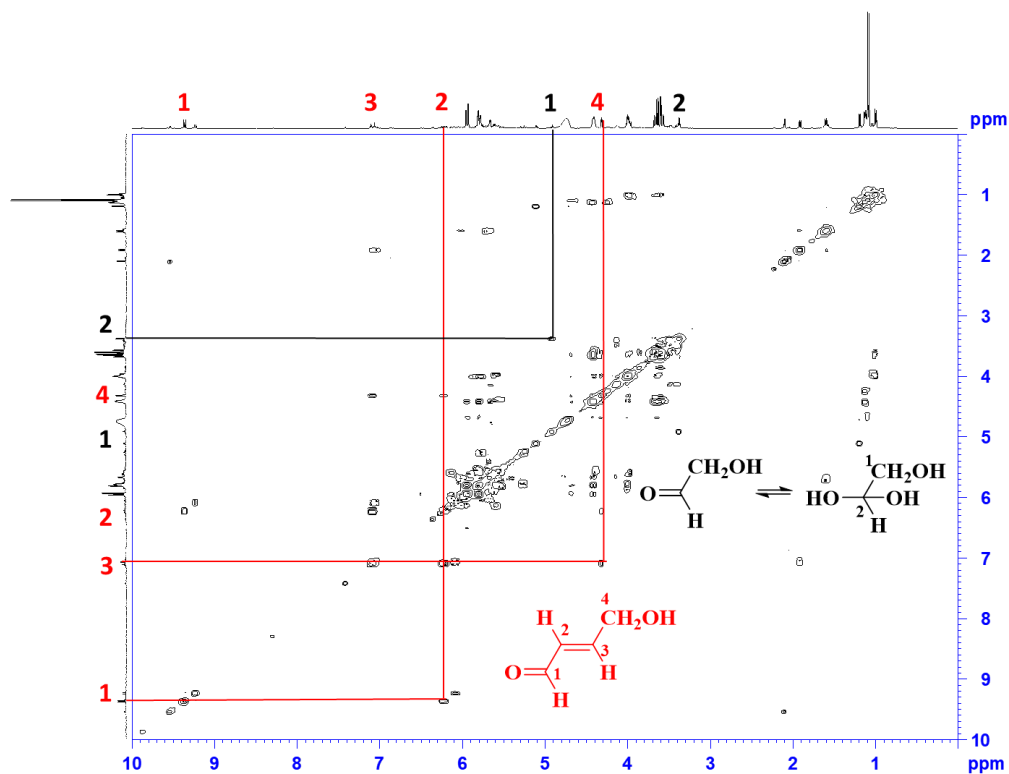


Figure 2.10. ¹H COSY NMR of photooxidation SOH product mixture. The molecule and the proton signal assignments of (*E*)-4-hydroxybut-2-enal are in red, and for 2-hydroxyacetaldehyde hydrate are in black. The solutions, prepared with 10 μM RB in D₂O, were continuously purged with oxygen as it was irradiated with a 150 W Xenon lamp. The temperature of the reaction was maintained at ~ 5 °C. The NMR spectra were obtained in the 400 Bruker NMR spectrometer.

The ¹H NMR of an authentic sample of acetaldehyde in D₂O shows signals at 1.2 ppm and 5.1 ppm, which are also present in the oxidation mixture (Figure 2.7). Low molecular weight aldehydes commonly trimerize and exhibit a different set of NMR peaks than the parent compound (27). Acetaldehyde trimer formation of the six-member, paraldehyde, produced *cis* and *trans* isomer. The *cis* isomer, with methyl groups in the equatorial positions, is sterically favored. The ratio of the *cis* trimer, and *trans* trimer, and

the monomer of acetaldehyde was 3.8:1:1 in the ^1H NMR of aqueous acetaldehyde authentic standard. The ^1H NMR of the reaction product mixture of $^1\text{O}_2$ with SOH had only the *cis* paraldehyde isomer signals present.

Homonuclear correlation spectroscopy was used to assign the signals corresponding to 4-hydroxycrotonaldehyde, the stoichiometric partner of acetaldehyde (Figure 2.8). The ratio of the integration of 4-hydroxycrotonaldehyde to acetaldehyde monomer to *cis* acetaldehyde trimer was 1.5:1:0.5. The $[2+2]_1$ cycloaddition reactions also yielded an excellent stoichiometric balance.

The SOH-EP from the $[4+2]$ pathway was the major product of the $^1\text{O}_2$ reaction with SOH (Table 2.1). Sorbic alcohol endoperoxide can have *cis* or *trans* geometry. The $[4+2]$ pathway, concerted $[4+2]$ addition of singlet oxygen to the *EE* isomer of SOH, can only produce the *cis* EP according to the Woodward Hoffman rules. Evidence for isomeric SOH-EP was not observed in these studies.

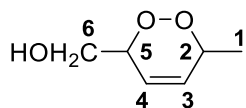


Table 2.1 ^{13}C NMR data for (6-methyl-3,6-dihydro-1,2-dioxin-3-yl)methanol

Carbon	Methanol, d4	D ₂ O
1	17.57	17.00
2	74.38	75.08
3	123.0	122.5
4	131.5	131.0
5	79.69	79.83
6	63.41	61.57

The transformation of EPs to furans has been catalyzed by 5, 10, 15, 20-Tetraphenyl-21H,23H-porphine cobalt (II) (CoTPP) (29). The CoTPP catalyzed reaction of EPSOH in CDCl_3 efficiently produced the furan derivative (5-methylfuran-2-yl)methanol (Table 2.2).

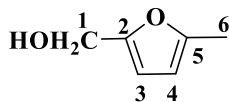


Table 2.2. ^{13}C NMR data of (5-methylfuran-2-yl)methanol

Carbon	Standard	Product
1	57.24	57.63
2	152.4	152.5
3	108.6	108.8
4	106.2	106.4
5	152.2	152.3
6	13.46	13.76

Similarly to SCOOH, the SOH-EP was the only product of the reactions when the solvents were CD_3OD or CD_3Cl .

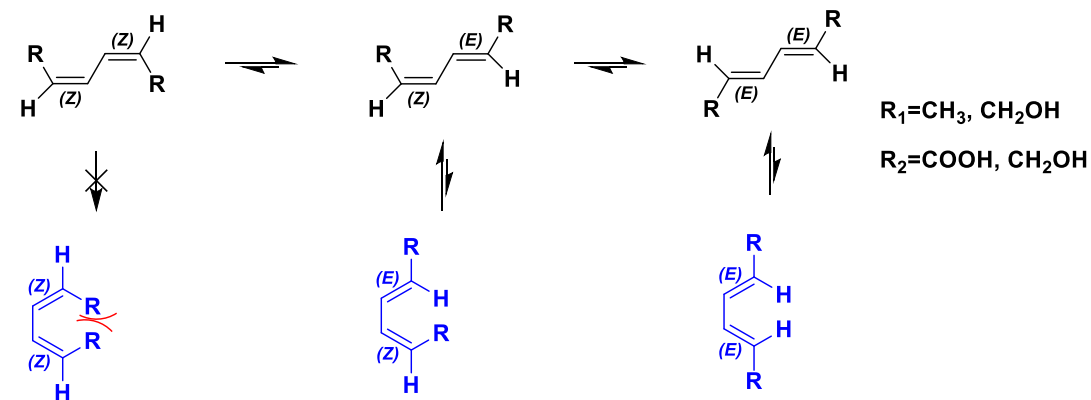
The reactions of $^1\text{O}_2$ with SCOOH and SOH followed mainly the [4+2] pathways to produce the corresponding endoperoxide derivatives. In contrast to SOH, the EP derivative of SCOOH degraded over time to *Z* and *E* 4-hydroxypent-2-enal. The reactions in D_2O produced products from the [2+2] pathway in low yields. However, the [2+2] products were not observed in methanol- d_4 or chloroform- d_3 . The observed solvent effect agrees with the literature reports. In general, the ene and [2+2] pathways occur through a peroxide intermediate, or open intermediate has been supported (11–15, 30). The solvent effect on product distribution suggests that the [2+2] cycloaddition may require water molecules to stabilize charged or polar intermediates, while the [4+2] pathway may have a less polar character or do not require such stabilization. Both concerted and non-concerted mechanisms for the [4+2] cycloaddition of hexadienes have been reported in organic

solvents (10, 16, 30). In the case of SCOOH, two sets of signals are observed in ^{13}C , ^1H , and NOESY NMR. Parekh, P., proposed an equilibrium between half-chair conformers of the SCOOH-EP_{cis}. On the other hand, for the SOH-EP from the [4+2] $^1\text{O}_2$ reaction, only one set of signals is observed. Studies of the $^1\text{O}_2$ reaction with the *E*, *Z* isomer of SCOOH can provide further support to the half-chair conformation proposal since the *trans* isomer is expected to exist as one conformer. Low-temperature NMR of the SOH-EP can also show the signals splitting into the different conformers reinforcing the proposed equilibrium.

2.5. Mechanistic Studies:

Isomeric 1, 3 hexadienes have served as mechanistic probes for the $^1\text{O}_2$ reactions (10). The [4+2] pathway concerted mechanism requires that the diene assumes an *s-cis* conformation (Scheme 2.3). The individual isomers are constrained by different energetics in assuming the *s-cis* conformation due to steric limitations. A concerted [4+2] cycloaddition of $^1\text{O}_2$ to isomeric dienes would yield a *cis* endoperoxide for the *E,E* isomer, a *trans* endoperoxide for the *Z,E* isomer, and no [4+2] reaction pathway for the *Z,Z* isomer based on inability to obtain an *s-cis* conformation (28). Previous studies revealed a mixture of *trans*, *cis* endoperoxides, and solvent trapped intermediates for the singlet oxygenation of isomeric 1, 3-hexadienes in methanol, indicating a stepwise non-concerted mechanism produced (10). Solvent effects also suggested a polar or open intermediate for the [4+2] pathway of cyclic 1,3-dienes in water (31). The cyclic dienes had a fixed *s-cis* conformation, which may favor a concerted pathway. In general, the available data for the $^1\text{O}_2$ reactions in aqueous media is minimal.

Dienes undergo excitation and isomerization of the π system under UV radiation (32). The UV isomerization of SCOOH, SOH, MuCOOH), and MuOH was conducted in order to study the reactions of the different isomers using the procedure described by Kralj Cigić and colleges (32). Irradiation of the hexadienes with UV light ($\lambda=254$ nm) produced isomers in relatively good yields. The ^1H NMR signals of indicative olefinic protons region of the UV isomerization of SCOOH are shown in Figure 2.11.



Scheme 2.5. Isomerization and s-cis conformations of hexadienes

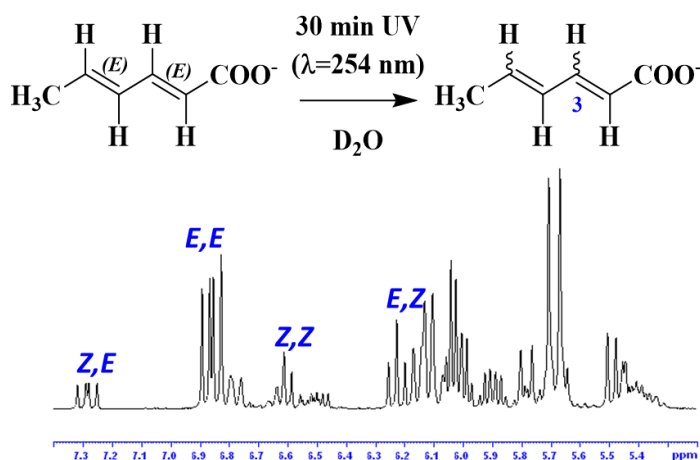


Figure 2.10. ^1H NMR of the UV mediated isomerization of SCOOH. A 10 mM solution of SCOOH in D_2O was argon saturated and irradiated with UV light ($\lambda=254\text{nm}$) for 30 minutes. The reactions were monitored and analyzed using the 400 MHz NMR spectrometer.

The isomers were identified using the coupling constants for the proton at carbon in position 3 (Figure 2.11) and comparison to literature reports (32). The relative ratio of the isomers was obtained using ^1H NMR signal integration. The major isomer in the product mixture was the *E,E*, which is sterically favored over the other isomers.

Table 2.3. The estimated product distribution of UV isomerization of SCOOH using NMR data C_3

SCOOH Isomer	δ (ppm)	J_{H3-H2}	Reported Ratio
<i>EE</i>	6.85	14.7	1
<i>EZ</i>	7.30	15.1	0.35
<i>ZE</i>	6.20	11.0	0.19
<i>ZZ</i>	6.61	11.5	0.28

The singlet oxygenation of the SOOH isomeric mixture yielded signals not present in the photooxidation of the *E,E* isomer alone. However, the insufficient quantity of the product(s) did not allow characterization.

Muconic Acids and Alcohols:

The preliminary results of the UV isomerization SCOOH isomers were encouraging, since all the isomers were obtained. However, the reactions of SCOOH and $^1\text{O}_2$ yields are low. The UV isomerization of *Z,Z* dienes to the *Z,E*, and *E,E* is generally sterically favored. The *Z,Z* muconic acids (MuCOOH) were purchased, since better photochemical isomerization yield of the *Z,E* and *E,E* isomers was expected. Despite the expectations, the isomerization yielded similar ratios of the isomers to *E,E* SCOOH. Singlet oxygen was, however, unreactive with the mixture of *Z,Z*, *E,Z*, and *Z,Z* MuCOOHs. The electron-withdrawing carboxylic acid groups may lower the electron density of the conjugated diene, hence lowering nucleophilic character and reactivity of the diene towards $^1\text{O}_2$.

The singlet oxygenation of SOH yielded ~80% transformation, whereas singlet oxygenation transformed ~30% of SCOOH, since the alcohol substitution increases the electron density of the diene. With this in mind, the reduction of the MuCOOH to MuOH was conducted (Figure 2.11). At first, the standard procedure of lithium aluminum hydride (LiAlH_4) in ether was attempted (33). However, solubility did not allow the reaction to proceed. Therefore, the esterification of the MuCOOH to MuCOOCH_3 was a critical step before reduction. The acid-catalyzed esterification in methanol produced a mixture of the *ZZ*, *ZE*, *EE* isomers suggesting protonation of the double bonds during the reaction (34).

Using a previously reported method (20), the Sn2 reaction of MuCOOH with methyl iodate in a basic solution produced MuCOOCH₃ at near quantitative yields. The reaction was followed by TLC and then separated via 100-200 mesh silica gel column chromatography. The reduction of the ester functionalities was carried out with diisobutyl aluminum hydride (DIBAL-H), as previously reported (20). An unexpected reduction of the double bond by LiAlH₄ was observed (20).

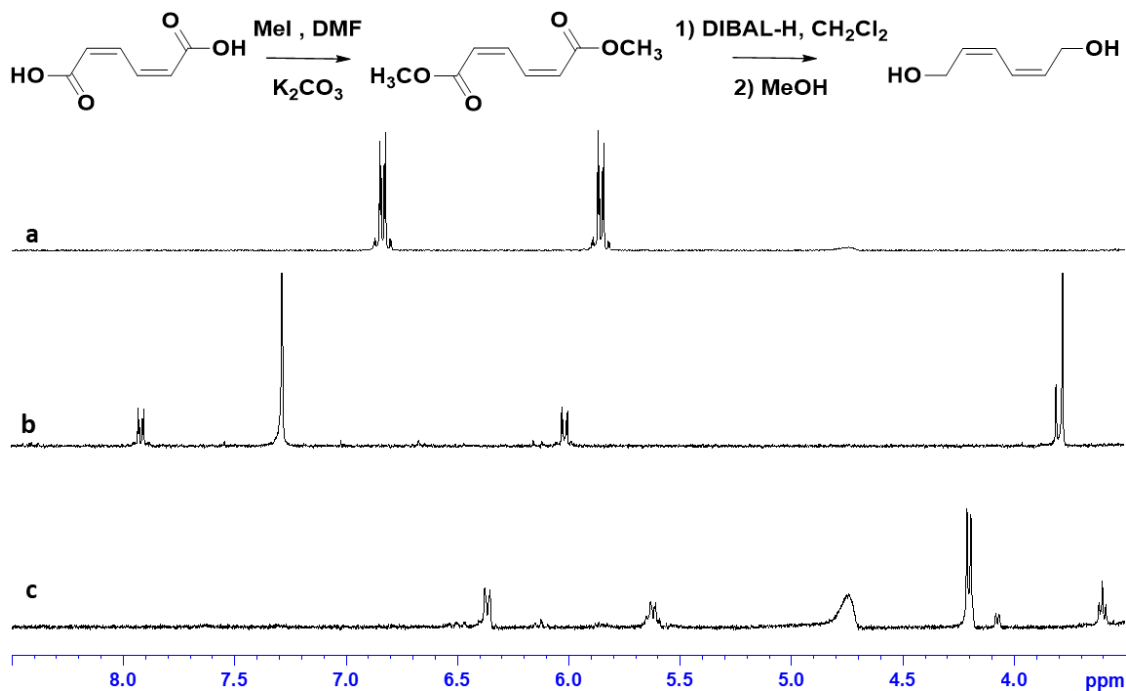


Figure 2.11. ¹H NMR of Z,Z MuCOOH (a), Z,Z MuCOOCH₃ (b), and of Z,Z MuOH (c). The reaction were conducted as described in literature reports (20) and the experimental section. The spectra was obtained using the 400 MHz NMR spectrometer.

Z,Z Muconic alcohol (10 mg) in D₂O was irradiated with UV, λ=254 nm for 30 minutes (Figure 2.12). The photochemical reaction produced the Z,Z, E,Z and E,E isomers

(Table 2.4). The specific isomer was identified by the chemical shift of the doublet, 6Hs, at C1 in the ^1H NMR spectrum. The *Z,Z* MuOH was the major isomer in the mixture, although sterics favors the *E,E* conformation.

Table 2.4. The estimated product distribution of UV isomerization of MuOH using NMR data C_3

MuOH Isomer	δ (ppm)	Ratio
<i>EE</i>	3.85	0.13
<i>EZ</i>	3.90	0.38
<i>ZZ</i>	4.15	1

The MuOH isomeric mixture was subjected to singlet oxygenation for two hours (Figure 2.12). $^1\text{O}_2$ was, however, unreactive towards MuOH. The lack of reactivity of might be related to the stability of the *Z,Z* isomer under UV radiation.

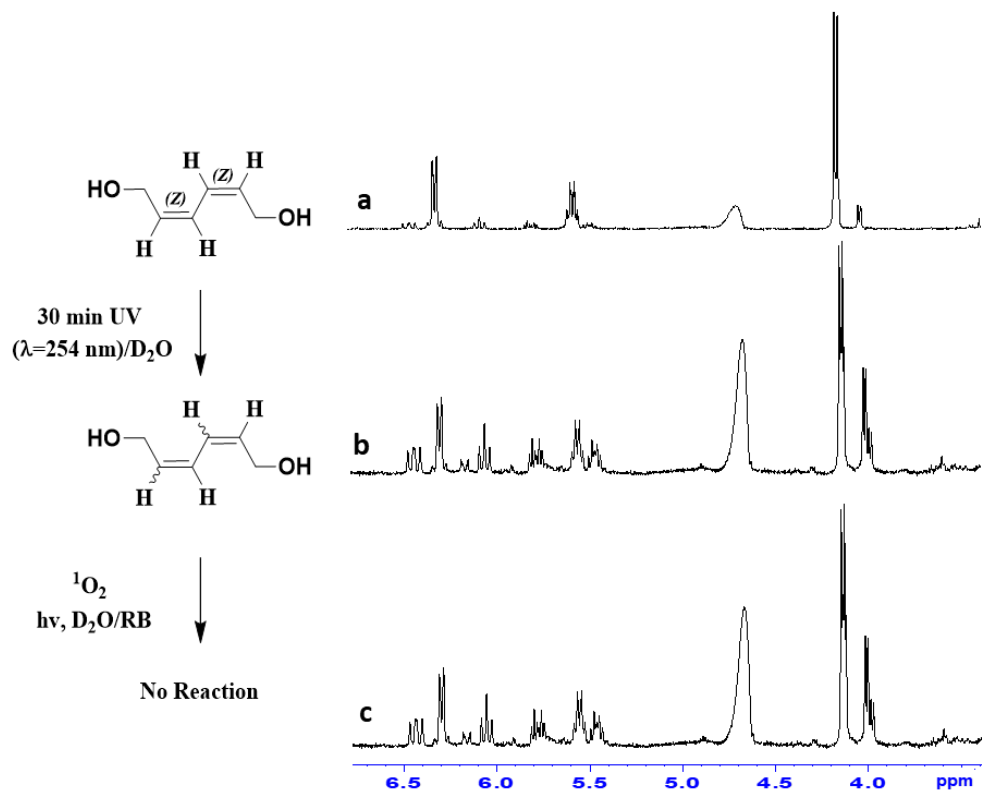


Figure 2.12 ^1H NMR of Z,Z MuOH (a), isomeric MuOH (b), and singlet oxygenation of isomeric MuOH (c). The spectra were obtained using the 400 MHz NMR spectrometer.

Although preliminary results of the singlet oxygenation of SCO OH isomers were encouraging, $^1\text{O}_2$ was unreactive to the mixture of isomeric MuCO OH s and MuOHs. In future studies, the isomers of SCO OH and SOH will be separated and singlet oxygenated. The kinetics of the reactions of SCO OH , SOH, and SNH $_3$ will be assessed using competition kinetics.

2.6. References

- (1) Bell, T. A.; Etchells, J. L.; Borg, A. F. Influence of Sorbic Acid on the Growth of Certain Species of Bacteria, Yeasts, and Filamentous Fungi. *J. Bacteriol.* **1959**, *77* (5), 573–580.
- (2) Parekh, P. K. The Photooxidation of Domoic Acid. **2012**.
- (3) Bellassoued, M.; Lensen, N.; Bakasse, M.; Mouelhi, S. Two-Carbon Homologation of Aldehydes via Silyl Ketene Acetals: A New Stereoselective Approach to (E)-Alkenoic Acids. *J. Org. Chem.* **1998**, *63* (24), 8785–8789.
- (4) Smith, D. P.; Rollin, N. J. Sorbic Acid as a Fungistatic Agent for Foods. *J. Food Sci.* **1954**, *19* (1–6), 59–65.
- (5) Velosa, A. C.; Baader, W. J.; Stevani, C. V.; Mano, C. M.; Bechara, E. J. H. 1,3-Diene Probes for Detection of Triplet Carbonyls in Biological Systems. *Chem. Res. Toxicol.* **2007**, *20* (8), 1162–1169.
- (6) McNeill, K.; Canonica, S. Triplet State Dissolved Organic Matter in Aquatic Photochemistry: Reaction Mechanisms, Substrate Scope, and Photophysical Properties. *Environ. Sci. Process. Impacts* **2016**, *18* (11), 1381–1399.
- (7) Parker, K. M.; Mitch, W. A. Halogen Radicals Contribute to Photooxidation in Coastal and Estuarine Waters. *Proc. Natl. Acad. Sci. U. S. A.* **2016**, *113* (21), 5868–5873.
- (8) Grebel, J. E.; Pignatello, J. J.; Mitch, W. A. Sorbic Acid as a Quantitative Probe for the Formation, Scavenging and Steady-State Concentrations of the Triplet-Excited State of Organic Compounds. *Water Res.* **2011**, *45* (19), 6535–6544.
- (9) Zhou, H.; Yan, S.; Ma, J.; Lian, L.; Song, W. Development of Novel Chemical Probes for Examining Triplet Natural Organic Matter under Solar Illumination. *Environ. Sci. Technol.* **2017**, *51* (19), 11066–11074.
- (10) O’Shea, K. E.; Foote, C. S. Chemistry of Singlet Oxygen. 51. Zwitterionic Intermediates from 2, 4-Hexadienes. *J. Am. Chem. Soc.* **1988**, *110* (21), 7167–7170.
- (11) Fudickar, W.; Linker, T. Intermediates in the Formation and Thermolysis of Peroxides from Oxidations with Singlet Oxygen. *Aust. J. Chem.* **2014**, *67* (3), 320.
- (12) Henson, L. M. Stereochemical Dependence of Isotope Effects in the Singlet Oxygen-Olefin Reaction. *Am. Chem. Soc.* **1979**, *39* (22), 3–5.
- (13) Orfanopoulos, M. Solvent Effects on the Side Selectivity of Singlet Oxygen with Alpha, Beta Unsaturated Esters. New Evidence for a Peroxide Intermediate. *Tetrahedron Lett.* **1991**, *32* (49), 7321–7324.

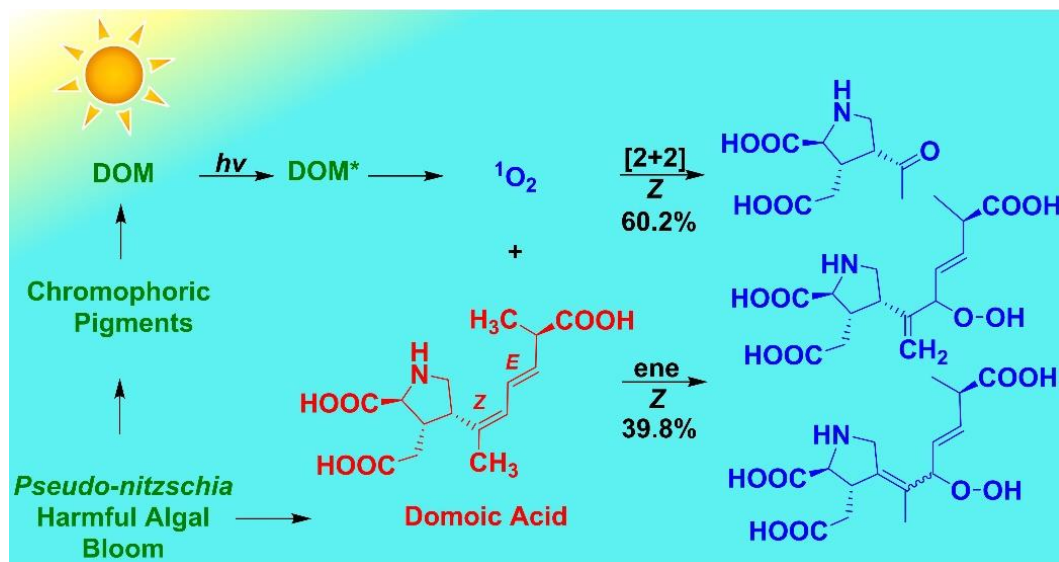
- (14) Poon, T. H. W.; Pringle, K.; Foote, C. S. Reaction of Cyclooctenes with Singlet Oxygen. Trapping of a Peroxide Intermediate. *J. Am. Chem. Soc.* **1995**, *117* (29), 7611–7618.
- (15) Adam, W.; Saha-Möller, C. R.; Schambony, S. B. A Highly Diastereoselective Dioxetane Formation by the Hydroxy-Directed [2+2] Cycloaddition of Singlet Oxygen to a Chiral Allylic Alcohol. *J. Am. Chem. Soc.* **1999**, *121* (9), 1834–1838.
- (16) Shea, K. E. O.; Foote, C. S. Reactions of TCNJ3 with Isomeric 2,4-Hexadienes. *Tetrahedron Lett.* **1990**, *31* (6), 841–844.
- (17) Zehm, D.; Fudickar, W.; Linker, T. Molecular Switches Flipped by Oxygen. *Angew. Chemie - Int. Ed.* **2007**, *46* (40), 7689–7692.
- (18) Fudickar, W.; Linker, T. Remote Substituent Effects on the Photooxygenation of 9,10-Diarylanthracenes: Strong Evidence for Polar Intermediates. *Chem. Commun.* **2008**, No. 15, 1771.
- (19) Aubry, J. M.; Mandard-Cazin, B.; Rougee, M.; Bensasson, R. V. Kinetic Studies of Singlet Oxygen [4 + 2]-Cycloadditions with Cyclic 1,3-Dienes in 28 Solvents. *J. Am. Chem. Soc.* **1995**, *117* (36), 9159–9164.
- (20) Bagal, S. K.; Davies, S. G.; Lee, J. A.; Roberts, P. M.; Scott, P. M.; Thomson, J. E. Syntheses of the Enantiomers of 1-Deoxyojirimycin and 1-Deoxyaltronojirimycin via Chemo- and Diastereoselective Olefinic Oxidation of Unsaturated Amines. *J. Org. Chem.* **2010**, *75* (23), 8133–8146.
- (21) Clayden, J.; Knowles, F. E.; Baldwin, I. R. The Synthesis of (-)-Isodomoic Acid C. *J. Am. Chem. Soc.* **2005**, *127* (8), 2412–2413.
- (22) Jaramillo, M.; Joens, J. A.; O'Shea, K. E. Fundamental Studies of the Singlet Oxygen Reactions with the Potent Marine Toxin Domoic Acid. *Environ. Sci. Technol.* **2020**, acs.est.9b07380.
- (23) Eske, A.; Goldfuss, B.; Griesbeck, A. G.; de Kiff, A.; Kleczka, M.; Leven, M.; Neudörfl, J.-M.; Vollmer, M. Ene–Diene Transmissive Cycloaddition Reactions with Singlet Oxygen: The Vinylogous Gem Effect and Its Use for Polyoxyfunctionalization of Dienes. *J. Org. Chem.* **2014**, *79* (4), 1818–1829.
- (24) Matsumoto, M.; Yamada, M.; Watanabe, N. Reversible 1,4-Cycloaddition of Singlet Oxygen to N-Substituted 2-Pyridones: 1,4-Endoperoxide as a Versatile Chemical Source of Singlet Oxygen. *Chem. Commun.* **2005**, No. 4, 483.
- (25) Adam, W.; Erden, I. Trapping of Unstable Alpha-Pyrone / Singlet Oxygen Adduct by Reduction with Diazene. *Angew. Chem. Int. Ed. Engl.* **1978**, *17* (3), 211.
- (26) Yong, K. W. L.; Lambert, L. K.; Hayes, P. Y.; De Voss, J. J.; Garson, M. J. Oxidative Processes in the Australian Marine Sponge *Plakinastrella Clathrata*: Isolation of Plakortolides with Oxidatively Modified Side Chains. *J. Nat. Prod.* **2012**, *75* (3), 351–360.

- (27) Dermer, O.; Jenkins, A. Notes: Aldehyde Cotrimers. *J. Org. Chem.* **1959**, *24* (6), 869–869.
- (28) Hoffmann, R.; Woodward, R. B. Selection Rules for Concerted Cycloaddition Reactions. *J. Am. Chem. Soc.* **1965**, *87* (9), 2046–2048.
- (29) O'Shea, K.; Foote, C. S. Quantitative Rearrangement of Monocyclic Endoperoxides to Furans Catalyzed by Co(II). *J. Org. Chem.* **1989**, *54* (14), 3475–3477.
- (30) Gollnick, K.; Griesbeck, A. Interactions of Singlet Oxygen with 2,5-Dimethyl-2,4-Hexadiene in Polar and Non-Polar Solvents Evidence for a Vinylog Ene-Reaction. *Tetrahedron* **1984**, *40* (17), 3235–3250.
- (31) Aubry, J.-M.; Mandard-Cazin, B.; Rougee, M.; Bensasson, R. V. Kinetic Studies of Singlet Oxygen [4 + 2]-Cycloadditions with Cyclic 1,3-Dienes in 28 Solvents. *J. Am. Chem. Soc.* **1995**, *117* (36), 9159–9164.
- (32) Kralj Cigić, I.; Plavec, J.; Možina, S. S.; Zupančič-Kralj, L. Characterisation of Sorbate Geometrical Isomers. *J. Chromatogr. A* **2001**, *905* (1–2), 359–366.
- (33) Nystrom, R. F.; Brown, W. G. Reduction of Organic Compounds by Lithium Aluminum Hydride. II. Carboxylic Acids. *J. Am. Chem. Soc.* **1947**, *69* (10), 2548–2549.
- (34) Zhang, J.; Jiang, L. Acid-Catalyzed Esterification of Zanthoxylum Bungeanum Seed Oil with High Free Fatty Acids for Biodiesel Production. *Bioresour. Technol.* **2008**, *99* (18), 8995–8998.

**CHAPTER 3 FUNDAMENTAL STUDIES OF THE SINGLET OXYGEN
REACTIONS WITH THE POTENT MARINE TOXIN DOMOIC ACID**

3.1. Abstract

Domoic acid (DA), a potent marine toxin, is readily oxidized upon reaction with singlet oxygen ($^1\text{O}_2$). Detailed product studies revealed the major singlet oxygenation reaction pathways were the [2+2] cycloaddition (60.2%) and ene reactions (39.8%) occurring at the Z double bond. Diene isomerization and [4+2] cycloaddition, common for conjugated diene systems, were not observed during the singlet oxygenation of DA. The bimolecular rate constant for the DA reaction with $^1\text{O}_2$ determined by competition kinetics was $5.1 \times 10^5 \text{ M}^{-1} \text{ s}^{-1}$. Based on the rate constant and steady-state concentrations of $^1\text{O}_2$ in surface waters, the environmental half-life of DA due to singlet oxygen-induced transformations is between 5 and 63 days. The $^1\text{O}_2$ reaction product mixture of DA did not exhibit significant biological activity based on ELISA studies indicating singlet oxygenation could be an important natural detoxification process. The characteristic oxidation products can provide valuable markers for the risk assessment of DA contaminated natural waters.



3.2. Introduction

Domoic acid (DA), a powerful neurotoxin, has been isolated from red algae *Chondria armata* (1, 2) and is also produced by the marine diatom *Pseudonitzschia*. (3). Shellfish, clams, and mussels bioaccumulate DA, leading to DA biomagnification through the food chain (3). The first reported incident of human toxic effect induced by DA occurred in Prince Edward Island, Canada in 1987 when three elderly people died and other victims suffered long-term neurological problems (4). Because the victims suffered from memory loss, the term “amnesic shellfish poisoning” (ASP) is used to describe DA toxic effect (4, 5). The ingestion of DA has led to the severe illness and/or death of seals, sea lions, whales, and other mammals worldwide (3). DA contamination of the Pacific Ocean on the west coast of the United States has resulted in numerous closures of the Dungeness crab fisheries with estimated lost incomes up to \$10 million USD per closure (6). The US EPA set a maximum allowed concentration of 20 µg DA per 1 g of seafood (7). DA contaminated water is particularly problematic where water desalination is critical to freshwater supplies, *e.g.*, the desalination plant at El Segundo, CA (8).

The glutamic acid-like moiety is critical for the strong binding of DA to the glutamate receptors in the brain and the heart, resulting in loss of cellular function, damage, and death (3). The conjugation and geometry of the diene functionality have, also, been reported to play an important role in the toxicity of DA. The most toxic isomer of DA possesses a conjugated diene with (*Z*, *E*) geometries (9). In comparison, isodomoic acid C with a non-conjugated diene system, a terminal alkene, and an (*E*) double bond, has 240 fold less affinity for the glutamate receptors compared to DA (9).

Photochemical transformations play important roles in the natural transformation and fate of a wide variety of contaminants and toxins (10). Photoexcited natural chromophoric materials, including dissolved organic matter (DOM), can lead to direct or indirect photochemical reactions through the generation of reactive oxygen species (ROS). In type I photooxidation reactions, an excited photosensitizer can react with a substrate or the solvent producing excited species and radicals, such as hydroxyl radical, $\cdot\text{OH}$, and/or radical ion (11). Alternatively, in type II, photooxidation processes the excited photosensitizer's energy is transferred to molecular oxygen, generating singlet oxygen (11). Electron transfer from the sensitizer to O_2 has also been reported, but this process is considerably less prevalent and has been described as both type II and type I (11). The energy difference between $^1\text{O}_2$ and ground-state O_2 is 94 kJ mol^{-1} (22 kcal mol^{-1}) (12). Representative energies of triplet excited dissolved organic matter ($^3\text{DOM}^*$) are in the range of $180\text{--}320 \text{ kJ mol}^{-1}$ (12). In natural systems, O_2 can readily function as a triplet energy acceptor (12). DA contains a number of functional groups that may be susceptible to photo-transformation. Thus, identification of the photo-transformation pathways and products of DA is required for accurate assessment of the environmental and human health impacts of DA contaminated aquatic systems.

A limited number of studies have been reported on the photoinduced transformations of DA (13–18). The indirect DOM photosensitized degradation of DA was enhanced significantly in the presence of Fe (III) (17). Parker and Mitch demonstrated the photosensitized production of halogen radicals (HRs) by $^3\text{DOM}^*$ increased the rate of the photodegradation of DA (15). Kinetic modeling studies showed the most important HRs

involved in the photodegradation of DA were $\text{Br}_2^{\cdot\cdot}$ and $\text{ClBr}^{\cdot\cdot}$ with estimated bimolecular rate constants of $k_{(\text{Br}_2^{\cdot\cdot}+\text{DA})}=1 \times 10^8 \text{ M}^{-1} \text{ s}^{-1}$ and $k_{(\text{ClBr}^{\cdot\cdot}+\text{DA})}=1.7 \times 10^9 \text{ M}^{-1} \text{ s}^{-1}$ (15). The DOM photosensitized transformation of DA produced complex reaction mixtures which were analyzed by ultra-high-performance liquid chromatography coupled to quadrupole time-of-flight mass spectrometry (UHPLC-QTOF-MS) (16). The study illustrates HRs yielded unique products via hydrogen abstraction from DA ultimately producing hydroperoxides and stable decarboxylated products (16). $^3\text{DOM}^*$ also leads to the photosensitized isomerization of the diene functionality of DA with a bimolecular rate constant of $3.8 \pm 0.2 \times 10^8 \text{ M}^{-1} \text{ s}^{-1}$ (16). Hydroxyl radical, which can be formed during photosensitization processes, reacts with DA with a bimolecular rate constant of $9.22 \pm 0.60 \times 10^9 \text{ M}^{-1} \text{ s}^{-1}$ (19). While a number of hydroxyl radical dominated pathways and products have been proposed (16), detailed kinetic and product studies of the $^1\text{O}_2$ reaction with DA have yet to be reported.

Singlet oxygen is continuously generated during daylight hours in natural surface waters, due to the presence of UV and visible light absorbing components and dissolved O_2 . Singlet oxygen has potential as an oxidant for a solar-based water decontamination and disinfection processes (20, 21) and is also used in a variety of processes from photodynamic cancer treatments (22) to regio or stereoselective steps in the synthesis of natural products (23–26). Singlet oxygen reacts with dienes via [4+2] cycloaddition, ene and/or [2+2] cycloaddition reactions (25). The common [4+2] cycloaddition of $^1\text{O}_2$ yields modestly stable endoperoxides (25). The ene reaction involves the abstraction of an allylic hydrogen by $^1\text{O}_2$ to form the corresponding hydroperoxide, while the [2+2] reaction produces

dioxetanes, which are unstable and typically collapse into their corresponding carbonyl compounds (25). While there is extensive literature on the products and general mechanisms of $^1\text{O}_2$ reactions in organic solvents (23–26), detailed product studies in aqueous media are limited (27, 28).

The natural production of DA occurs during harmful algal blooms along with high levels of chromophoric pigments (CP). In the presence of CP, sunlight, and O_2 , $^1\text{O}_2$ can be continually generated. Singlet oxygen has limited chemical reactivity with amine and carboxylic acid groups but is generally highly reactive towards the electron-rich diene functionality (25). Since the diene functionality plays a critical role in the toxicity of DA, its reaction with $^1\text{O}_2$ may represent an important pathway for the photochemical decontamination of DA. Preliminary results for product studies were obtained by Parekh, P. K, a previous member of Dr. O’Shea’s research group (29). Parekh, P. K. proposed the (*E*)-2-methyl-5-oxopent-3-enoic acid (MOP) from the [2+2], (Figure 3.3), the endoperoxide, from the [4+2], and (HP1), from the ene reaction at proton CH_{3f} as the major product(Figure 1) in a 1:2:2.5 ratio respectively (29).

Building on Parekh, P. K. work, we report the detailed study of $^1\text{O}_2$ reactions with DA, using advanced NMR and LC-HR/MS techniques to elucidate the reaction products and pathways. A modified relative rate method was adapted and used to determine the bimolecular rate constant of the $^1\text{O}_2$ reaction with DA, $k(^1\text{O}_2+\text{DA})$. Reported steady-state concentrations for common reactive species $[\text{RS}]_{\text{ss}}$ along with their bimolecular rate constants were used to assess their contributions in the environmental photodegradation of DA. The biological activity of the reaction product mixture from the reaction of DA with

$^1\text{O}_2$ was evaluated using competitive enzyme-linked immunosorbent assay (cELISA). Our results demonstrate, the singlet oxygenation of DA results predominantly in the oxidative cleavage of the Z double bond, thus eliminating the conjugated diene functionality critical to the toxicity of DA. Kinetic and ELISA studies suggest $^1\text{O}_2$ could be an important and effective oxidant for the natural detoxification of DA.

3.3. Materials and methods

Materials: Domoic acid (CAS Number 14277-97-5, MW: 311.3 g/mol), kainic acid (CAS Number 58002-62-3, MW= 231.3 g/mol), Rose Bengal (RB) (CAS Number 632-69-9), and furfuryl alcohol (FFA) (CAS Number 98-00-0, MW= 98.1 g/mol) were purchased from Sigma Aldrich, and KH_2PO_4 (CAS number 10049-21-5) was purchased from Fisher Scientific. Reagents had purity > 95% and were used without purification. The NMR tubes (OD 5 mm) were purchased from Kimble Chase. Deuterium oxide (D_2O) was purchased from Cambridge Isotope Laboratories Incorporated. The solvents used for the HPLC analysis were acetonitrile and formic acid of LC-grade supplied by Fisher Scientific. Millipore filtered water (18 M Ω) was used for the preparation of aqueous solutions during kinetic studies.

Stock Solutions: A stock solution of 3.21 mM (1 mg/mL) of DA or FFA and 1×10^{-2} mM RB was prepared in D_2O for NMR studies. The samples were diluted in Millipore filtered water (18 M Ω) for HPLC analysis and ELISA assays. A potassium phosphate buffer, 20 mM KH_2PO_4 adjusted with NaOH to pH=8, was used as the solvent to simulate oceanic pH.

Photooxidation: An NMR tube or Pyrex test tube (12 x 75 mm) containing DA or FFA stock solution was submerged in a water-ice bath in a Pyrex windowed Dewar flask to maintain a temperature at ~ 5 °C. Pyrex glass blocks wavelengths < 310 nm. Samples were aligned and irradiated with a 150 W Xenon lamp (Oriel), equipped with a focusing lens fitted with a heat filter containing deionized water.

Control reactions: RB was chosen as the photosensitizer because of its well-established property to produce $^1\text{O}_2$ cleanly. The transformations of DA by direct photolysis (in the absence of a sensitizer) and type I photosensitized reactions (in argon-saturated solution) were negligible. Furthermore, the photooxidative transformation of DA in artificial D_2O seawater (halide containing), prepared as described by Parker and Mitch, under our conditions generated the same products and similar kinetics as in halide free-water (15).

Product studies: The DA stock solution was subjected to photooxidation and monitored by ^1H and COSY NMR spectroscopy at specific irradiation times employing a 400 MHz Bruker NMR spectrometer. A 600 MHz Bruker NMR spectrometer was used to assess product stability, resolve overlapping signals and determine coupling constants.

Synthesis of (2*S*, 3*S*, 4*R*)-4-acetyl-3-(carboxymethyl)pyrrolidine-2-carboxylic acid (PAC): The synthesis of PAC was achieved by Lemieux–Johnson oxidation of approximately 10 mg kainic acid in 0.016 mM osmium tetroxide (OsO_4) and 10 mM periodate (IO_4^-) in D_2O for 5 h (30). The yield for the reaction was nearly quantitative. The product has $\text{M}+1$ ion of 216.0867 m/z and ^1H NMR (D_2O , 400 MHz) signals of 2.12 (dd,

J=5.3, 16.1 Hz, 1 H), 2.20 (s, 3 H), 2.50 (dd, J=11.2, 16.1 Hz, 1 H), 3.00 (m, 1 H), 3.42 (m, 2 H), 3.70 (m, 1 H), and 3.81 ppm (d, J=6.6, 1 H).

HPLC Analysis: A Varian Pro star 210 HPLC equipped with a C18 column (250 × 4.60 mm; 5 μm) and UV diode-array detector (DAD) was used. The flow rate was 1 mL per min of eluent composed of acetonitrile (ACN) and 0.35 μM aqueous formic acid (FA), ACN/FA at a 13:87, v/v ratio, following a procedure modified from Parker and Mitch (15). A 10:90 solvent (ACN/FA) ratio afforded better peak resolution and was employed for product studies. The injection volume was 30 μL and analysis run times were 13 and 25 minutes for 13:87 and 10:90 solvent systems, respectively. The detection wavelength was 242 nm (15). The photooxidations of 200 μM DA were conducted in 12 x 75 mm Pyrex test tubes as reaction vessels and diluted 1:1 with an aqueous solution of FA to improve peak shape.

Kinetics Studies: A relative rate method, summarized below, was used to determine the second-order rate constant for the reaction of $^1\text{O}_2$ with DA, $k_{(^1\text{O}_2+\text{DA})}$ (31). The rate of the reaction of FFA with $^1\text{O}_2$ is well-established and has been extensively used in competition kinetics with a variety of organic compounds (32). The rate equations for the reactions of DA and FFA with $^1\text{O}_2$ are expressed in equations 1 and 2,

$$\frac{dLn(DA)}{dt} = -k_{(^1\text{O}_2+\text{DA})}[^1\text{O}_2] \quad (1)$$

$$\frac{dLn(FFA)}{dt} = -k_{(^1\text{O}_2+\text{FFA})}[^1\text{O}_2] \quad (2)$$

which can be used to derive the kinetic equation 3 based on the ratio of the reactions,

$$\text{Ln} \frac{[DA]_t}{[DA]_0} = \frac{k(^1\text{O}_2+DA)}{k(^1\text{O}_2+FFA)} \text{Ln} \frac{[FFA]_t}{[FFA]_0} \quad (3)$$

Multiplying the slope of the natural log of the $^1\text{O}_2$ degradation rate of FFA versus that of DA by the FFA second-order rate constant, $k(^1\text{O}_2+FFA)$, yields the $k(^1\text{O}_2+DA)$. The value $1.2 \times 10^8 \text{ M}^{-1}\text{s}^{-1}$ has been widely used for the $k(^1\text{O}_2+FFA)$ in these types of kinetic studies (33). Recent work, however, recommends a value of $1.0 \times 10^8 \text{ M}^{-1}\text{s}^{-1}$ for studies in solutions with low ionic strength (34). The latter rate constant was selected for the determination of the rate constant in our study. We found the rate of the reaction of $^1\text{O}_2$ with FFA is much faster than with DA, thus it is impractical to simultaneously monitor these as competing reactions. To address this limitation, the individual rate expressions were considered under identical photooxidative conditions to allow the qualitative assessment of the $k(^1\text{O}_2+DA)$ using the ratio of the observed rates (k_{obs}) of the two reactions, following equation 4.

$$k(^1\text{O}_2+DA) = k_{\text{obs} DA} \frac{k(^1\text{O}_2+FFA)}{k_{\text{obs} FFA}} \quad (4)$$

Application of a steady-state assumption for singlet oxygen, $[^1\text{O}_2]_{\text{ss}}$, yields equation 5 which can be used to extract the half-life of DA upon reaction with $^1\text{O}_2$ ($t_{1/2} (^1\text{O}_2+DA)$). Derivation of equation 5 can be found in the supporting information (SI) (page S15, Derivation S1).

$$t_{1/2} (^1\text{O}_2+DA) = \frac{\text{Ln}(2)}{k(^1\text{O}_2+DA)[^1\text{O}_2]_{\text{ss}}} \quad (5)$$

LC-MS Analysis: The MS data were obtained employing a Surveyor HPLC system equipped with a Dionex Acclaim 120 C18 column (50 x 2.1 mm; 5 μ m). The HPLC system was equipped with a photodiode array (PDA) UV-VIS detector operated at 5 Hz under a full spectrum mode. High-resolution mass spectrometry (HR/MS) detection was performed by a 7 T Bruker Solarix FT-ICR mass spectrometer equipped with an ESI source. The instrument was operated in positive mode, at a resolving power of 500,000 (at $m/z = 400$). The scan range was 100-1000 m/z , and the instrument was internally calibrated using ions from the Agilent ESI tuning mixture.

Biological activity of the domoic acid oxidation reaction mixture: The biological activity of the reaction products was assessed using ELISA assay. Domoic acid ELISA kits were purchased from Mercury Science Product # DAK-36. The quantitative range of the assay was from concentrations of 0.2 to 2.8 nM DA with a linear least-squares regression of 0.9964 and reproducibility within 10 %.

3.4. Results and discussion

Product Studies: For a typical experiment, an oxygen-saturated solution of D₂O containing DA and RB was irradiated in an NMR tube. The reaction with singlet oxygen was monitored by ¹H NMR and HPLC. Control experiments in the absence of oxygen or sensitizer showed insignificant DA transformation from direct photolysis or energy transfer from RB. Singlet oxygenation of DA (3.21 mM) resulted in a mixture of products, defined as DA_{ox}, for the purpose of this study. The characteristic ¹H NMR aliphatic and olefinic peaks of DA disappeared with the simultaneous formation of a complex array of new peaks, illustrated in the supplementary material (Figure 3.1). Parker and Mitch reported fast

reaction rates and unique products for the reactions of DA with HRs generated during photooxidation in seawater (15). To assess the role of HRs under our experimental conditions, the photooxidation reactions were conducted in synthetic D₂O seawater. We observed identical products and similar kinetics for the reactions of ¹O₂ with DA in synthetic seawater in D₂O and in D₂O in the absence of halide ions. These findings indicate that HRs are not involved in the reactions under our photolysis conditions. Previous studies showed that increasing the ionic strength (IS) of the solutions can also stabilize ³DOM* and offset the lower concentrations of dissolved oxygen in synthetic sea-water (35). While the past studies did not address the quenching of ¹O₂ by halogen ions, such as Cl⁻, $k_q(^1O_2+Cl^-) = 1000 \text{ M}^{-1}$ (36), the quenching effect may have also been balanced by the reported IS effect. Analogously, the stabilization of RB in our experiments may explain the observed similar kinetics with and without halogen ions.

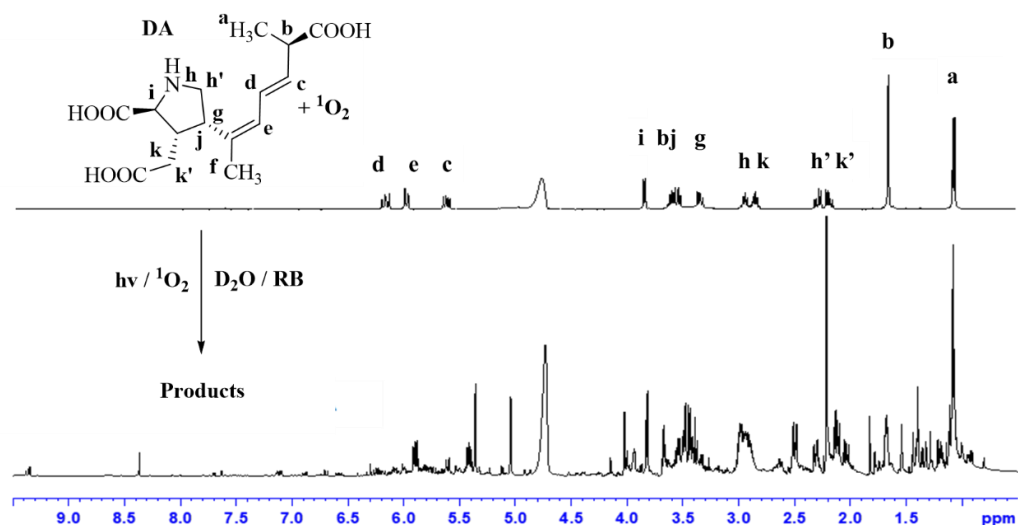


Figure 3.1. ¹H NMR spectra of Domoic acid and singlet oxygenated Domoic acid. ¹H NMR spectrum of 3.21 mM DA (top) and after 25 minutes of reaction with ¹O₂ reaction (bottom). The solutions were prepared with 10 μM RB in D₂O, buffered at pH 8 in an NMR tube, constantly purged with oxygen, and irradiated with a 150 W Xenon lamp while maintaining the temperature at ~ 5 °C. The NMR spectra were recorded in the 400 Bruker NMR spectrometer.

Notable changes in the ¹H NMR spectrum of DA upon reaction with ¹O₂, include the disappearance of the methyl singlet, CH_{3f}, at 1.6 ppm with the complementary formation of a singlet at 2.2 ppm. The doublet at 1.1 ppm corresponding to CH_{3a} in DA did not appreciably shift upon reaction with ¹O₂. The signals for the olefinic protons H_d, H_e, and H_c decreased, with the growth of two doublets of doublets at 5.9 ppm, *J*=7.6, 15.5 Hz and 5.4 ppm, *J*=8.2, 15.4 Hz. Further discussion and detailed assignment of the NMR results are presented after HPLC and MS results.

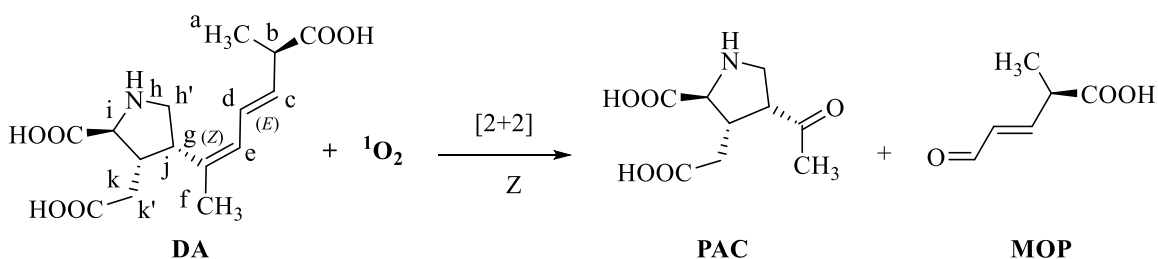
Based on the integration of the corresponding HPLC peaks, 17.0 % residual DA was present in the DA_{ox} product mixture with the characteristic retention time of 19.29

minutes and UV absorbance ($\lambda_{\text{max}} = 242$ nm). Three major product peaks were observed with retention times of 4.92 (60.2%), 18.23 (9.7%) and 20.29 (30.1%) minutes and λ_{max} at 226, 235 and 235 nm, respectively. The most prevalent M+1 peaks for the three major products were 216.0867, 282.1333 and 282.1333 m/z, in the order of retention times stated above.

The reactions products were characterized by HPLC and MS results in combination with careful analysis of the ^1H and COSY NMR spectra as detailed below. The [4+2] reaction pathway leading to an endoperoxide with a cyclic *cis* alkene is among the most common pathways for the reaction of conjugated dienes with singlet oxygen (37). Parekh, P. K. reported the EP as the second major product of the reactions (29). However, the ^1H NMR of the proposed molecule had trans coupling for the olefinic protons (dd at 6.87 ppm, $J=7.3, 15.7$ Hz, and integration of 0.27, and 6.71 ppm, $J=15.8$ Hz and integration of 0.2315.8 Hz. (29). Similarly, we did not observe any characteristic signals with a *cis* proton-proton coupling constant ($J_{\text{cis}} = 10\text{-}12$ Hz) in the olefinic region, indicating that the endoperoxide formed in the reaction of singlet oxygen and DA. The lack of endoperoxide formation is likely due to the steric inhibition of the *s-cis* confirmation of the *Z, E* diene in DA required for the [4+2] cycloaddition reaction pathway. While singlet oxygen-induced $Z \rightleftharpoons E$ isomerization of dienes has been reported in organic solvents (38), the ^1H NMR shows the diene in DA does not undergo isomerization under our photochemical conditions.

Singlet oxygen can react with olefins by [2+2] reaction pathways to form dioxetanes, which generally are unstable and collapse to the corresponding carbonyl compounds, ultimately resulting in the oxidative cleavage of the olefin. In the case of DA,

the [2+2] reaction could occur at the *E* or *Z* double bond of the diene. The singlet formation at 2.2 ppm in the proton NMR spectrum is consistent with the expected chemical shift and multiplicity of the methyl ketone PAC and MOP resulting from the [2+2] addition of $^1\text{O}_2$ to the *Z* double bond of DA, shown below in Scheme 3.1.



Scheme 3.1. The [2+2] cycloaddition reaction of $^1\text{O}_2$ with the *Z* double of the diene functionality of Domoic acid. PAC and MOP, (*R*, *E*)-2-methyl-5-oxopent-3-enoic acid are the products of the reaction.

Parekh, P. K. attempted several strategies to oxidize kainic acid to produce the authentic standard of PAC (29). However, the attempts were unsuccessful (29). We carried out the Lemieux–Johnson oxidation of kainic acid was used to synthesize an authentic standard of PAC. A comparison of the NMR spectral features of the DA_{ox} and the PAC authentic standard reveals a direct correlation between the ^1H NMR spectra of the two samples (Figure 3.2.). PAC had a retention time of 4.92 min and λ_{max} of 226 nm under the 90:10 HPLC solvent system described in the methods, and it was observed in ~ 60 % yield in the DA_{ox} reaction mixture using the peak area of the chromatogram. LC-MS/MS shows an $\text{M}+1$ signal at 216.0866 m/z in the analysis of the PAC authentic standard and the DA_{ox} . Based on the absence of products with corresponding MS signals and characteristic aldehyde peaks in the ^1H NMR spectrum of DA_{ox} , we conclude singlet oxygen does not mediate oxidative cleavage via 2+2 addition at the *E* double bond in DA. The results

provide convincing evidence of the [2+2] pathway occurring at the more electron-rich trisubstituted *Z* double bond was the major reaction pathway for the singlet oxygenation of DA.

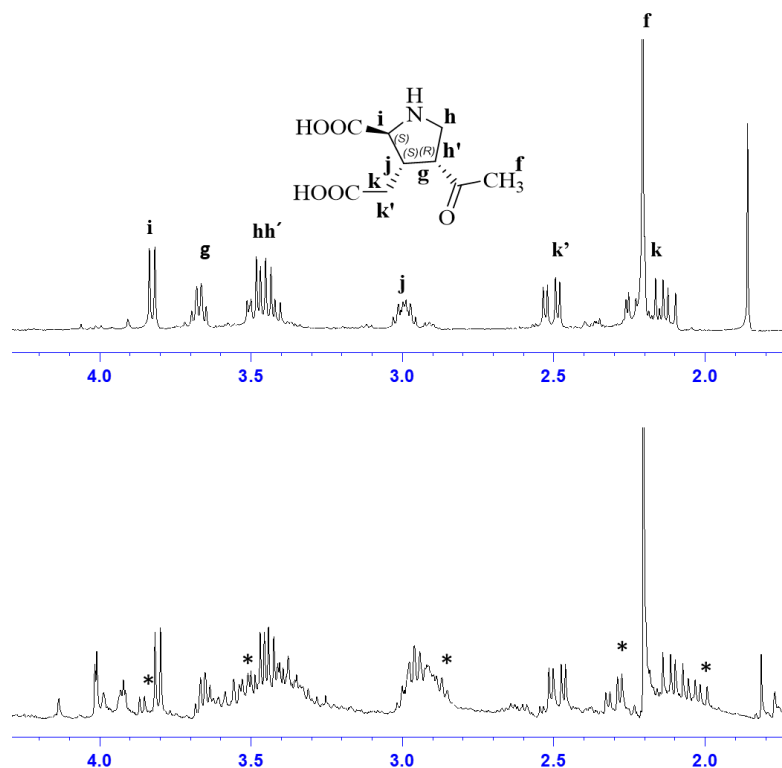


Figure 3.2. ¹H NMR of 10 mg (*2S*, *3S*, *4R*)-4-acetyl-3-(carboxymethyl)pyrrolidine-2-carboxylic acid, PAC, authentic per mL of D₂O standard (top). ¹H NMR of 25 min ¹O₂ reaction with 3.21 mM DA (bottom). The peaks labeled with * are assigned to the ene reaction products. The 3.21 mM DA solution was prepared with 10 μM RB in D₂O, buffered at pH=8 in an NMR tube, continuously purged with oxygen, and irradiated with at 150 W Xenon lamp while maintaining the temperature at ~ 5 °C. The NMR spectra were recorded in the 400 Bruker NMR spectrometer.

The observed major product, PAC, offers an attractive marker to monitor the singlet oxygen reaction with DA in natural settings using equation 6.

$$[\text{DA}] \text{ } ^1\text{O}_2 = [\text{DA}]_o - [\text{PAC}]x\left(\frac{100}{60.2}\right) \quad (6)$$

Where $[\text{DA}] \text{ } ^1\text{O}_2$ represents the degree of the singlet oxygenation of DA, $[\text{DA}]_{\text{ox}}$, represents the initial DA concentration. Initially, we proposed the ^1H NMR signals labeled * in Figure 3.2 are consistent with the isomer of PAC resulting from the epimerization of PAC- H_g . Attempts to epimerize PAC- H_g via a one-pot oxidation-base-catalyzed epimerization reaction produced the quantitative oxidation of the methyl ketone to a carboxylic acid. The transformation of PAC under our conditions may be due to the presence of residual I_2 impurities from the periodate reaction, which could lead to oxidation of the methyl ketone through an iodoform type reaction mechanism. Alternatively, oxidation of methyl ketones by periodate under alkaline conditions has also been reported (39)

The ^1H NMR spectrum of DA_{ox} has the characteristic signals of MOP, formed from the collapse of the dioxetane at the *Z* double bond (complementary to PAC). The signal MOP- H_e is assigned to the observed aldehyde doublet at 9.3 ppm, $J=8.0$ Hz, correlating to a MOP- H_d at 7.1 ppm, $J=8.0$, 16 Hz, which in turn correlates to a MOP- H_c dd at 6.6 ppm, $J=8.0$, 15.6 Hz. Parekh, P. K also observed MOP in her studies; however, as a minor product (29). In the present work, we observed that during the initial stages of photooxidation of DA, MOP was observed in parallel concentration to PAC using the integration of the ^1H NMR signals. As the reaction proceeded, the MOP:PAC ratio gradually decreased (Figure 3.3).

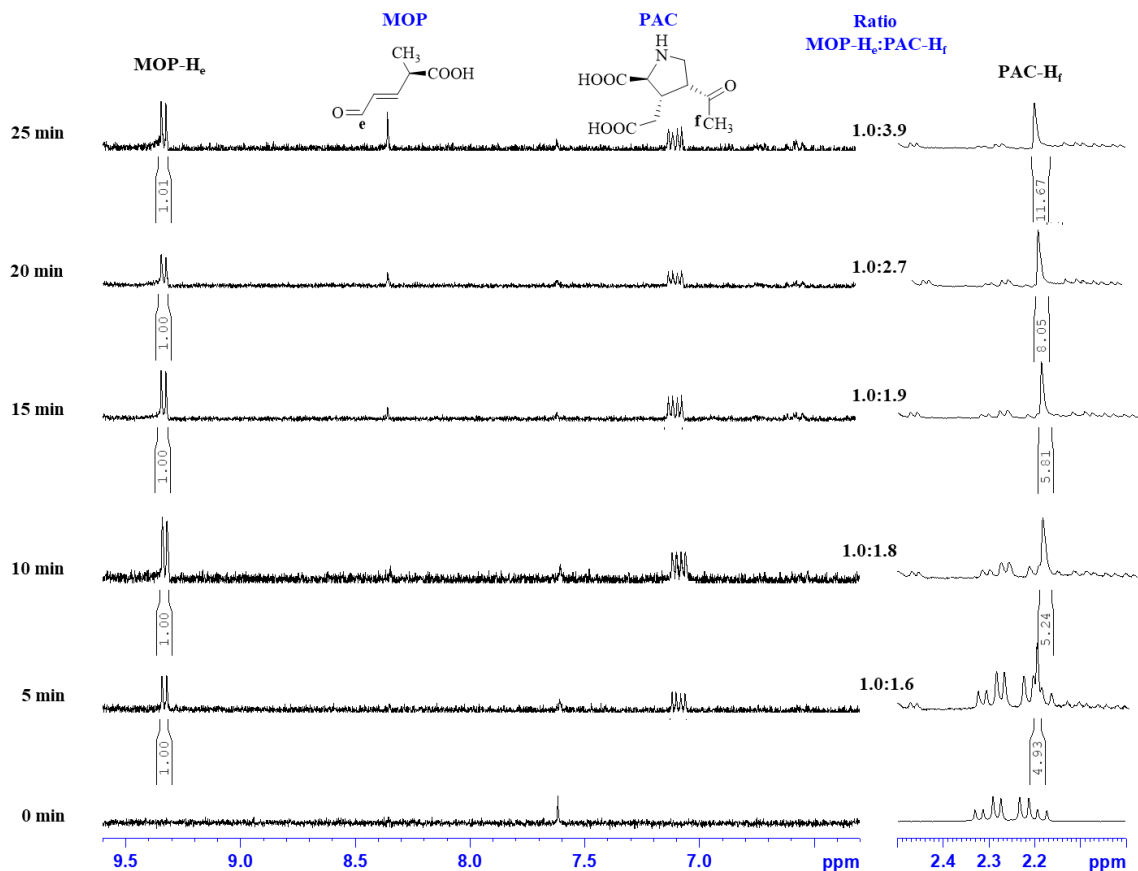


Figure 3.3. Time profile of aldehyde and aliphatic regions of the ^1H NMR spectrum of singlet oxygenated Domoic acid. The ratio of MOP- H_e and PAC- H_f signals over the course of the reaction is shown. The integration of PAC- H_f corresponds to the 3 hydrogens of the methyl group. The solutions were prepared with 10 μM RB in D_2O , buffered at pH ~ 8 in an NMR tube, constantly purged with oxygen, and irradiated with a 150 W Xenon lamp temperature while maintaining the temperature at $\sim 5^\circ\text{C}$. The NMR spectra were recorded in the 400 Bruker NMR spectrometer.

The spectrum of DA_{ox} after 1 hour in the dark shows significant tautomerization of MOP to the enol form, shown below in Figure 3.4 and referred to as enol-MOP. The tautomerization of MOP extends the conjugation of the molecule and therefore enhances the stability of the enol form relative to the keto form. The ^1H NMR spectrum of DA_{ox} after 1 hour minus the spectrum after 3 hours in the dark shows the complete disappearance of

MOP. The peaks assigned to enol-MOP [Enol-MOP H_d dd at 6.9 ppm ($J = 8.9, 15$ Hz), Enol-MOP H_c d at 6.7 ppm ($J = 15$), the assignment Enol-MOP H_e was not possible due to overlapping olefinic signals] were observed after 3 hours in the dark. Figure 3.4 below summarizes these results.

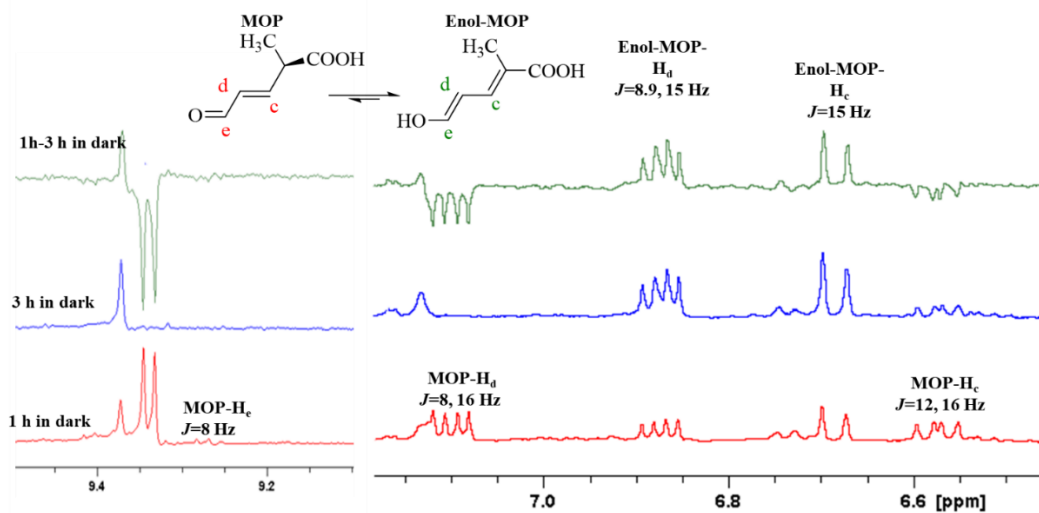


Figure 3.4. The ¹H NMR time profile of the singlet oxygenation of Domoic acid showing characteristic (*R, E*)-2-methyl-5-oxopent-3-enoic acid, MOP, and enol-(*R, E*)-2-methyl-5-oxopent-3-enoic acid, enol-MOP signals. Spectrum (bottom) was recorded 1 hour in the dark after the photooxidation. Spectrum (middle) was taken 3 hours in the dark the photooxidation. The spectrum at the top is the difference between the bottom and middle spectra. The signals for the enol tautomer, enol-MOP, are labeled. The NMR spectra were recorded in the 600 Bruker NMR spectrometer.

The cyclization of enol-MOP may form 3-methyl-2H-pyran-2-one (Lactone-MOP). The Lactone-MOP is locked in the *s-cis* diene conformation, which can readily undergo [4+2] cycloaddition with ¹O₂. For comparison, the endoperoxide produced by the ¹O₂ reaction with a similar cyclic lactone, 2-pyrone produced 4-oxo-2-pentenoic acid and CO₂ at 30 °C (40). Lactone-MOP differs from 2-pyrone by a methyl group CH₃ at the α position

instead of an H. The electron-donating CH_3 is expected to enhance the $^1\text{O}_2$ reaction compared to 2-pyrone. We, thus, propose that the [4+2] reaction of MOP-lactone with singlet oxygen can yield an endoperoxide that could readily rearrange to produce the stable (Z)-4-oxopent-2-enal and CO_2 . The details for the proposed reaction pathway can be found in Figure 3.5.

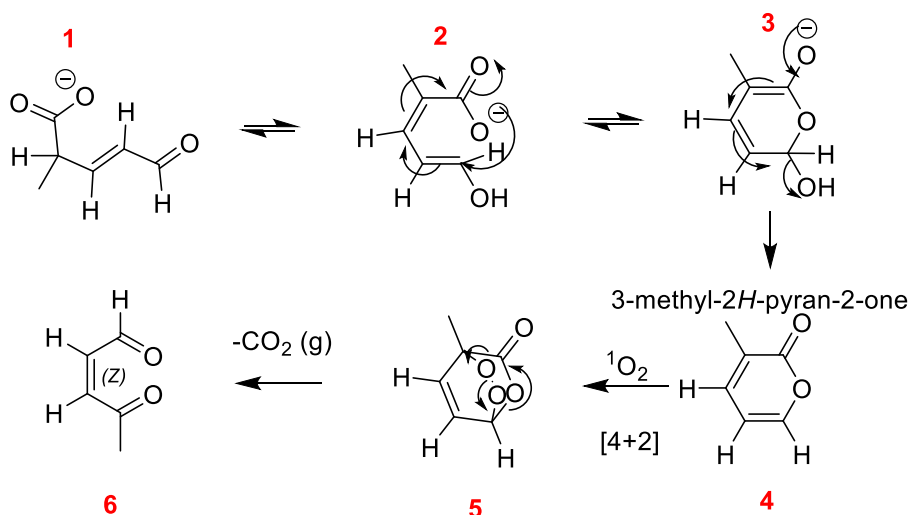


Figure 3.5. Proposed Transformation of (R, E)-2-methyl-5-oxopent-3-enoic acid (MOP) under $^1\text{O}_2$ reaction conditions. Proposed MOP (1) enolization to molecule 2 extends conjugation, and subsequently, intermolecular cyclization and dehydration produce 3-methyl-2H-pyran-2-one (4), which is locked in an s-cis conformation, which is highly susceptible to [4+2] cycloaddition of $^1\text{O}_2$. The resulting 5 can decompose to CO_2 and (Z)-4-oxopent-2-enal.

The remaining two products observed in the HPLC chromatogram had retention times of 18.23 (9.7 %) and 20.29 (30.1%) minutes and strong M+1 signals at 282.1333 m/z. Based on this information, along with the detailed interpretation of NMR presented below, we assigned these two products as ene products. The signals in ^1H NMR include a

doublet of doublets at 2.0 and 2.3 ppm in the DA_{ox} mixture with approximately in a 1:2 peak area ratio compared to PAC based on the NMR integration (Figure 3.6).

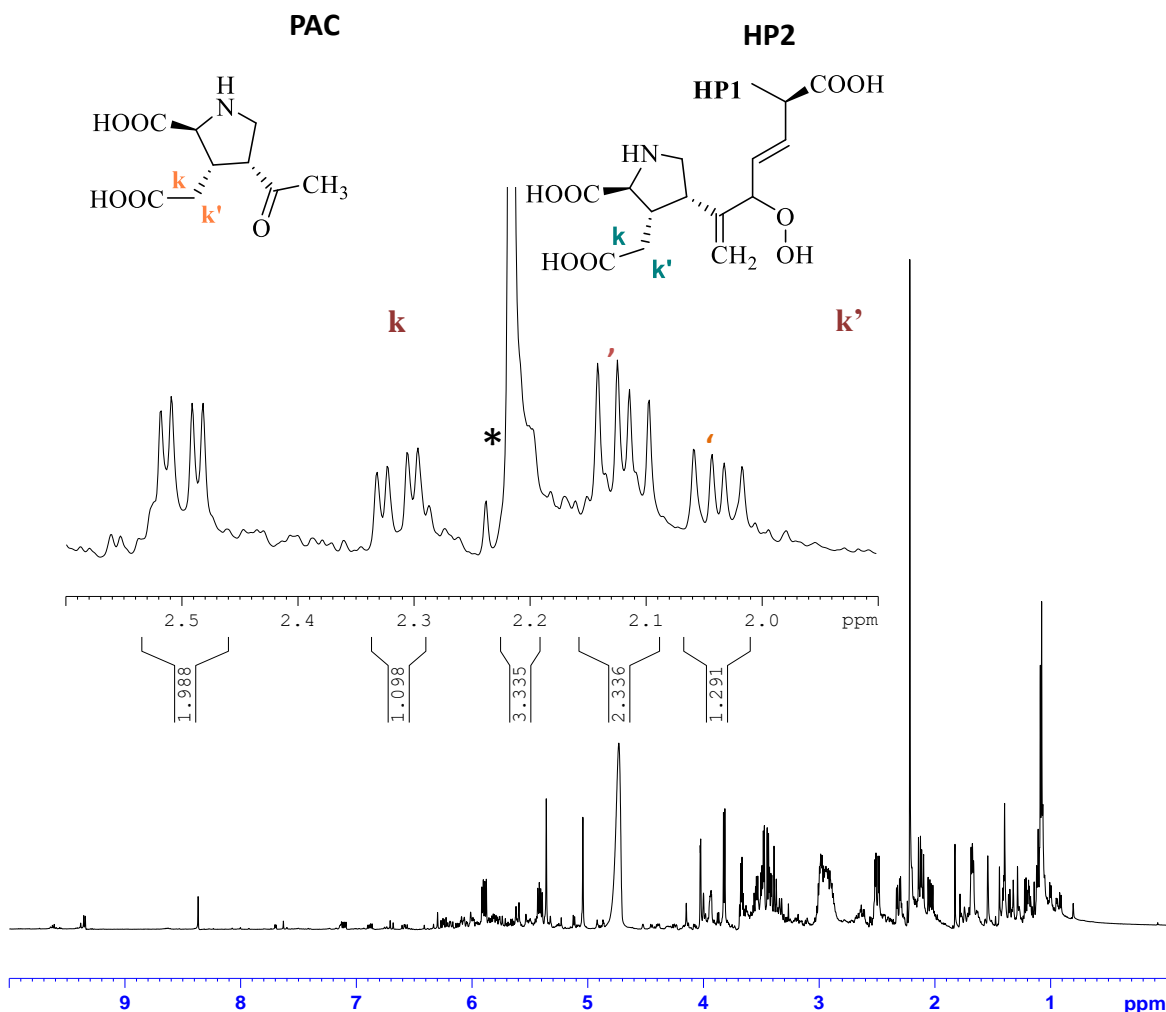


Figure 3.6. ¹H NMR spectra of singlet oxygenated Domoic acid illustrating the integration ratio of (2*S*, 3*S*, 4*R*)-4-acetyl-3-(carboxymethyl)pyrrolidine-2-carboxylic acid (PAC) to (2*S*, 3*S*, 4*S*)-4-((6*R*, *E*)-6-carboxy-3-hydroperoxyhepta-1,4-dien-2-yl)-3-(carboxymethyl)pyrrolidine-2-carboxylic acid (HP1). The solutions were prepared in 10 μM Rose Bengal in D₂O, buffered at pH ~ 8 in an NMR tube, constantly purged with oxygen and irradiated with a 150 W Xenon lamp temperature while maintaining the temperature at ~ 5 °C. The NMR spectra were recorded in the 400 Bruker NMR spectrometer.

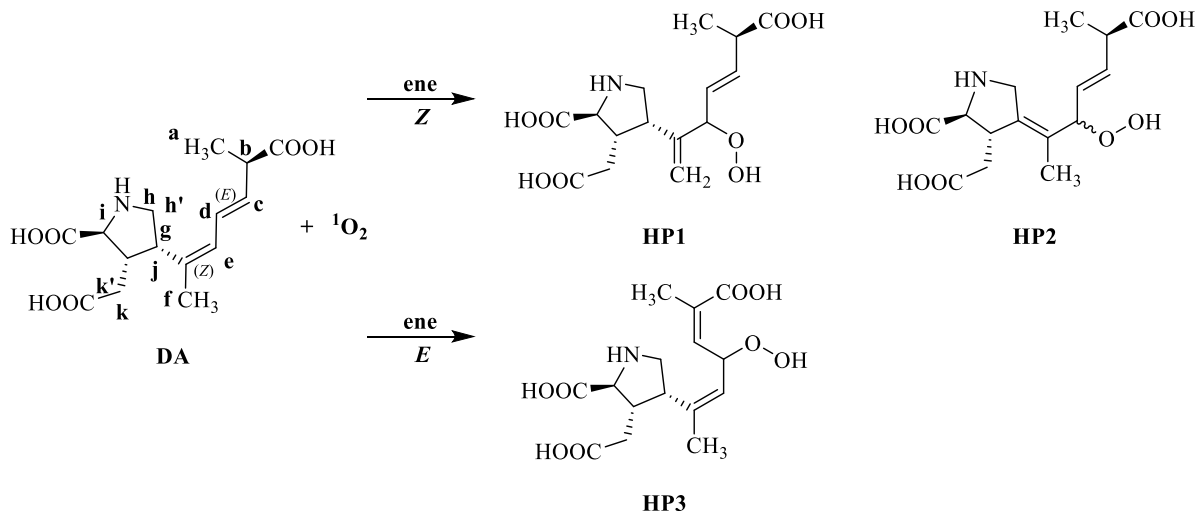
The product with a retention time of 20.29 min in the HPLC chromatogram, also, exhibited a 1:2 peak area ratio compared to PAC (Table 3.1).

Table 3.1. Summary of HPLC and LC-HR/MS analyses of Domoic acid and major products of singlet oxygenated Domoic acid

Molecule	Peak Area at λ_{\max}	Percentage (%)	λ_{\max}	Retention Time (min) in HPLC	M+1 (m/z) (HRLC-MS)
DA	3.4	17	242	19.29	312.1447
PAC	9.9	50	226	4.92	216.0867
HP1	5	25	235	20.29	282.1333
HP2	1.7	9	235	18.23	282.1333

The solutions were prepared with 10 μ M Rose Bengal in D₂O, buffered at pH ~ 8 in an NMR tube, constantly purged with oxygen, and irradiated with a 150 W Xenon lamp while maintaining the temperature at ~ 5 °C. Reaction and analytical conditions are detailed in text S1, S3 and S4.

The ene reaction pathways common to singlet oxygen require allylic hydrogens. DA contains three different allylic hydrogens, H_b, H_f, and H_g. The ene reaction at the *Z* olefin can produce HP1, and HP2, while reaction at the *E* olefin would yield HP3, as defined below (Scheme 3.2).



Scheme 3.2. The ene reaction of $^1\text{O}_2$ pathway at the E and Z double of the diene functionality of Domoic acid. HP1 ((2S,3S,4S)-4-((6R,E)-6-carboxy-3-hydroperoxyhepta-1,4-dien-2-yl)-3-(carboxymethyl) pyrrolidine-2-carboxylic acid) and HP2 ((2S,3S,Z)-4-((6R,E)-6-carboxy-3-hydroperoxyhept-4-en-2-ylidene)-3-(carboxymethyl)pyrrolidine-2-carboxylic acid) are the products of the reaction at the Z double bond. HP3, ((2S,3S,4S)-4-((2Z,5E)-6-carboxy-4-hydroperoxyhepta-2,5-dien-2-yl)-3 (carboxymethyl)pyrrolidine-2-carboxylic acid) was not observed.

The ene reaction involving the proton abstraction of the H_f yields a hydroperoxide labeled HP1 illustrated in Scheme 3.2. The characteristic peaks assigned to HP1 observed in the ^1H NMR spectrum included two doublets of doublets with *trans* coupling constants in the olefinic region at HP1- H_c 5.9 ppm, $J=7.7, 15.5$ Hz and HP1- H_d 5.4 ppm, $J=8.2, 15.4$ Hz in the ^1H NMR spectrum of DA_{ox} . Parekh, P. K also proposed HP1 as one of the products for the reactions (29). However, our interpretation of ^1H NMR for HP1 is very different. The ^1H NMR signals and splitting patterns from the azolidine rings of HP1 and in PAC should be similar with the exception of small differences in chemical shifts. The signals labeled * in Figure 3.2 were assigned to HP1. In addition, two broad singlets in the olefinic region

characteristic of a terminal alkene and assigned to HP1-H_f based correlations in the COSY NMR spectrum of DA_{ox} are shown in Figure 3.7.

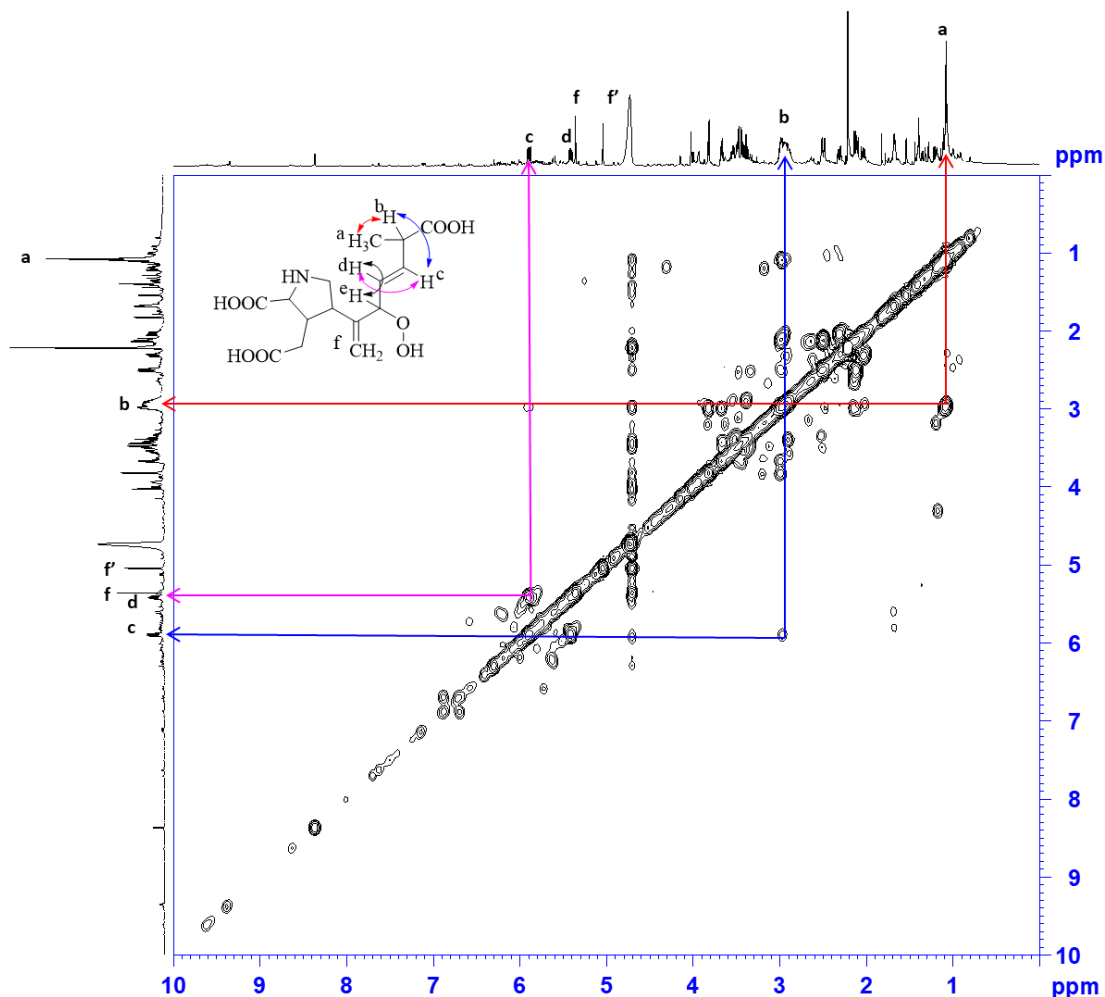


Figure 3.7. COSY NMR of singlet oxygenated Domoic acid. The proton correlations for the ene product, HP1 is shown. Protons in the azolidine ring are not shown for simplicity. HP1-H_e chemical shift is expected to be around 5 ppm, which coincides with the water peak. The solutions were prepared with 10 μ M Rose Bengal in D₂O, buffered at pH ~ 8 in an NMR tube, constantly purged with oxygen and irradiated with a 150 W Xenon lamp temperature while maintaining the temperature at ~ 5 °C. The NMR spectra were recorded in the 400 Bruker NMR spectrometer.

In comparison, isodomoic acid C exhibits analogous signals for its terminal alkene group (41). In addition, the COSY NMR spectrum of DA_{ox} shows individual correlations among protons HP1-H_a ⇔ HP1-H_b ⇔ HP1-H_c ⇔ HP1-H_d unique to HP1 and HP2, which would be absent for HP3. Based on the absence of characteristic signals for HP3 (Scheme 3.2) in DA_{ox}, the presence of HP3 in the reaction mixture is ruled out.

The product assigned HP1 (30.1%) has LC-HR/MS spectrum with four major fragments at 344.1073, 300.1435, 282.1329, and 198.0706 m/z. The LC-HR/MS spectrum of the product with a peak at 18.3 minutes in HPLC (9.7 %) exhibited the same four major fragments (Figure 3.8). The λ_{\max} of both HP1 and the product with a peak at 18.3 min in HPLC (9.7 %) were slightly blue-shifted to 235 nm relative to the λ_{\max} of DA=242 nm. The chromophores in these products absorbed higher energy wavelengths than DA. Indicating a change in the conjugation and/or bonding when compared to DA, but similar conjugation and/or bonding when compared to each other. This information illustrates the structural similarity among these molecules consistent with the proposed products HP1 and HP2 shown in Scheme 3.2.

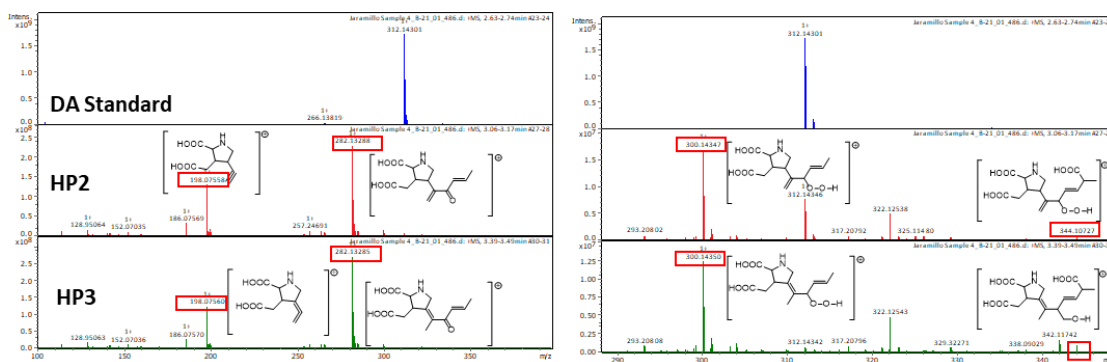


Figure 3.8. LC-HR/MS spectra of singlet oxygenation of Domoic acid and Domoic acid after singlet oxygenation. The proposed fragmentation pattern for HP1 and HP2. LC-HR/MS of 32.1 μM DA Standard (Top) LC-HR/MS of 1:100 dilution of 25 min $^1\text{O}_2$ reaction with 3.21 mM DA, HP1 (middle), and HP2 (bottom). Left to right are squared the proposed fragmentation patterns for HP1 and HP2. The solutions were prepared in 10 μM Rose Bengal in D_2O , buffered at pH ~ 8 in an NMR tube, constantly purged with oxygen, and irradiated with a 150 W Xenon lamp while maintaining the temperature at $\sim 5^\circ\text{C}$. The MS data were obtained employing a Surveyor HPLC for chromatographic separation, and HR/MS detection was performed by a 7 T Bruker Solarix FT-ICR mass spectrometer equipped with an ESI source.

Biological Activity: DA_{ox} was diluted to ppb levels and analyzed using cELISA assay. The observed rate of disappearance of DA was $6.8 \times 10^{-5} \text{ s}^{-1}$ using ELISA, which is in reasonable agreement with the HPLC determination, $4.4 \times 10^{-5} \text{ s}^{-1}$. The ELISA results indicate the major DA singlet oxygenation by-products do not bind to the anti-DA antibodies in the assay. Therefore, these by-products do not possess the same type of biological activity as DA. Further biological, either cellular or systemic assays, are needed to confirm or define the overall toxicity of the DA_{ox} .

Kinetic Studies: The fundamental kinetic parameters for the singlet oxygenation of DA are important to assess the environmental fate of DA and the possibility of using $^1\text{O}_2$ as a detoxification agent for water contaminated with DA. Competition kinetics

between DA and FFA for the reaction with $^1\text{O}_2$ were used to determine $k(^1\text{O}_2+\text{DA})$. The observed rates at 5 °C for the reaction of $^1\text{O}_2$ with FFA and DA were $8.6 \pm 0.16 \times 10^{-3} \text{ s}^{-1}$ and $4.4 \pm 0.06 \times 10^{-5} \text{ s}^{-1}$, respectively producing a $k(^1\text{O}_2+\text{DA})=5.1 \times 10^5 \text{ M}^{-1} \text{ s}^{-1}$ at 95 % confidence level. It is important to note that the primary uncertainty in our calculations arises from $k(^1\text{O}_2+\text{FFA})=1.0 \pm 0.6 \times 10^8 \text{ M}^{-1}\text{s}^{-1}$. These reaction rates are not expected to have a significant temperature dependence (34). Our results show the reaction of $^1\text{O}_2$ with FFA is approximately 200 times faster than the reaction of $^1\text{O}_2$ with DA. This observation is consistent with our mechanistic assessment and product assignment. The main pathway for the reaction $^1\text{O}_2$ with FFA is the [4+2] cycloaddition, which is generally faster than the [2+2] and ene pathways (42). The major processes involved in the reaction of $^1\text{O}_2$ with DA established from our product studies are the [2+2] cycloaddition and the ene reaction, which is consistent with the slower reaction compared to the reaction of $^1\text{O}_2$ with FFA.

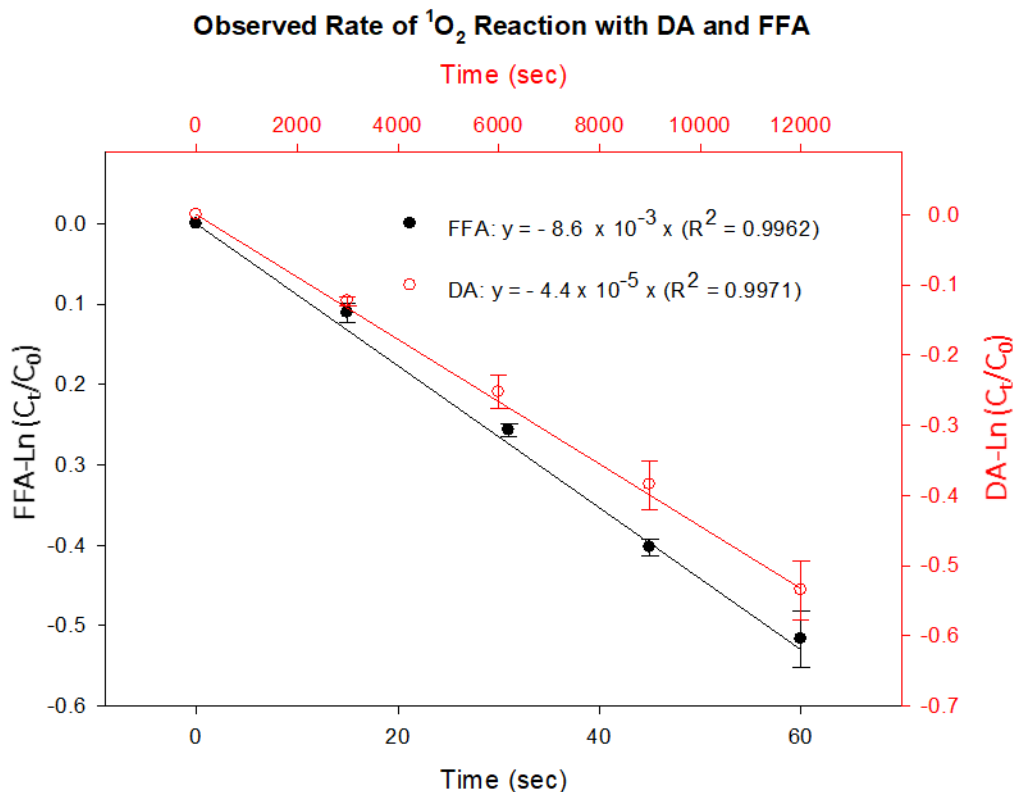
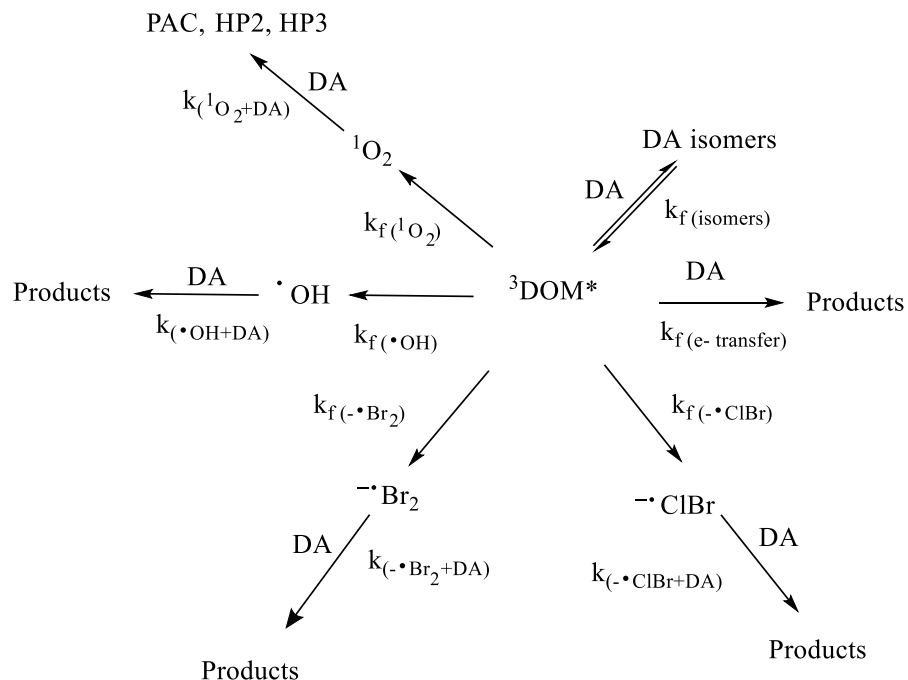


Figure 3.9. Red and black circles represent the rate of singlet oxygenation of 200 μM of Domoic acid and FFA. The solutions were prepared in 10 μM RB Millipore filtered water (18 $\text{M}\Omega$) buffered by 20 mM KH_2PO_4 at $\text{pH}=8$. The photochemical reaction was carried out in a Pyrex test tube (12 x 75 mm) and constantly purged with oxygen. A 150 W Xenon lamp equipped with a water-filled Pyrex filter, was used for irradiation at a reaction temperature of $\sim 5^\circ\text{C}$. The reactions were monitored using the Varian Pro star 210 HPLC.

A summary of the possible reactions of DA with the reactive species (RS) generated by photosensitized processes reported in natural aqueous systems is illustrated in Scheme 3.3. The photochemical half-life of DA can be calculated using equation 5 and the reported steady-state concentrations of $^1\text{O}_2$ [$^1\text{O}_2$]_{ss}, or other RS such as $\cdot\text{OH}$, [$\cdot\text{OH}$]_{ss}, halogen radicals, [HR]_{ss} and $^3\text{DOM}^*$, [$^3\text{DOM}^*$]_{ss}, in sunlit surface waters to assess the environmental importance and the role of each RS. The steady-state concentrations of RS, [RS]_{ss} are highly dependent on the specific environmental or laboratory conditions,

including concentration DOM, quality of DOM, wavelengths of irradiation, and light intensity (12, 15, 32, 43).



Scheme 3.3. Major photosensitized transformations of Domoic acid

Burns *et al.* reported a photosensitized half-life for DA in the range of 12 - 34 hours in synthetic seawater solutions of DOM from Suwanee River (SR) (44). However, the RS involved in the photochemical transformation of DA was not elucidated in this particular study. There are also reports of diene isomerizations via energy transfer from $^3\text{DOM}^*$ (12). DA photoisomerization is reported to account for approximately 30 % of the total photo-induced processes in synthetic seawater solutions (15). Using the reported photoisomerization rate constant of DA, $k_{f(\text{isomers})}=3.6 \times 10^8 \text{ M}^{-1}\text{s}^{-1}$ (16) and 30 % of the generalized environmental range of $[\text{}^3\text{DOM}^*]_{\text{ss}}$ (1.00 to $0.01 \times 10^{-12} \text{ M}$) (12) the half-life of

DA would be between 2 hours and 7 days. The relatively short photosensitized half-lives reported by Burns *et al.* could be due to energy transfer from $^3\text{DOM}^*$ to DA leading to diene isomerization. Since the isomers of DA are also highly toxic and dissolved O_2 is inversely correlated to the initial rate of the formation of DA isomers (16), it is important to assess the degree of other photochemical reactions outlined in Scheme 3.3.

Based on rate constants in the literature under relevant environmental conditions, the $t_{1/2} (^1\text{O}_2 + \text{DA})$ could range from hours to years (Table 3.2.). Application of available $[^1\text{O}_2]_{\text{ss}}$ and $[\cdot\text{OH}]_{\text{ss}}$ values for coastal conditions yielded $t_{1/2}$ values for DA of 63 and 29 days for degradation from $^1\text{O}_2$ and $\cdot\text{OH}$, respectively. These relatively long half-life values are due to the generally low steady-state concentrations of $^1\text{O}_2$ and $\cdot\text{OH}$ in marine environments with low DOM concentrations. However, under bloom conditions, O_2 concentrations can be expected to be elevated at the surface due to superior photosynthetic activity. As mention earlier, O_2 is capable of accepting energy from most $^3\text{DOM}^*$ moieties leading to the generation of $^1\text{O}_2$ (12). Also, during algal blooms, large amounts of marine DOM are produced, including pigments, such as chlorophyll, and particulate organic matter (POM). The photosensitized generation of $^1\text{O}_2$ extracellularly by algal cultures, principally by chlorophyll sensitization (45) and intracellularly by porphin-like sensitizers, have been recorded (46). $[^1\text{O}_2]_{\text{ss}}$ was produced up to $0.576 \pm 0.052 \times 10^{-12}$ M in the extracellular matrix of *C. reinhardtii* algal culture under simulated sunlight (47). The authors also reported the apparent quantum yield for $^1\text{O}_2$ during the algal exponential phase and late stationary phases were similar to SR DOM solutions (47). A recent study demonstrated $[^1\text{O}_2]_{\text{ss}} = 3 \times 10^{-12}$ M using hydrophobic probes with the concentrations of $^1\text{O}_2$ having a

“sigmoidal” profile with the highest values in the middle of the DOM particle and lowest values in the bulk solution (48). Large amounts of marine POM and DOM are produced during algal blooms, and the highest [DA] is found in the particulate fraction of DOM where the $[^1\text{O}_2]_{\text{ss}}$ may resemble the steady-state concentrations recorded with hydrophobic probes (49). Table 3.2 summarizes the $t_{1/2}$ of DA based on the reaction with $^1\text{O}_2$ and the $t_{1/2}$ of DA based on the reaction with other common RS.

Table 3.2. The half-life of Domoic acid based on the reaction with reactive species			
Reactive species, conditions	[RS] _{ss} (M)	$t_{1/2}$	Ref.
$[^1\text{O}_2]_{\text{ss}}$ (M), costal	2.5×10^{-13}	63 days	(32)
$[^1\text{O}_2]_{\text{ss}}$ (M), algal cultures	5.8×10^{-13}	27 days	(47)
$[^1\text{O}_2]_{\text{ss}}$ (M), hydrophobic probe and Aldrich humic acid	3.0×10^{-12}	5 days	(48)
30 % $[^3\text{DOM}^*]_{\text{ss}}$ (M), generalized environmental range	$1.0 - 0.01 \times 10^{-12}$	2 hours-7 days	(12)
$[\text{Br}_2\cdot^-]_{\text{ss}}$ (M), kinetic modeling estimated range	$3.2 - 0.81 \times 10^{-14}$	3 - 10 days	(15)
$[\text{ClBr}^-]_{\text{ss}}$ (M), kinetic modeling estimated range	$1.2 - 0.3 \times 10^{-14}$	9 hours - 2 days	(15)
$[\cdot\text{OH}]_{\text{ss}}$ (M), costal	3.0×10^{-17}	29 days	(50)
$[\cdot\text{OH}]_{\text{ss}}$ (M), midday, June, sunlight 1 kWm^{-2} with DOM	2.5×10^{-17}	35 days	(19)
$[\text{DA}]_0=96 \mu\text{M}$, $[\text{Fe(III)}]$, $[\text{PO}_4^{3-}]$ and [DOM]	N/A	12 - 36 hours	(17)

Calculations are based on the bimolecular rates constants $k(^1\text{O}_2+\text{DA}) = 5.1 \times 10^5 \text{ M}^{-1}\text{s}^{-1}$ (this work), $k(\cdot\text{OH}+\text{DA}) = 9.22 \times 10^9 \text{ M}^{-1}\text{s}^{-1}$ (19) and $k_{\text{f(isomers)}} = 3.8 \times 10^8 \text{ M}^{-1}\text{s}^{-1}$ (16), $k(\text{Br}_2\cdot^-+\text{DA}) = 1 \times 10^8 \text{ M}^{-1}\text{s}^{-1}$ and $k(\text{ClBr}^-+\text{DA}) = 1 \times 10^9 \text{ M}^{-1}\text{s}^{-1}$ (15). Reported DA $t_{1/2}$ in iron Fe(III) containing solutions are included. The $t_{1/2}$ values refer to time of continuous irradiation.

The most significant contribution to the transformation of DA is the $^3\text{DOM}^*$ induced diene isomerization, which is reversible and leads to toxic products. Although Fe(III) promoted the photochemical transformation of DA, the products have not been elucidated. HRs yielded $t_{1/2}$ in the range of 9 hours to 10 days, using the modeled steady-state concentrations and bimolecular rate constants previously reported (15). The $t_{1/2}$ of DA for the transformation by the other reactive species are similar, suggesting that all RS should be considered important for the photochemical transformation of DA. Equation 7 can be used to estimate the total DA photosensitization half-life ($t_{1/2}^{\text{DA photosensitization}}$), measuring the steady states of the different reactive species by means of quenching with well-study probes.

$$t_{1/2}^{\text{(Photosensitization of DA)}} = \frac{\text{Ln}(2)}{\sum k_{(RS+DA)} \sum [\text{RS}]_{ss}} \quad (7)$$

The DA photooxidation in bloom conditions may be very different from laboratory settings, and the photochemically generated RS may react with, quench and/or generate other RS. Products of the reactions of DA with photochemically generated RS, namely $^1\text{O}_2$, $\text{Br}_2^{\cdot\cdot}$, $\text{ClBr}^{\cdot\cdot}$, $\cdot\text{OH}$, $^3\text{DOM}^*$, have been well-studied and reported. Our studies indicate the reaction of $^1\text{O}_2$ with DA appears to yield non-toxic products. The products of the reactions of DA with the radical RS can lead to complex reaction mixtures as expected for radical mechanisms, as discussed in detail by Jin et al (16). Additional insight on DA photochemistry can be gained by quantification of DA, isomers of DA, PAC, HP1, HP2, and radical-mediated products during bloom conditions.

3.5. References

- (1) Maeno, Y.; Kotaki, Y.; Terada, R.; Cho, Y.; Konoki, K.; Yotsu-Yamashita, M. Six Domoic Acid Related Compounds from the Red Alga, *Chondria Armata*, and Domoic Acid Biosynthesis by the Diatom, *Pseudo-Nitzschia Multiseriata*. *Sci. Rep.* **2018**, *8* (1), 1–10.
- (2) Takemoto, T.; Daigo, K. Constituents of *Chondria Armata*. *Chem. Pharm. Bull.* **1958**, *6* (5), 578–580.
- (3) Saeed, A. F.; Awan, S. A.; Ling, S.; Wang, R.; Wang, S. Domoic Acid: Attributes, Exposure Risks, Innovative Detection Techniques and Therapeutics. *Algal Res.* **2017**, *24*, 97–110.
- (4) Perl, T.; Bedard, L.; Kosatsky, T.; Hockin, J.; Todd, E.; Remis, R. An Outbreak of Toxic Encephalopathy Caused by Eating Mussels Contaminated with Domoic Acid. *New Engl. J. Med.* **1990**, *322* (25), 1775–1779.
- (5) Todd, E. C. D. Domoic Acid and Amnesic Shellfish Poisoning - A Review. *J. Food Prot.* **1993**, *56* (1), 69–83.
- (6) Huppert, D. D.; Trainer, V. L. Economics of Razor Clam Fishery Closures Due to Harmful Algal Blooms in Washington State. *PICES Sci. Rep.* **2014**, (47), 59–71.
- (7) Appendix 5: FDA and EPA Safety Levels in Regulations and Guidance. *Fish and Fishery Products Hazards and Controls Guidance*; SGR 129, United States Department of Health and Human Services; Food and Drug Administration; Center for Food Safety and Applied Nutrition; Office of Food Safety. <https://www.fda.gov/media/80637/download>. **2019**, A5-8.
- (8) Bandala, E. R.; Brito, L.; Pelaez, M. Degradation of Domoic Acid Toxin by UV-Promoted Fenton-like Processes in Seawater. *Desalination.* **2009**, *245*, (1), 135–145.
- (9) Holland, P. T.; Selwood, A. I.; Mountfort, D. O.; Wilkins, A. L.; McNabb, P.; Rhodes, L. L.; Doucette, G. J.; Mikulski, C. M.; King, K. L. Isodomoic Acid C, an Unusual Amnesic Shellfish Poisoning Toxin from *Pseudo-Nitzschia Australis*. *Chem. Res. Toxicol.* **2005**, *18* (5), 814–816.
- (10) Kieber, D. J.; Peake, B. M.; Scully, N. M. Chapter 8 Reactive oxygen species in aquatic ecosystems. *UV Effects in Aquatic Organisms and Ecosystems*; Helbling, E. W., Zagarese, H., Eds.; Comprehensive Series in Photochemical & Photobiological Sciences; Royal Society of Chemistry: Cambridge, 2007; Vol. 1, pp 251-276., and references within.

- (11) Foote, C. S. Mechanisms of Photosensitized Oxidation. *Science*. **1968**, *162* (3857), 963-970.
- (12) McNeill, K.; Canonica, S. Triplet State Dissolved Organic Matter in Aquatic Photochemistry: Reaction Mechanisms, Substrate Scope, and Photophysical Properties. *Environ. Sci. Process. Impacts*. **2016**, *18*, 1381–1399.
- (13) Gagez, A. L.; Bonnet, A.; Pineau, P.; Graber, M. Identification and Quantification of Domoic Acid by UHPLC/QTOF Tandem Mass Spectrometry, with Simultaneous Identification of Non-Target Photodegradation Products. *Int. J. Environ. Anal. Chem.* **2017**, *97* (12), 1192–1205.
- (14) Bouillon, R. C.; Kieber, R. J.; Skrabal, S. A.; Wright, J. L. C. Photochemistry and Identification of Photodegradation Products of the Marine Toxin Domoic Acid. *Mar. Chem.* **2008**, *110*, 18–27.
- (15) Parker, K. M.; Mitch, W. A. Halogen Radicals Contribute to Photooxidation in Coastal and Estuarine Waters. *Proc. Natl. Acad. Sci. U.S.A.* **2016**, *113* (21), 5868–5873.
- (16) Jin, H.; Lian, L.; Zhou, H.; Yan, S.; Song, W. Mechanistic Consideration of the Photochemical Transformation of Domoic Acid (Algal Toxin) in DOM-Rich Brackish Water. *Chemosphere*. **2018**, *209*, 328–337.
- (17) Fisher, J. M.; Reese, J. G.; Pellechia, P. J.; Moeller, P. L.; Ferry, J. L. Role of Fe(III), Phosphate, Dissolved Organic Matter, and Nitrate during the Photodegradation of Domoic Acid in the Marine Environment. *Environ. Sci. Technol.* **2006**, *40* (7), 2200–2205.
- (18) Djaoued, Y.; Robichaud, J.; Thibodeau, M.; Balaji, S.; Tchoukanova, N.; Bates, S. S. Photocatalytic Properties of Nanocrystalline Titanium Dioxide Films in the Degradation of Domoic Acid in Aqueous Solution: Potential for Use in Molluscan Shellfish Biotoxin Depuration Facilities. *Food Addit. Contam.* **2009**, *26* (2), 248–257.
- (19) Jones, K. G.; Cooper, W. J.; Mezyk, S. P. Bimolecular Rate Constant Determination for the Reaction of Hydroxyl Radicals with Domoic and Kainic Acid in Aqueous Solution. *Environ. Sci. Technol.* **2009**, *43* (17), 6764–6768.
- (20) Kim, H.; Kim, W.; MacKeyev, Y.; Lee, G. S.; Kim, H. J. K.; Tachikawa, T.; Hong, S.; Lee, S.; Kim, H. J. K.; Wilson, L. J.; Tachikawa, T.; Hong, S.; Lee, S.; Kim, J.; Wilson, L. J.; Majima, T.; Alvarez, P. J.J.; Choi, W.; Lee, J. Selective Oxidative Degradation of Organic Pollutants by Singlet Oxygen-Mediated Photosensitization: Tin Porphyrin versus C60 Aminofullerene Systems. *Environ. Sci. Technol.* **2012**, *46* (17), 9606–9613.

- (21) Delcanale, P.; Montali, C.; Rodríguez-Amigo, B.; Abbruzzetti, S.; Bruno, S.; Bianchini, P.; Diaspro, A.; Agut, M.; Nonell, S.; Viappiani, C. Zinc-Substituted Myoglobin Is a Naturally Occurring Photo-Antimicrobial Agent with Potential Applications in Food Decontamination. *J. Agric. Food Chem.* **2016**, *64* (45), 8633–8639.
- (22) DeRosa, M. C.; Crutchley, R. J. Photosensitized Singlet Oxygen and Its Applications. *Coord. Chem. Rev.* **2002**, *234*, 351–371., and references within.
- (23) Adam, W.; Prein, M. π -Facial Diastereoselectivity in the [4+2] Cycloaddition of Singlet Oxygen as a Mechanistic Probe. *Acc. Chem. Res.* **1996**, *29* (6), 275–283.
- (24) Tzirakis, M. D.; Alberti, M. N. On the Mechanism of the [4+2] Cycloaddition of $^1\text{O}_2$ with 1, 3-Dienes : Identifying the Putative Biradical/Dipolar Intermediate by Employing the Gem -Diphenylcyclopropylcarbinyl Radical Clock as a Mechanistic Probe. *Arch. Org. Chem.* **2015**, *iii*, 83–100.
- (25) Adam, W.; Saha-Möller, C. R.; Schambony, S. B. A Highly Diastereoselective Dioxetane Formation by the Hydroxy-Directed [2+2] Cycloaddition of Singlet Oxygen to a Chiral Allylic Alcohol. *J. Am. Chem. Soc.* **1999**, *121* (9), 1834–1838.
- (26) Stratakis, M.; Orfanopoulos, M. Regioselectivity in the Ene Reaction of Singlet Oxygen with Alkenes. *Tetrahedron.* **2000**, *56*, 1595–1615.
- (27) Gracanin, M.; Hawkins, C. L.; Pattison, D. I.; Davies, M. J. Singlet-Oxygen-Mediated Amino Acid and Protein Oxidation: Formation of Tryptophan Peroxides and Decomposition Products. *Free Radic. Biol. Med.* **2009**, *47* (1), 92–102.
- (28) Davies, M. J. Singlet Oxygen-Mediated Damage to Proteins and Its Consequences. *Biochem. Biophys. Res. Commun.* **2003**, *305* (3), 761–770., and references within.
- (29) Parekh, P. K. The Photooxidation of Domoic Acid. 2012.for the Oxidative Cleavage of Olefins by $\text{OsO}_4 - \text{NaIO}_4$. *Org. Lett.* **2004**, *6* (19), 3217–3219.
- (30) Atkinson, R.; Aschmann, S. M.; Pitts, J. N. Rate Constants for the Gas-Phase Reactions of the OH Radical with a Series of Monoterpenes at 294 ± 1 K. *Int. J. Chem. Kinet.* **1986**, *18* (3), 287–299.
- (31) Haag, W. R.; Hoigne, J. Singlet Oxygen in Surface Waters. 3. Photochemical Formation and Steady-State Concentrations in Various Types of Waters. *Environ. Sci. Technol.* **1986**, *20* (4), 341–348.
- (32) Latch, D.; Stender, B. L.; Packer, J. L.; Arnold, W. A.; McNeill, K. Photochemical Fate of Pharmaceuticals in the Environment : Cimetidine and Ranitidine. *Environ. Sci. Technol.* **2003**, *37* (15), 3342–3350.

- (33) Appiani, E.; Ossola, R.; Latch, D. E.; Erickson, P. R.; McNeill, K. Aqueous Singlet Oxygen Reaction Kinetics of Furfuryl Alcohol: Effect of Temperature, pH, and Salt Content. *Environ. Sci. Process. Impacts*. **2017**, *19* (4), 507–516.
- (34) Parker, K. M.; Pignatello, J. J.; Mitch, W. A. Influence of Ionic Strength on Triplet-State Natural Organic Matter Loss by Energy Transfer and Electron Transfer Pathways. *Environ. Sci. Technol.* **2013**, *47* (19), 10987–10994.
- (35) Egorov, S.; Krasnovsky Jr, A. Quenching of Singlet Molecular Oxygen by Components of the Media Used for Isolation of Chloroplasts and Testing Their Photosynthetic Activity. *Russ. J. Plant Physiol.* **1986**, *33*, 10–14.
- (36) Eske, A.; Goldfuss, B.; Griesbeck, A. G.; de Kiff, A.; Kleczka, M.; Leven, M.; Neudörfl, J.-M.; Vollmer, M. Ene–Diene Transmissive Cycloaddition Reactions with Singlet Oxygen: The Vinylogous Gem Effect and Its Use for Polyoxoxygenation of Dienes. *J. Org. Chem.* **2014**, *79* (4), 1818–1829.
- (37) O’Shea, K. E.; Foote, C. S. Chemistry of Singlet Oxygen. 51. Zwitterionic Intermediates from 2, 4-Hexadienes. *J. Am. Chem. Soc.* **1988**, *110* (21), 7167–7170.
- (38) Panigrahi, G. P.; Misro, P. K. Kinetics & Mechanism of Oxidation of Aliphatic Ketones by Sodium Metaperiodate: A Comparative Study of Uncatalysed versus OsO₄-Catalysed Oxidation. *Indian J. Chem.* **1978**, *16A* (9), 762–766.
- (39) Adam, W.; Erden, I. Trapping of Unstable Alpha-Pyrone / Singlet Oxygen Adduct by Reduction with Diazene. *Angew. Chem. Int. Ed. Engl.* **1978**, *17* (3), 211.
- (40) Clayden, J.; Knowles, F. E.; Baldwin, I. R. The Synthesis of (—)-Isodomoic Acid. *J. Am. Chem. Soc.* **2005**, *127* (8), 2412–2413.
- (41) Clennan, E. L. Synthetic and Mechanistic Aspects of 1,3-Diene Photooxidation. *Tetrahedron* **1991**, *47* (8), 1343–1382.
- (42) Zepp, R. G.; Wolfe, N. L.; Baughman, G. L.; Hollis, R. C. Singlet Oxygen in Natural Waters. *Nature*. **1977**, *267* (June), 190–192.
- (43) Burns, J. M.; Schock, T. B.; Hsia, M. H.; Moeller, P. D. R.; Ferry, J. L. Photostability of Kainic Acid in Seawater. *J. Agric. Food Chem.* **2007**, *55* (24), 9951–9955.
- (44) Luo, L.; Lai, X.; Chen, B.; Lin, L.; Fang, L.; Tam, N. F. Y.; Luan, T. Chlorophyll Catalyse the Photo-Transformation of Carcinogenic Benzo[a]Pyrene in Water. *Sci. Rep.* **2015**, *5*, 1–11.

- (45) Skovsen, E.; Snyder, J. W.; Lambert, J. D. C.; Ogilby, P. R. Lifetime and Diffusion of Singlet Oxygen in a Cell. *J. Phys. Chem. B.* **2005**, *109* (18), 8570–8573.
- (46) Tenorio, R.; Fedders, A. C.; Strathmann, T. J.; Guest, J. S. Impact of Growth Phases on Photochemically Produced Reactive Species in the Extracellular Matrix of Algal Cultivation Systems. *Environ. Sci. Water Res. Technol.* **2017**, *3* (6), 1095–1108.
- (47) Latch, D. E.; McNeill, K. Microheterogeneity of Singlet Oxygen Distributions in Irradiated Humic Acid Solutions. *Science.* **2006**, *311* (5768), 1743–1747.
- (48) Schnetzer, A.; Lampe, R. H.; Benitez-Nelson, C. R.; Marchetti, A.; Osburn, C. L.; Tatters, A. O. Marine Snow Formation by the Toxin-Producing Diatom, *Pseudo-Nitzschia Australis*. *Harmful Algae.* **2017**, *61*, 23–30.
- (49) Mopper, K.; Zhou, X. Hydroxyl Radical Photoproduction in the Sea and Its Potential Impact on Marine Processes. *Science.* **1990**, *250* (4981), 661–664.

**CHAPTER 4 REACTIONS OF THE SINGLET OXYGENATION OF WATER-
SOLUBLE PYRROLES: PRODUCTS, KINETICS, AND MECHANISTIC
STUDIES**

4.1. Abstract

Melanin, a pyrrole based photoprotective pigment in skin pigment, is subject to irreversible damage by photooxidation. The reactions of $^1\text{O}_2$ with water-soluble pyrroles (Py) were studied as model compounds to understand the photooxidative damage to the primary Melanin structure. The reactions of singlet oxygen with these pyrroles produced hydroxypyrrolones (HPOnes) as the major products. The singlet oxygenation of several pyrroles despite varying substitution at the α -carbon yielded identical major products. The reactions of all the pyrroles in this study were fast but significantly different, with bimolecular rate constants from 1.18 to 18.9 $\text{M}^{-1}\text{s}^{-1}$. Our studies also demonstrate that *N*-alkyl substitution enhanced the reactivity of the Py towards $^1\text{O}_2$ and yielded a more complex mixture of products than the *N*-H based pyrroles. 1H-pyrrole-2,3,4-tricarboxylic acid (TCOOH-Py), commonly used as a marker to assess melanin photoaging, reacts with $^1\text{O}_2$ at rates near diffusion control, $k(^1\text{O}_2+\text{TCOOH-Py})=1.89\pm 0.047 \times 10^9 \text{ M}^{-1}\text{s}^{-1}$. Using TCOOH-Py concentrations as a measure of melanin damage under photodynamic conditions may underestimate skin damage due to sun exposure. The HPOnes products identified in our study may serve as markers for assessing the $^1\text{O}_2$ -mediated damage to melanin. Our results provide fundamental mechanistic insight on the singlet oxygenation of pyrroles in aqueous media, which may extend to the understanding of photooxidation of numerous biologically and environmentally important pyrrole based molecules and polymers. The reactions produced nearly quantitative transformation pyrroles providing a green method for synthesizing HPOne based natural products and drugs.

4.2. Introduction

Pyrrole functionalities are critical to living organisms as melanin and bile pigments and in biologically active compounds, including Atorvastatin (ATV), Fluvastatin (FLV), and Fludioxonil (FLD). The pyrrole systems present in the skin or natural aquatic systems as pollutants are susceptible to photooxidation. Melanin, a vital natural pigment, plays a protective role against Ultra Violet (UV) radiation and reactive oxygen species damage, including $^1\text{O}_2$ (1, 2). The melanin biopolymer is composed of indole and pyrrole subunits (1, 3, 4). In the presence of light, melanin in hair produced $^1\text{O}_2$ through self-sensitization (5). Using near IR emission, the lifetime of $^1\text{O}_2$ in hair was (0.1 μs) significantly shorter than water (4 μs) (6, 7), indicating efficient quenching of $^1\text{O}_2$ by melanin (5). Phosphorescence of $^1\text{O}_2$ was used to support the generation of $^1\text{O}_2$ by DHICA-melanin (8). The reactions of $^1\text{O}_2$ with the indole functionalities undergone mainly ene and [2+2] cycloadditions (9). The singlet oxygenation of melanin in hair was proposed to produce the hydroperoxide of the indol ring through the ene pathway (8). The proposal was supported by a signal appearing at 8.4 ppm in the ^1H NMR spectrum (8). The melanin $^1\text{O}_2$ quenching rate was $1.34 \times 10^8 \text{ M}^{-1}\text{s}^{-1}$ (8). Melanin is chemically oxidized to TCOOH-Py for HPLC and LC-MS analysis (1). The ratio of free and total TCOOH-Py is used as photodegradation and aging measurement (1). 2, 3, 4-TCOOH-Py was found in fossil ink sacs more than 160 million years old (2). 2, 3, 4-TCOOH-Py was observed in eumelanin aging (cross-linking) experiments (10). The reactions of $^1\text{O}_2$ with the chemical marker, TCOOH-Py, may underestimate the photochemical damage of melanin. The singlet oxygenation of TCOOH-Py can also provide insights into photochemical transformations, photoprotection, and singlet oxygenation of melanin. Bilirubin, a tetrapyrrole bile pigment, reacts with $^1\text{O}_2$ at a

rate of $4 \times 10^8 \text{ M}^{-1}\text{s}^{-1}$, accounting for the rapid disappearance of bilirubin during the photodynamic therapy of neonatal jaundice (11). Recently, the reactive oxygen species (ROS) quenching ability of bilirubin has been a research topic in the nanomedicine field (12, 13). The cholesterol-lowering pyrrole based drugs, ATV, and FLV are extensively prescribed for reducing human blood cholesterol (14). These hyperlipidemia medicines are introduced into the environment through wastewater systems (14). ATV and FLV pose a threat to drinking water sources because of the extensive use and the lack of appropriate treatment of wastewater (14–16). Singlet oxygen was the primary reactive oxygen species (ROS) involved in the DOM mediated photochemical transformation of ATV, accounting for 67.14% of transformation, while $\text{OH}\cdot$ only accounted for 0.66% (14). Although the lifetime of $^1\text{O}_2$ is shorter in water than in methanol, the bimolecular rate constant for the reaction of $^1\text{O}_2$ with ATV has been reported to be higher in water ($k_r=3.1 \pm 0.2 \times 10^8 \text{ M}^{-1}\text{s}^{-1}$ (16)) than in $\text{MeOH}/\text{H}_2\text{O}$ (1:8) ($k_r= 1.5 \pm 0.2 \times 10^8 \text{ M}^{-1} \text{ s}^{-1}$ (17)). Similarly fast kinetics have also been reported for Fluvastatin ($k_r=1.64 \pm 0.18 \times 10^8 \text{ M}^{-1} \text{ s}^{-1}$ (18)) and the pyrrole-based pesticide, Fludioxonil ($k_r=4.90 \pm 0.20 \times 10^7 \text{ M}^{-1} \text{ s}^{-1}$ (19)) in aqueous media.

The reductive dearomatization of pyrroles has been extensively used in synthetic methodologies (20, 21). The oxidation of pyrroles can result in product mixtures and is often considered impractical (21–23). Photooxygenation of individual pyrrole ring systems has been extensively studied in organic solvents (20, 21, 24–26). The singlet oxygenation of pyrroles can yield complex product mixtures from the competing [4+2], [2+2], and ene reaction pathways depending on the substitution of the pyrrole (20, 21, 24–26). The reaction of kryptopyrrole (2,4-dimethyl-3-ethylpyrrole) with $^1\text{O}_2$ in methanol yielded the

methoxy or hydroxyl pyrrolinones substituted derivatives (21). Pyrroles with alkyl, formyl, carbomethoxy, or acyl groups at the α position produced hydroxy or methoxy pyrrolones upon reaction with $^1\text{O}_2$ (in what solvent) (27). Alkyl substitution on the pyrrole nitrogen significantly increased the complexity of the $^1\text{O}_2$ reactions (26). Rearrangement or hydrolysis of an unstable endoperoxide intermediate was proposed to rationalize the formation of the observed products (21). Unsaturated γ -lactams were isolated in yields of 58–76 % upon the singlet oxygenation of N-substituted pyrroles (28). The hydroxy pyrrolones were also observed in the reaction mixture, but acid workup caused dehydration to yield unsaturated γ -lactams (28). In general, the $^1\text{O}_2$ reactions with pyrroles are relatively clean for rings substituted with both electron-releasing and electron-withdrawing groups compared to N-alkyl pyrroles (27).

While detailed mechanistic studies of the reactions of pyrroles with singlet oxygen have been studied in organic solvents (20, 21, 24–26), reports on the singlet oxygenation of pyrroles in aqueous media are limited (16, 19). Singlet oxygen reactions are notorious for exhibiting strong solvent dependence (29–31). Nucleophiles trapped an imino hydroperoxide intermediate in the singlet oxygenation of 5-substituted pyrroles (25). David A. Lightner et al. observed the unstable endoperoxides (EPs) of *N*-methylpyrroles with low-temperature and used ^{18}O to elucidate the internal rearrangement of the EPs as the primary reaction mechanism, except when water was the reaction solvent (30). The authors proposed that the water attacks one of the EP carbons producing a hydroperoxide that rearranges to the corresponding HPOne (30). Extraction of a proton from the endoperoxide carbon can also lead to the formation of the HPOne (30).

HPOne functionality is attractive in medicinal chemistry and is observed on several important natural products. Biologically active γ -hydroxy- γ -butyrolactams, such as Jatropham and Oteromycin are known for their anticancer and anti-HIV-1 activity, respectively (32). The synthesis of HPOnes traditionally requires a multi-step reaction sequence, as illustrated in the synthesis of Lucilactaene, a cancer inhibitory compound (33). However, the self-sensitized photooxidation reaction of pyrrolo[2,1-a]isoquinoline produced the HPO in a single step in ~ 70 % yield (34). The importance and syntheses of 3-pyrrolin-2-ones have been studied and reviewed by Pelkey et al. (35).

The kinetics of the singlet oxygen reactions with pyrroles are also dependent on the substitution of the pyrrole. The $^1\text{O}_2$ reaction rate of 3-phenyl substituted pyrrole, $k = 7.9 \times 10^8 \text{ M}^{-1}\text{s}^{-1}$, was faster than the unsubstituted pyrrole, $k=4.95 \times 10^8 \text{ M}^{-1}\text{s}^{-1}$, which in turn was faster than the rate of 3-cyanopyrrole, $k=0.438 \times 10^8 \text{ M}^{-1}\text{s}^{-1}$ in aqueous media (19). There are only a limited number of reports on the bimolecular rate constants for the reaction of $^1\text{O}_2$ with pyrrole containing compounds in aqueous media (19).

We report herein the singlet oxygenation of several water-soluble pyrroles. We describe the products, mechanisms, and kinetics of the reactions. Our product studies indicate that water may attack the functional group at the α -carbon position of the unstable endoperoxide, producing stable HPone and complementary acid in a very controlled, efficient, and clean manner. These results build on existing knowledge and demonstrate the critical role water plays in the reaction mechanisms of singlet oxygen. Also, the kinetics of the reactions were very fast, with biomolecular rate constants in the $10^8 \text{ M}^{-1} \text{ s}^{-1}$ magnitudes.

4.3. Materials and methods

Materials: 3,5-dimethyl-1H-pyrrole-2,4-dicarboxylic (COOH-Py) (CAS number 5434-29-7, MW= 183.16 g mol⁻¹), 5-acetyl-2,4-dimethyl-1H-pyrrole-3-carboxylic acid (Ac-Py) (CAS number 17106-15-9, MW= 181.19 g mol⁻¹), 2,4-dimethylpyrrole-3-carboxylic acid (H-Py) (CAS 17106-13-7, MW= 139.15 g mol⁻¹), 5-formyl-2,4-dimethyl-3-pyrrolecarboxylic Acid (F-Py) (CAS number 253870-02-9, MW= 167.16 g mol⁻¹), Rose Bengal disodium salt (RB) (CAS Number 632-69-9, MW= 1,017.65167.16 g mol⁻¹), and furfuryl alcohol (CAS Number 98-00-0, MW= 98.1 g mol⁻¹) were purchased from Sigma Aldrich. All reagents had purity > 95% and were used without purification. The NMR tubes (OD 5 mm) were purchased from Kimble Chase. Deuterium oxide (D₂O), was purchased from Cambridge Isotope Laboratories Incorporated.

Stock Solutions: A stock solution of 0.5 M pyrrole (Py) and 10 μM RB was prepared in D₂O for product studies. A stock solution of 0.5 M Py/0.5 M furfuryl alcohol (FFA), Py/FFA, and 10 μM RB was prepared in D₂O for the kinetic studies. The pH was adjusted with NaOD to ~ 8 to enhance solubility.

Photooxidation: The NMR tube containing Py or Py/FFA stock solution was placed in a Pyrex glass (cutoff $\lambda < 310$ nm) windowed Dewar flask filled with a water-ice bath (~ 5 °C). A 150 W Xenon lamp (Oriel) was used as the irradiation source.

Controls for the reactions: The transformation of Py by direct photolysis (in the absence of a sensitizer) and type I photosensitized reactions (argon-saturated solution) were negligible.

Synthesis of methyl 5-acetyl-2,4-dimethyl-1H-pyrrole-3-carboxylate, Ac-Py-DM: The esterification of 50 mg Ac-Py was modified from the procedure initially described by Bagal et al., 2010 (36). 5-acetyl-2,4-dimethyl-1H-pyrrole-3-carboxylic acid (50 mg, 70.4 μmol) was added to solution of MeI (18 μL , 70.4 μmol) and K_2CO_3 (155 mg, 281 μmol) in DMF (2 mL) while stirring. The mixture was stirred for 24 hours at room temperature. The product was extracted with $\text{H}_2\text{O}/\text{Et}_2\text{O}$, the final extraction of the organic layer was done with a NaCl saturated brine solution, and then dried over CaCl_2 . The solvent was evaporated in vacuo to give AC-Py-ES. ^1H NMR δ ppm (400 MHz, CDCl_3) 3.76 (3H, s, CO_2CH_3), 2.55 (3H, s, COCH_3), 2.43 (3H, s, CH_3), 2.41 (3H, s, CH_3).

Synthesis of methyl 5-acetyl-1,2,4-trimethyl-pyrrole-3-carboxylate, Ac-Py-TM: The same procedure, as described above for the synthesis of AC-Py-DM, was used to synthesize AC-Py-TM from 5-acetyl-2,4-dimethyl-1H-pyrrole-3-carboxylic acid by adding 2 eq. (36 μL , 140.8 μmol) MeI to give the AC-Py-TM. ^1H NMR δ ppm (400 MHz, CDCl_3) 3.88 (3H, s, CO_2CH_3), 3.78 (3H, s, NCH_3), 2.6 (3H, s, COCH_3), 2.50 (3H, s, CH_3), 2.50 (3H, s, CH_3).

Kinetics Studies: competition kinetics of the reaction of $^1\text{O}_2$ with Py, $k_{(\text{O}_2+\text{Py})}$, and FFA was employed to determine the individual singlet oxygen rate constants with the different pyrroles (37). The pyrroles bimolecular rate constants were calculated by

comparing the rate of the singlet oxygenation of FFA $k_{(O_1+FFA)}$, $0.94 \pm 0.01 \times 10^8 \text{ M}^{-1} \text{ s}^{-1}$ (38–41). Derivation Equation 1 and 2 can be found in the introductory chapter.

$$\text{Ln} \frac{[Py]_t}{[Py]_0} = \frac{k_{(^1O_2+Py)}}{k_{(^1O_2+FFA)}} \text{Ln} \frac{[FFA]_t}{[FFA]_0} \quad (1)$$

Assuming singlet oxygen is in a steady-state concentration, $[^1O_2]_{ss}$, in our system, the half-life of Py upon reaction with 1O_2 ($t_{1/2} (^1O_2+Py)$) is given by Equation 2.

$$t_{1/2} (^1O_2+Py) = \frac{\text{Ln}(2)}{k_{(^1O_2+Py)}[^1O_2]_{ss}} \quad (2)$$

MS Analysis: The samples were provided as liquids (solvent) with stated concentrations of 2 mg/mL. The sample was initially diluted to 20 ppm in a 1:1 Optima grace Acetonitrile: Water solvent mixture (5 % Agilent TuneMix). Thereafter, the samples were infused/analyzed by (+/-) ESI mode on a Solarix FT-ICR MS operated in low-resolution mode: 256 KWord. The Solarix FT-ICR MS instrument was calibrated with 4 calibration points between the mass range of 100 to 900 Da., applying a quadratic calibration with a mass tolerance of 10 ppm for low-resolution operation. Mass spectra were collected with 20 co-added scans.

Product studies: The Py stock solution was subjected to photooxidation and monitored by ^1H and ^{13}C NMR spectroscopy at specific irradiation times employing a 400 MHz Bruker NMR spectrometer. The product assignment was verified using The Solarix FT-ICR MS. The main product of the 1O_2 reaction of Ac-Py, F-Py, COOH-Py, and H-Py was **2-hydroxy-2,4-dimethyl-5-oxo-2,5-dihydro-1H-pyrrole-3-carboxylic acid (OHOxo-Py)**. OHOxo-Py ^1H NMR δ ppm (400 MHz, D_2O); 1.55 (3H, s), 1.75 (3H, s),

1.85 (H, s), ^{13}C NMR δ ppm (400 MHz, D_2O); 174.36, 171.01, 153.10, 130.07, 86.37, 23.64, 23.35, 8.80, and M-1 ion 170.04538 m/z.

4.4. Results and discussion

Product Studies: Under our experimental conditions, the singlet oxygenation of the water-soluble pyrroles was typically fast and clean. The reactions were run without RB as a control for direct photolysis and with RB under argon saturation, in the absence of oxygen, as controls for type I photochemical reactions showed insignificant transformation. The singlet oxygenation of 0.5 M Ac-Py produces a single product. The production of singlet oxygen upon thermal decomposition of EPs has been used as support for the presence of EPs in singlet oxygen reaction products (30). The singlet oxygenation product of AcPy heated to 100 °C for 30 mins remained unchanged, indicating the EP is unlikely the product of the reaction. Detailed analysis by ^1H and ^{13}C NMR and HR/MS confirmed the product of the reaction as **OHOxo-Py**,

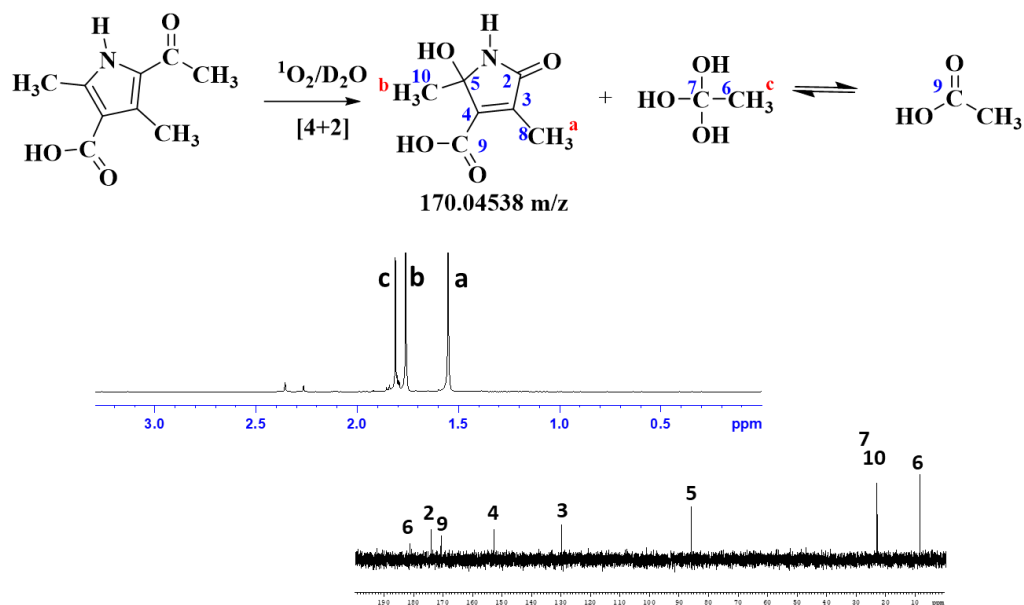
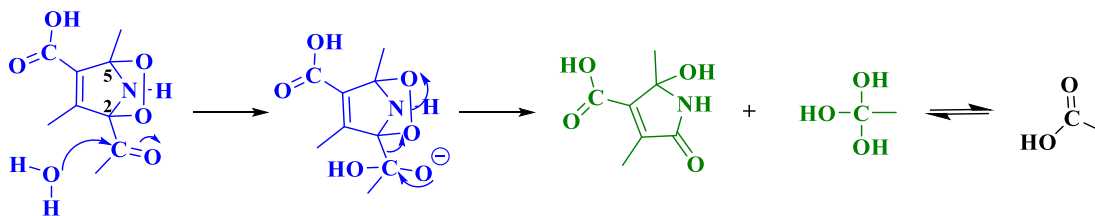


Figure 4.1. Elucidation of the product from 20 min Photooxidation of 0.5 M, 5-acetyl-2,4-dimethyl-1H-pyrrole-3-carboxylic acid (Ac-Py), 2-hydroxy-2,4-dimethyl-5-oxo-2,5-dihydro-1H-pyrrole-3-carboxylic acid (OHOxo-Py). The ^1H (Top) and ^{13}C (Bottom) NMR spectra were recorded in the 400 Bruker NMR spectrometer. The solution was prepared with 10 μM RB in D_2O , continuously purged with oxygen, and irradiated with at 150 W Xenon lamp while maintaining the temperature at $\sim 5^\circ\text{C}$.

In previous studies employing H_2O^{18} and MS analysis, the formation of HPOne was proposed to occur via water attack at an endoperoxide carbon at position 5 or 2 (Scheme 4.1) (30). However, the $^1\text{O}_2$ reaction of Ac-Py leads mainly to a single product, atypical for endoperoxide rearrangements. We hypothesized that the rearrangement is initially driven by water attacking the electron-deficient carbonyl carbon of the methyl ketone. Following, loss of acetic acid and opening of endoperoxide through cleavage of the peroxide bond with the formation of hydroxyl and carbonyl functionalities at the endoperoxide carbons to yield OHOxo-Py, as illustrated in Scheme 4.1.



Scheme 4.1. Proposed mechanism for the 5-acetyl-2,4-dimethyl-1H-pyrrole-3-carboxylic acid, Ac-Py, endoperoxide rearrangement into 2-hydroxy-2,4-dimethyl-5-oxo-2,5-dihydro-1H-pyrrole-3-carboxylic acid, OHOxo-Py.

To probe the mechanism proposed in Scheme 4.1, we conducted the photooxidation of dimethyl pyrrole carboxylic acids differing from Ac-Py only by the substitution at the α position with an -H, -CHO, and $-\text{CO}_2^-$. Abbreviated as H-Py, F-Py, and COOH-Py and shown in Figure 4.2.

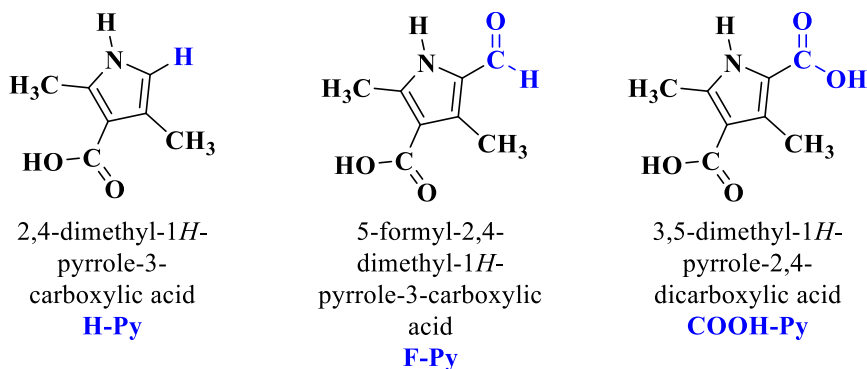


Figure 4.2. Structure of mechanistic probes for the $^1\text{O}_2$ reactions with pyrroles.

The reactions of singlet oxygen with H-Py, F-Py, and COOH-Py produced **OHOxo-Py** as the major product. However, the rates and products varied depending on the substitution at the α position. 0.5 M F-Py yielded OHOxo-Py exclusively. Formic acid, a byproduct of the reaction, protonated and precipitated OHOxo-Py from the solution. Acid

workup provides an attractive and economical route to purify OHOxo-Py for synthetic applications.

0.5 M COOH-Py also produced OHOxo-Py upon reaction with $^1\text{O}_2$ as the major product, $71.2 \pm 2.9\%$, based on the ^1H NMR integration signals compared to an unidentified minor product, $28.8 \pm 2.9\%$. When hydrogen was at the alpha position of the Py, OHOxo-Py was the main product in $65.5 \pm 7.5\%$ relative to a minor product, not elucidated, 34.5% . The singlet oxygenation of pyrrolo[2,1-a]isoquinoline and coumarin-fused pentacyclic produced the HPOs in 68 to 78% (34). The H substitution at one of the α positions was critical to the reactivity of the compounds (34). Our results indicate that H- α substituted Py would react with $^1\text{O}_2$ to produce HPOs in similar yields. The α -methyl ketone or formyl substituted pyrrolo[2,1-a]isoquinoline, and coumarin-fused pentacyclic, thus, may offer cleaner but slower conversion in the syntheses of HPOs than the α -H substituted pyrroles.

To conduct low-temperature NMR to observe the unstable EP intermediates, we synthesized Ac-Py-DM and Ac-Py-TM (Figure 4.3 and 4.4). The esterification of Ac-Py to Ac-Py-DM was conducted as described by Bagal et al., 2010 (36). The esterification is an $\text{S}_{\text{N}}2$ reaction of MeI by deprotonated Ac-Py.

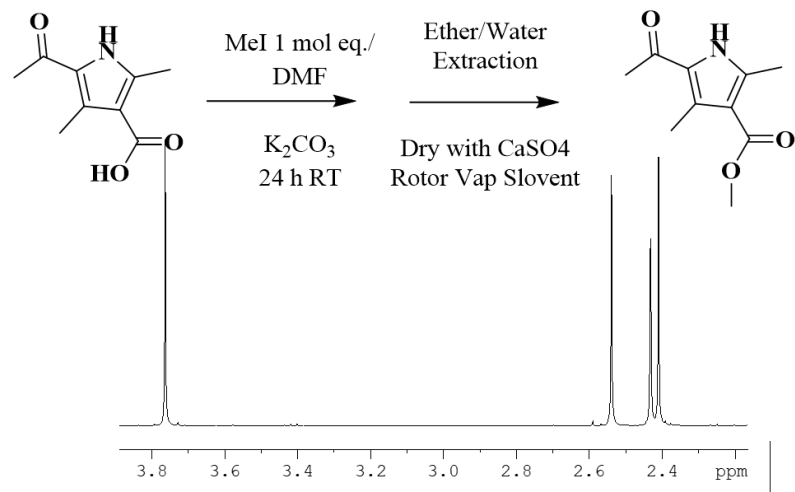


Figure 4.3. Synthesis of methyl 5-acetyl-2,4-dimethyl-1H-pyrrole-3-carboxylate, Ac-Py-DM. The esterification of 50 mg Ac-Py was modified from the procedure initially described by Bagal et al., 2010 (36). 5-Acetyl-2,4-dimethyl-1H-pyrrole-3-carboxylic acid (50 mg, 70.4 mmol) was added to solution of MeI (18 μ L, 70.4 mmol) and K₂CO₃ (155 mg, 281 mmol) in DMF (2 mL) while stirring. The mixture was stirred for 24 hours at room temperature. The product was extracted with H₂O/Et₂O, the final extraction of the organic layer was done with a NaCl saturated brine solution, and then dried over CaCl₂. The solvent was evaporated in vacuo to give AC-Py-ES. ¹H NMR δ ppm (400 MHz, CDCl₃) 3.76 (3H, s, CO₂CH₃), 2.55 (3H, s, COCH₃), 2.43 (3H, s, CH₃), 2.41 (3H, s, CH₃).

Ac-TM-Py was also synthesized from Ac-Py. The double methylation was achieved using a 2:1 ratio of MeI to Ac-Py concentration (Figure 4.4).

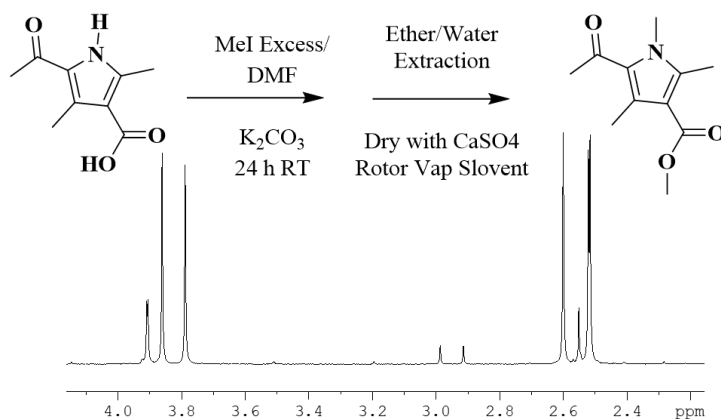


Figure 4.4. Synthesis of methyl 5-acetyl-1,2,4-trimethyl-pyrrole-3-carboxylate, Ac-Py-TM. The esterification of 50 mg Ac-Py was modified from the procedure initially described by Bagal et al., 2010 (36). 5-Acetyl-2,4-dimethyl-1H-pyrrole-3-carboxylic acid (50 mg, 70.4 mmol) was added to solution of MeI (36 μ L, 140.8 mmol) and K_2CO_3 (155 mg, 281 mmol) in DMF (2 mL) while stirring. The mixture was stirred for 24 hours at room temperature. The product was extracted with H_2O/Et_2O , the final extraction of the organic layer was done with a NaCl saturated brine solution, and then dried over $CaCl_2$. The

The singlet oxygen reactions of 0.5 M Ac-Py-DM in CD_2Cl_2 produced the OHOxo-Ac-DM-Py as the main product along with minor products as observed in the spectrum (Figure 4.5). The 1O_2 reactions of Ac-Py (D_2O) and the ester derivative Ac-DM-Py (CD_2Cl_2) products were analogous. However, the reactions of the water-soluble derivative were cleaner, producing OHOxo-Ac-Py at high purity (Figure 4.1).

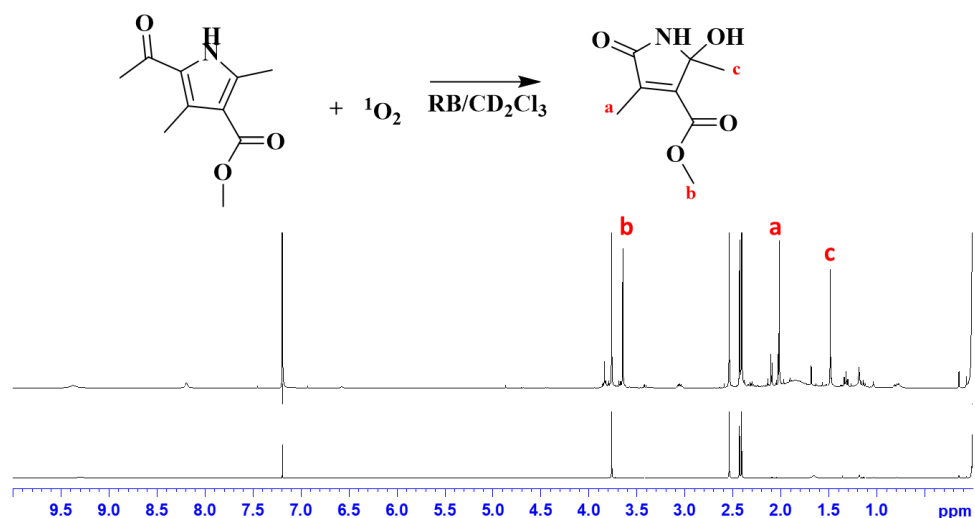


Figure 4.5. Photooxidation of 0.5 M Synthesis of methyl 5-acetyl-2,4-dimethyl-1H-pyrrole-3-carboxylate, Ac-Py-DM, in CD₂Cl₂. ¹H NMR Ac-Py-DM (bottom) and ¹H NMR product upon 25 min photooxidation, OHoxoEs-Py, methyl 2-hydroxy-2,4-dimethyl-5-oxo-2,5-dihydro-1H-pyrrole-3-carboxylate. The solutions were prepared with 10 μM Rose Bengal in D₂O in an NMR tube, constantly purged with oxygen and irradiated with a 150 W Xenon lamp temperature while maintaining the temperature at ~ 5 °C. The spectra were recorded in the 400 Bruker NMR spectrometer.

The singlet oxygen reaction of 0.5 M Ac-Py-TM in CD₂Cl₂ was extremely fast, complete within 90 seconds yielding a complex mixture of products (Figure 4.6). Our results demonstrate the reactions of singlet oxygen with Ac-Py-TM, *N*-methyl substituted, resulted in a more complex product mixture than for the *N*-H-pyrroles in agreement with previous reports (27).

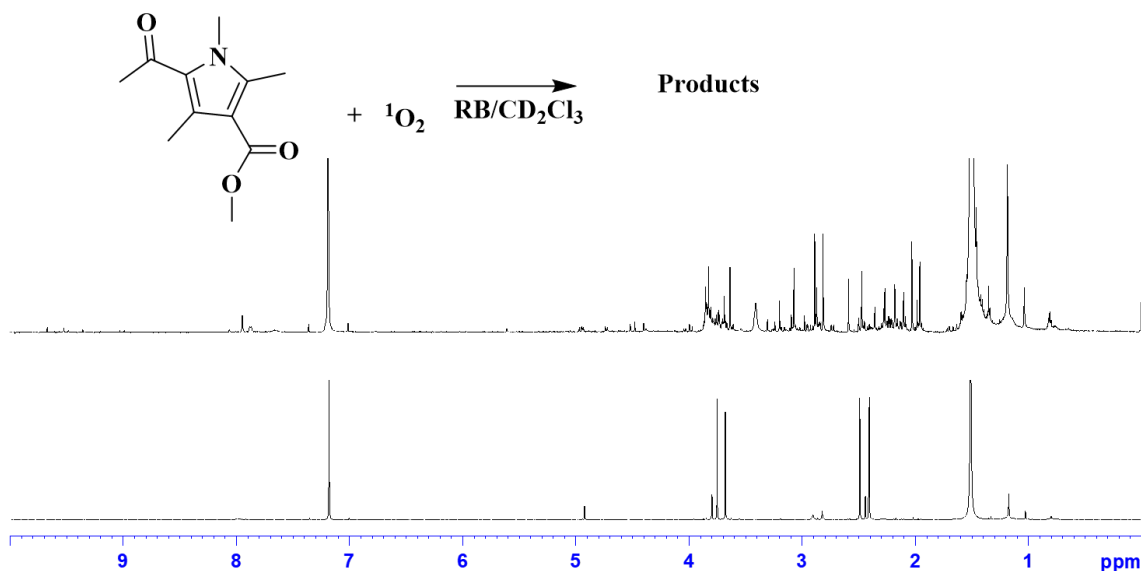


Figure 4.6 Photooxidation of 0.5 M methyl 5-acetyl-1,2,4-trimethyl-pyrrole-3-carboxylate, Ac-Py-TM, in CD_2Cl_2 . ^1H NMR Ac-Py-TM (bottom) and ^1H NMR product mixture upon 90 seconds photooxidation. The solutions were prepared with $10\ \mu\text{M}$ Rose Bengal in D_2O in an NMR tube, constantly purged with oxygen and irradiated with a 150 W Xenon lamp temperature while maintaining the temperature at $\sim 5\ ^\circ\text{C}$. The spectra were recorded in the 400 Bruker NMR spectrometer.

The photodegradation of melanin is implicated in skin cancer (10). 2, 3, 4-TCOOH-Py indicate eumelanin cross-linking due to photodamage or photoaging. The reactions of $^1\text{O}_2$ with the chemical marker, TCOOH-Py, may underestimate photochemical damage of melanin. Thus a fundamental understanding of its reactions with $^1\text{O}_2$ is essential. Singlet oxygen reactions with TCOOH-Py yielded clean reaction product(s). Figure 4.7 shows the ^1H NMR of the singlet oxygenation of TCOOH-Py. Future ^{13}C NMR and MS tools will be used for the structure elucidation of the product(s).

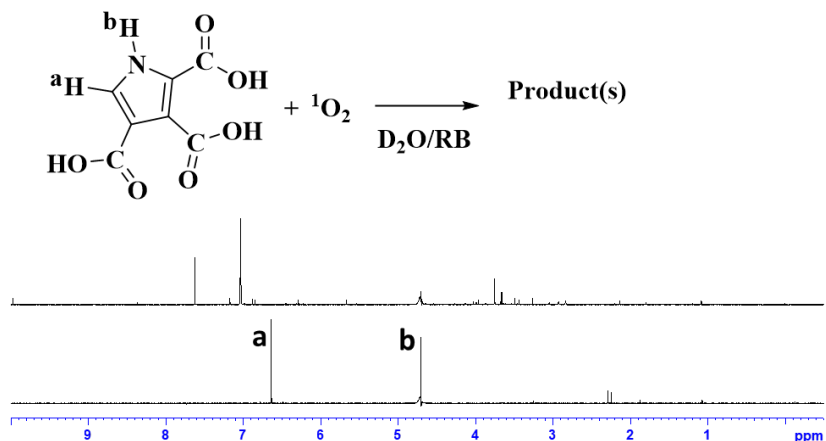


Figure 4.7. ^1H NMR of the photooxidation of 0.5 M 1H-pyrrole-2,3,4-tricarboxylic acid (TCOOH-Py) in 1 ml^{-1} D_2O . ^1H NMR TCOOH-Py before reaction (bottom) and ^1H NMR of the product of 10 min photooxidation of TCOOH-Py (top). The solutions were prepared with $10\ \mu\text{M}$ Rose Bengal in D_2O in an NMR tube, continuously purged with oxygen and irradiated with a 150 W Xenon lamp temperature while maintaining the temperature at $\sim 5\ ^\circ\text{C}$. The spectra were recorded in the 400 Bruker NMR spectrometer.

4.5. Kinetic studies

The relative rate method was used to calculate the bimolecular rate constants of the singlet oxygenation of Pys. The standard kinetic probe FFA was used as the reference. The reaction rates were qualitatively assessed using ^1H NMR peak integration of the disappearance of signals from starting material and the emergence of indicative product signals.

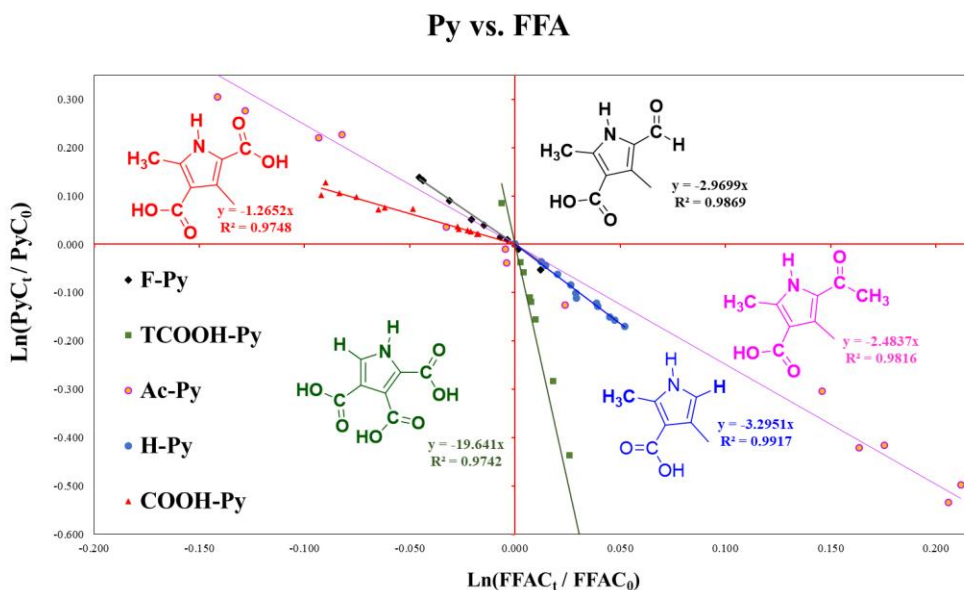


Figure 4.8. The relative reaction rate of singlet oxygenation of 0.5 M model Pyrrole and 0.5 M FFA. Detailed reaction conditions are provided in the experimental section. Red triangles represent COOH-Py, gray squares represent TCOOH-Py, black diamonds represent F-Py, yellow circles represent Ac-Py, and blue circles represent H-Py.

The pyrroles in this study exhibited fast reactions with second-order reaction rate constants from 0.188 to $18.9 \times 10^8 \text{ M}^{-1}\text{s}^{-1}$ (Figure 4.8 and Table 4.2). Substitution at the α -carbon of the pyrrole ring significantly affected the kinetics of the reactions. The rates constants from slowest to fastest based on the functional group at the α -carbon were $\text{COOH} < \text{COCH}_3 < \text{COH} < \text{H}$. The pH of the solution was slightly basic, $\text{pH} \sim 8$. We propose that the enhanced reactivity for H-Py compared to substituted pyrroles consistent with previous reports is dependent on the ease of elimination of the α -H (30). The basic pH conditions may also facilitate the OH-/H₂O attack to the partial-positive carbon at the aldehyde and ketone groups, initiating rearrangement, as proposed above. The second-order rate constants of the pyrroles in this study follow the trend $\text{COOH-Py} < \text{Ac-Py} < \text{F-Py} < \text{H-Py}$. Electronic and steric effects can explain the observed kinetic trend. More

electron-withdrawing groups, such as carboxylate, at the α -position, had slower singlet oxygenation rates. The smallest, H substituted pyrrole, showed the fastest kinetics, indicating that sterics also play an essential factor—the reactions of TCOOH-Py bimolecular rate constant for the $^1\text{O}_2$ reaction of $18.9 \pm 0.047 \times 10^8 \text{ M}^{-1}\text{s}^{-1}$. The effect of electronics for TCOOH-Py seems to be overpowered by having an H and a COOH at α positions. The COOH and H were selectively lost upon the $^1\text{O}_2$ reaction based on the product studies for model pyrroles. Therefore, the kinetics of the reactions are dependant on the leaving ability of the α carbon substituents. The singlet oxygenation rate of TCOOH-Py was 4.7 times higher than the reported rate for bilirubin, $k(^1\text{O}_2+\text{Bil}) = 4 \times 10^8 \text{ M}^{-1}\text{s}^{-1}$ (11), which is one of the fastest $^1\text{O}_2$ reaction rates reported. These findings could be useful in pyrrole-based nanomedicines (12). In melanin photochemical studies, TCOOH-Py is expected to chemically quench most $^1\text{O}_2$ in the system since the rates of the reactions are near diffusion controlled.

Table 4.1. Summary of the $^1\text{O}_2$ reactions with Pyrroles

Name	R ₁	R ₂	R ₃	R ₄	R ₅	$k_{(\text{Py}+^1\text{O}_2)}$, $10^8\text{M}^{-1}\text{s}^{-1}$	Evidence for 3-Pyrrolin-2-ones derivative
COOH-py	H	COOH	CH ₃	COOH	CH ₃	1.18±0.044	¹ H, MS
Ac-py	H	COCH ₃	CH ₃	COOH	CH ₃	2.33±0.036	¹ H, ¹³ C, DEP, MS
F-py	H	COH	CH ₃	COOH	CH ₃	2.92±0.029	¹ H, ¹³ C, DEP, MS
H-py	H	H	CH ₃	COOH	CH ₃	3.12±0.028	¹ H, MS
TCOOH-py	H	H	COOH	COOH	COOH	18.9±0.047	Not elucidated
Ac-DM-Py	H	COCH ₃	CH ₃	COOCH ₃	CH ₃	N/A	¹ H
DiMeA-py	CH ₃	COCH ₃	CH ₃	COOCH ₃	CH ₃	N/A	Not elucidated

Calculations are based on the bimolecular rates constants $k(^1\text{O}_2+\text{FFA}) = 0.94\pm 0.01 \times 10^8 \text{ M}^{-1}\text{s}^{-1}$ (41)

The singlet oxygenation of the model pyrroles followed the [4+2] reaction pathways exclusively in D₂O. We did not obtain any evidence for the [2+2] cycloaddition or ene reaction pathways. The pyrrole endoperoxides were unstable, rearranging to the hydroxypyrrolone derivative. The pyrrole reactivity and kinetics with singlet oxygen are highly dependent on the substitution. The substitution at the α position of the pyrrole was critical for the singlet oxygenation. Sterics, electronics, and leaving group capacity may account for the strong substituent effect. Melanin generates and quenches ¹O₂ under photodynamic conditions. TCOOH-Py would chemically quench most ¹O₂ in the system since the rates of the reactions are near diffusion controlled. Using TCOOH-Py as a marker for UV degradation of melanin could underestimate the damage. The products identified in our study likely can serve as accurate markers for assessing the ¹O₂-mediated damage to melanin. Our results provide fundamental mechanistic insight on the singlet oxygenation pyrroles in aqueous media, which may contribute to a better assessment of melanin aging, photochemistry of other important biological pigments, and pyrroles based contaminants.

4.6. References

- (1) Ito, S.; Kikuta, M.; Koike, S.; Szewczyk, G.; Sarna, M.; Zadlo, A.; Sarna, T.; Wakamatsu, K. Roles of Reactive Oxygen Species in UVA-Induced Oxidation of 5,6-Dihydroxyindole-2-Carboxylic Acid-Melanin as Studied by Differential Spectrophotometric Method. *Pigment Cell Melanoma Res.* **2016**, *29* (3), 340–351.
- (2) Glass, K.; Ito, S.; Wilby, P. R.; Sota, T.; Nakamura, A.; Bowers, C. R.; Vinther, J.; Dutta, S.; Summons, R.; Briggs, D. E. G.; Wakamatsu, K.; Simon, J. D. Direct Chemical Evidence for Eumelanin Pigment from the Jurassic Period. *Proc. Natl. Acad. Sci. U. S. A.* **2012**, *109* (26), 10218–10223.
- (3) Xiao, M.; Chen, W.; Li, W.; Zhao, J.; Hong, Y. lee; Nishiyama, Y.; Miyoshi, T.; Shawkey, M. D.; Dhinojwala, A. Elucidation of the Hierarchical Structure of Natural Eumelanins. *J. R. Soc. Interface* **2018**, *15* (140).

- (4) Ward, W. C.; Lamb, E. C.; Gooden, D.; Chen, X.; Burinsky, D. J.; Simon, J. D. Quantification of Naturally Occurring Pyrrole Acids in Melanosomes. *Photochem. Photobiol.* **2008**, *84* (3), 700–705.
- (5) Chiarelli-Neto, O.; Pavani, C.; S. Ferreira, A.; Uchoa, A. F.; Severino, D.; Baptista, M. S. Generation and Suppression of Singlet Oxygen in Hair by Photosensitization of Melanin. *Free Radic. Biol. Med.* **2011**, *51* (6), 1195–1202.
- (6) Rodgers, M. A. J.; Snowden, P. T. Lifetime of $^1\text{O}_2$ in Liquid Water As Determined by Time-Resolved Infrared Luminescence Measurements. **1982**, (6), 5541–5543.
- (7) Lindig, B. A.; Rodgers, M. A. J.; Schaaplc, A. P. Determination of the Lifetime of Singlet Oxygen in D₂O Using 9,10-Anthracenedipropionic Acid, a Water-Soluble Probe. *J. Am. Chem. Soc.* **1980**, *102* (17), 5590–5593.
- (8) Ito, S.; Kikuta, M.; Koike, S.; Szewczyk, G.; Sarna, M.; Zadlo, A.; Sarna, T.; Wakamatsu, K. Roles of Reactive Oxygen Species in UVA-Induced Oxidation of 5,6-Dihydroxyindole-2-Carboxylic Acid-Melanin as Studied by Differential Spectrophotometric Method. *Pigment Cell Melanoma Res.* **2016**, *29* (3), 340–351.
- (9) Zhang, X.; Foote, C. S.; Khan, S. I. Reactions of N-Acylated Indoles with Singlet Oxygen. *J. Org. Chem.* **1993**, *58* (1), 47–51.
- (10) Ito, S.; Wakamatsu, K.; Glass, K.; Simon, J. D. High-Performance Liquid Chromatography Estimation of Cross-Linking of Dihydroxyindole Moiety in Eumelanin. *Anal. Biochem.* **2013**, *434* (2), 221–225.
- (11) Foote, C. S.; Ching, T. Y. Chemistry of Singlet Oxygen. XXI. Kinetics of Bilirubin Photooxygenation. *J. Am. Chem. Soc.* **1975**, *97* (21), 6209–6214.
- (12) Chen, Z.; Vong, C. T.; Gao, C.; Chen, S.; Wu, X.; Wang, S.; Wang, Y. Bilirubin Nanomedicines for the Treatment of Reactive Oxygen Species (ROS)-Mediated Diseases. *Mol. Pharm.* **2020**, *17* (7), 2260–2274.
- (13) Tian, J.; Huang, B.; Nawaz, M. H.; Zhang, W. Recent Advances of Multi-Dimensional Porphyrin-Based Functional Materials in Photodynamic Therapy. *Coord. Chem. Rev.* **2020**, *420*, 213410.
- (14) Wang, M.; Li, J.; Shi, H.; Miao, D.; Yang, Y.; Qian, L.; Gao, S. Photolysis of Atorvastatin in Aquatic Environment: Influencing Factors, Products, and Pathways. *Chemosphere* **2018**, *212*, 467–475.
- (15) Cermola, F.; DellaGreca, M.; Iesce, M. R.; Montanaro, S.; Previtera, L.; Temussi, F. Photochemical Behavior of the Drug Atorvastatin in Water. *Tetrahedron* **2006**, *62* (31), 7390–7395.

- (16) Razavi, B.; Abdelmelek, S. Ben; Song, W.; Cooper, W. J.; O'Shea, K. E. Photochemical Fate of Atorvastatin (Lipitor) in Simulated Natural Waters. *Water Res.* **2011**, *45* (September 2016), 625–631.
- (17) Montanaro, S.; Lhiaubet-Vallet, V.; Iesce, M.; Previtera, L.; Miranda, M. A. A Mechanistic Study on the Phototoxicity of Atorvastatin: Singlet Oxygen Generation by a Phenanthrene-Like Photoproduct. *Chem. Res. Toxicol.* **2009**, *22* (1), 173–178.
- (18) Santoke, H.; Cooper, W. J. Environmental Photochemical Fate of Selected Pharmaceutical Compounds in Natural and Reconstituted Suwannee River Water: Role of Reactive Species in Indirect Photolysis. *Sci. Total Environ.* **2017**, *580*, 626–631.
- (19) Apell, J. N.; Pflug, N. C.; McNeill, K. Photodegradation of Fludioxonil and Other Pyrroles: The Importance of Indirect Photodegradation for Understanding Environmental Fate and Photoproduct Formation. *Environ. Sci. Technol.* **2019**, *53* (19), 11240–11250.
- (20) Howard, J. K.; Rihak, K. J.; Bissember, A. C.; Smith, J. A. The Oxidation of Pyrrole. *Chem. - An Asian J.* **2016**, *11* (2), 155–167.
- (21) Lightner, D. A. Yearly reviews photochemistry of pyrroles , bile pigments and porphyrins. *Phnlorhemistry and Pholobiology* **1974**, *19*, 457–459.
- (22) Alberti, M. N.; Vougioukalakis, G. C.; Orfanopoulos, M. Photosensitized Oxidations of Substituted Pyrroles: Unanticipated Radical-Derived Oxygenated Products. *J. Org. Chem.* **2009**, *74* (19), 7274–7282.
- (23) Lightner, D. A. The Photoreactivity of Bilirubin and Related Pyrroles. *Photochem. Photobiol.* **1977**, *26* (4), 427–436.
- (24) Wasserman, H. H.; Xia, M.; Wang, J.; Petersen, A. K.; Jorgensen, M.; Power, P.; Parr, J. Singlet Oxygen Reactions of 3-Methoxy-2-Pyrrole Carboxylic Acid Tert-Butyl Esters. A Route to 5-Substituted Pyrrole Precursors of Prodigiosin and Analogs. *Tetrahedron* **2004**, *60* (34), 7419–7425.
- (25) Wasserman, H. H.; Xia, M.; Wang, J.; Petersen, A. K.; Jorgensen, M. Singlet Oxygen Oxidation of Pyrroles. Formation of 5-Substituted Derivatives. *Tetrahedron Lett.* **1999**, *40* (34), 6145–6148.
- (26) Wasserman, H. H.; Frechette, R.; Rotello, V. M. Singlet Oxygen Reactions of 2-Carbalkoxy-3-Methoxypyrroles. *Tetrahedron Lett.* **1991**, *32* (51), 7571–7574.
- (27) Iesce, M.; Cermola, F.; Temussi, F. Photooxygenation of Heterocycles. *Curr. Org. Chem.* **2005**, *9* (2), 109–139.

- (28) Demir, A. S.; Aydogan, F.; Akhmedov, I. M. The Synthesis of Chiral 5-Methylene Pyrrol-2(5H)-Ones via Photooxygenation of Homochiral 2-Methylpyrrole Derivatives. *Tetrahedron Asymmetry* **2002**, *13* (6), 601–605.
- (29) Merkel, P. B.; Kearns, D. R. Remarkable Solvent Effects on the Lifetime of $^1\Delta_g$ Oxygen. *J. Am. Chem. Soc.* **1972**, *94* (3), 1029–1030.
- (30) Lightner, D. A.; Bisacchi, G. S.; Norris, R. D. On the Mechanism of the Sensitized Photooxygenation of Pyrroles. *J. Am. Chem. Soc.* **1976**, *98* (3), 802–807.
- (31) Aubry, J. M.; Mandard-Cazin, B.; Rougee, M.; Bensasson, R. V. Kinetic Studies of Singlet Oxygen [4 + 2]-Cycloadditions with Cyclic 1,3-Dienes in 28 Solvents. *J. Am. Chem. Soc.* **1995**, *117* (36), 9159–9164.
- (32) Mardjan, M.; Parrain, J.-L.; Commeiras, L. Strategies To Access γ -Hydroxy- γ -Butyrolactams. *Synthesis (Stuttg.)* **2018**, *50* (06), 1175–1198.
- (33) Coleman, R. S.; Walczak, M. C.; Campbell, E. L. Total Synthesis of Lucilactaene, A Cell Cycle Inhibitor Active in P53-Inactive Cells. *J. Am. Chem. Soc.* **2005**, *127* (46), 16038–
- (34) Vyasamudri, S.; Yang, D.-Y. Base-Dependent Divergent Annulation of 4-Chloro-3-Formylcoumarin and Tetrahydroisoquinoline: Application to the Synthesis of Isolamellarins and Hydroxypyrrones. *J. Org. Chem.* **2019**, *84* (6), 3662–3670.
- (35) Pelkey, E. T.; Pelkey, S. J.; Greger, J. G. *De Novo Synthesis of 3-Pyrrolin-2-Ones*; Elsevier Ltd, 2015; Vol. 115.
- (36) Bagal, S. K.; Davies, S. G.; Lee, J. A.; Roberts, P. M.; Scott, P. M.; Thomson, J. E. Syntheses of the Enantiomers of 1-Deoxynojirimycin and 1-Deoxyaltronojirimycin via Chemo- and Diastereoselective Olefinic Oxidation of Unsaturated Amines. *J. Org. Chem.* **2010**, *75* (23), 8133–8146.
- (37) Atkinson, R. Kinetics and Mechanisms of the Gas-Phase Reactions of the Hydroxyl Radical with Organic Compounds under Atmospheric Conditions. *Chem. Rev.* **1985**, *85* (1), 69–201.
- (38) Atkinson, R.; Aschmann, S. M.; Pitts, J. N. Rate Constants for the Gas-Phase Reactions of the OH Radical with a Series of Monoterpenes at 294 ± 1 K. *Int. J. Chem. Kinet.* **1986**, *18* (3), 287–299.
- (39) Jaramillo, M.; Joens, J. A.; O’Shea, K. E. Fundamental Studies of the Singlet Oxygen Reactions with the Potent Marine Toxin Domoic Acid. *Environ. Sci. Technol.* **2020**, *54* (10), 6073–6081.

- (40) Haag, W. R.; Hoigne, J. Singlet Oxygen in Surface Waters. 3. Photochemical Formation and Steady-State Concentrations in Various Types of Waters. *Environ. Sci. Technol.* **1986**, *20* (4), 341–348.
- (41) Appiani, E.; Ossola, R.; Latch, D. E.; Erickson, P. R.; McNeill, K. Aqueous Singlet Oxygen Reaction Kinetics of Furfuryl Alcohol: Effect of Temperature, PH, and Salt Content. *Environ. Sci. Process. Impacts* **2017**, *19* (4), 507–516.

VITA

MARCELA JARAMILLO ARCILA

2015 – 2020	Environmental Chemistry, Ph.D., Florida International University, Miami FL
2017-2020	National Science Foundation (NSF) Graduate Research Fellowship Program
2015-2017	NSF GRFP Fellowship Honorable Mention
2016	NSF GRFP Fellowship Honorable Mention
2009 – 2011	Bachelor of Science Biology and Chemistry with honors, St. Thomas University, Miami Gardens, FL
2009-2011	Science, Technology, Engineering, and Mathematics Fellows Scholarship
2009-2011	Science, Technology, Engineering, and Mathematics Fellows Scholarship
2006-2007	NSF Science, Technology, Engineering, and Mathematics Scholarship

PUBLICATIONS AND PRESENTATIONS

- 1) Jaramillo, M.; O'Shea, K. E. Analytical Methods for Assessment of Cyanotoxin Contamination in Drinking Water Sources. *Curr. Opin. Environ. Sci. Heal.* 2019, 7, 45–51.
- 2) Jaramillo, M.; Joens, J. A.; O'Shea, K. E. Fundamental Studies of the Singlet Oxygen Reactions with the Potent Marine Toxin Domoic Acid. *Environ. Sci. Technol.* 2020, 54 10, 6073–6081.
- 3) Oral, Fundamental Studies of Singlet Oxygen Reactions with Melanin Model Compounds, Presenters: Marcela Jaramillo and Kevin E. as part of the Division of Physical Organic Chemistry, March 31st- April 4th, 2019, 257ACS Spring National Meeting, Orlando
- 4) Oral, Studies of the singlet oxygenation of Domoic acid: Mechanisms, kinetics, and biological significance, Presenters: Marcela Jaramillo and Kevin E. as part of the Division of Environmental Chemistry and Aquatic Photochemistry, March 31st- April 4th, 2019, 257ACS Spring National Meeting, Orlando
- 5) Oral, Studies of the singlet oxygenation of Domoic acid: Mechanisms and biological significance, Presenters: Marcela Jaramillo and Kevin E. as part of the Division of Environmental Chemistry and Aquatic, Photochemistry, March 18th- 22nd, 2018, 255 National American Chemical Society Meeting & Expo, New Orleans, LA
- 6) Oral, Singlet Oxygenation of dienes in water and methanol: Domoic Acid, Sorbate, and Sorbic Alcohol, Presenters: Marcela Jaramillo and Kevin E. O'Shea as part of Division of Environmental Chemistry and Aquatic Photochemistry, April 2nd-6th, 2017, 253rd National American Chemical Society in San Francisco, CA
- 7) Oral, Singlet Oxygenation of dienes in water and methanol: Domoic Acid, Sorbate, and Sorbic Alcohol, Presenters: Marcela Jaramillo and Kevin E. O'Shea as part of Division of Environmental Chemistry and Aquatic Photochemistry, April 2nd-6th, 2017, 253rd National American Chemical Society in San Francisco, CA